Bioconjugate Chemistry

Review

pubs.acs.org/bc

Radiolabeled Cyclic RGD Peptide Bioconjugates as Radiotracers Targeting Multiple Integrins

Shuang Liu*

School of Health Sciences, Purdue University, 550 Stadium Mall Drive, West Lafayette, Indiana 47907, United States

ABSTRACT: Angiogenesis is a requirement for tumor growth and metastasis. The angiogenic process depends on vascular endothelial cell migration and invasion, and is regulated by various cell adhesion receptors. Integrins are such a family of receptors that facilitate the cellular adhesion to and migration on extracellular matrix proteins in the intercellular spaces and basement membranes. Among 24 members of the integrin family, $\alpha_v\beta_3$ is studied most extensively for its role in tumor angiogenesis and metastasis. The $\alpha_v\beta_3$ is expressed at relatively low levels on epithelial cells and mature endothelial cells, but it is highly expressed on the activated endothelial cells of tumor neovasculature and some tumor cells. This restricted expression makes $\alpha_v\beta_3$ an excellent target to develop antiangiogenic drugs and diagnostic molecular imaging probes. Since $\alpha_v\beta_3$ is a receptor for extracellular matrix proteins with one or more RGD tripeptide sequence, many radiolabeled cyclic RGD peptides have been evaluated as "$\alpha_v\beta_3$−targeted" radiotracers for tumor imaging over the past decade. This article will use the dimeric and tetrameric cyclic RGD peptides developed in our laboratories as examples to illustrate basic principles for development of $\alpha_v\beta_3$-targeted radiotracers. It will focus on different approaches to maximize the radiotracer tumor uptake and tumor/background ratios. This article will also discuss some important assays for preclinical evaluations of integrin-targeted radiotracers. In general, multimerization of cyclic RGD peptides increases their integrin binding affinity and the tumor uptake and retention times of their radiotracers. Regardless of their multiplicity, the capability of cyclic RGD peptides to bind other integrins (namely, $\alpha_v\beta_5$, $\alpha_5\beta_1$, $\alpha_6\beta_4$, $\alpha_4\beta_1$, and $\alpha_v\beta_6$) is expected to enhance the radiotracer tumor uptake due to the increased integrin population. The results from preclinical and clinical studies clearly show that radiolabeled cyclic RGD peptides (such as ^{99m}Tc-3P-RGD$_2$, ^{18}F-Alfatide-I, and ^{18}F-Alfatide-II) are useful as the molecular imaging probes for early cancer detection and noninvasive monitoring of the tumor response to antiangiogenic therapy.

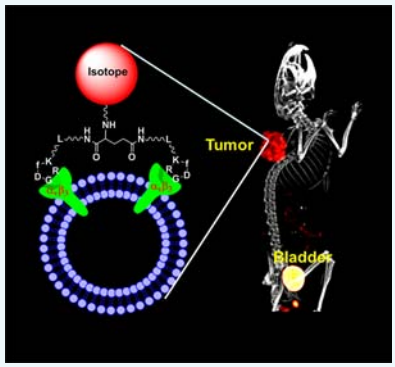

INTRODUCTION

Cancer is the second leading cause of death worldwide.[1] Most cancer patients will survive if it can be detected at the early stage. The sooner cancer is diagnosed and treated, the better chance a cancer patient will have for a full recovery. Thus, early detection is of great clinical importance for implementation of a therapeutic regimen before primary tumors become widely spread. In fact, early detection is the best option to substantially reduce deaths from cancer.

There are several imaging modalities available for diagnosis of cancer, including X-ray computed tomography (CT), ultrasound (US), nuclear magnetic resonance imaging (MRI), positron emission tomography (PET), and single photon emission computed tomography (SPECT). While CT, US, and MRI techniques are better suited for anatomic analysis of solid tumors, it is difficult to use them for evaluation of biochemical changes in tumor tissues due to the fact that they require a high concentration of contrast agent in order to achieve sufficient contrast. The specificity and sensitivity of CT and US for high-incidence tumors (e.g., breast, colorectal, lung, and prostate) are relatively low.[2] In contrast, PET or SPECT offers significant advantages with respect to specificity and sensitivity ($\sim 10^{-10}$ M for SPECT and 10^{-10}−10^{-12} M for PET).[2−4] Both modalities are able to provide the detailed information related to biochemical changes in tumor tissues at the cellular and molecular levels.

Nuclear imaging with PET or SPECT requires administration of radiopharmaceuticals (also called radiotracers), which are drugs containing a radionuclide for routine diagnosis of diseases. According to their biodistribution characteristics, diagnostic radiotracers can be divided into two classes: those whose biodistribution is determined almost exclusively by their chemical and physical properties, and those whose ultimate distribution properties are determined by their receptor binding affinity and receptor population in the diseased tissue. The latter ones are often called target-specific radiotracers. A number of target-specific radiotracers have been developed to target the receptors overexpressed on tumor cells and/or tumor vasculature.[2−10] In many cases, small peptides are used as targeting biomolecules (BM) for receptor binding in order to achieve high tumor specificity and selectivity.

Many radiolabeled cyclic RGD peptides have been evaluated as SPECT and PET radiotracers for tumor imaging.[11−50] A number of review articles have appeared to cover their nuclear medicine applications.[51−65] Instead of being an exhaustive

Received: June 9, 2015
Revised: July 16, 2015
Published: July 20, 2015

DOI: 10.1021/acs.bioconjchem.5b00327
Bioconjugate Chem. 2015, 26, 1413−1438

Chart 1. Schematic Presentation of Receptor Binding

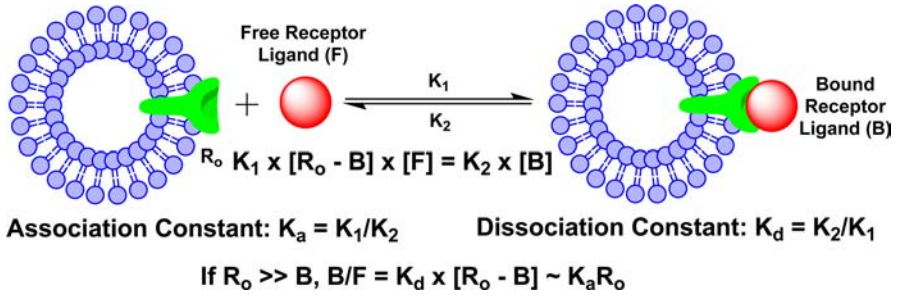

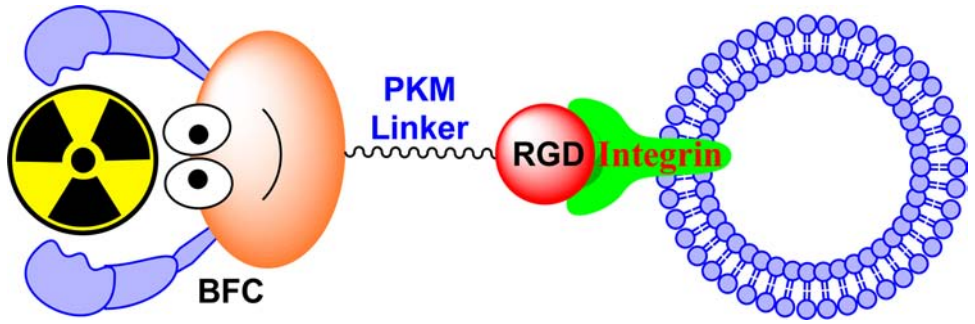

Figure 1. Schematic presentation of integrin-targeted radiotracers. The cyclic RGD peptide (monomeric, dimeric, or multimeric) serves as the targeting biomolecule to carry an isotope to the integrins (particularly $\alpha_v\beta_3$ and $\alpha_v\beta_5$). The bifunctional coupling agent (BFC) is used to attach the isotope to the targeting biomolecule. The PKM linker is often utilized to modify its pharmacokinetics.

review of current literature on radiolabeled cyclic RGD peptides, this article will use the dimeric and tetrameric cyclic RGD peptides developed in our laboratories as examples to illustrate the basic principles for development of $\alpha_v\beta_3$-targeted radiotracers. It will focus on different approaches to maximize radiotracer tumor uptake and tumor/background (T/B) ratios. It will also discuss some important biological assays for evaluations of $\alpha_v\beta_3$-targeted radiotracers, and their potential as molecular imaging probes for noninvasive monitoring of tumor metastasis and early detection of tumor response to treatment (chemotherapy, antiangiogenic therapy, radiation therapy, or combination thereof). The same basic principles illustrated in this Review may also apply to the radiotracers based on other receptors. Whenever possible, it will use the references published over the last 10 years. The author would apologize to those whose work has not been cited in this article.

RADIOTRACER DESIGN

Requirements for New Radiotracers. For a new radiotracer to be successful, it must show clinical indications for several high-incidence tumor types (namely, breast, lung, and prostate cancers). Its localization in tumors has to be sufficient so that clinically useful diagnostic images can be obtained within hours after intravenous administration of the radiotracer. Since most of the high-incidence tumor types occur in the torso (e.g., lung, colorectal, and breast cancers), renal excretion without significant kidney retention is necessary in order to maximize the T/B ratios. The main objective of tumor imaging is to achieve one or more of the following goals: (1) to detect the presence of tumor at an early stage, (2) to distinguish between benign and malignant tumors, (3) to follow the tumor growth and tumor response to a specific therapy (chemotherapy, antiangiogenic therapy, radiation therapy, or combination thereof), (4) to predict the success or failure of a specific therapeutic regimen, and (5) to assess the prognosis of a particular tumor in a specific cancer patient.

Basics of Receptor Binding. Receptor−ligand binding is defined by noncovalent interactions between a receptor and its ligand. These include hydrogen-bonding, lipophilic interactions, and static interactions between negative and positive charges. Using steady-state approximation, the association (K_a) and dissociation (K_d) constants could be calculated according to the equations illustrated in Chart 1. Frequently the dissociation constant K_d is preferred as the receptor binding affinity of a specific receptor ligand. K_1 and K_2 are association and dissociation rates, respectively. For receptor-based radiotracers, R_o is the total receptor population (bound and unbound), [B] is the concentration of receptor-bound radiotracer, and [F] is the unbound free radiotracer in blood circulation. If the total receptor population is much higher than the number of radiotracer molecules (radiolabeled receptor ligand), the target/background ratio will be directly proportional to K_a and R_o (Chart 1). Both binding affinity of the targeting biomolecule and receptor population are important to the tumor uptake and T/B ratios of a receptor-based radiotracer. Ligand binding is characterized in terms of the concentration of ligand at which half of the receptor binding sites are occupied, known as the IC_{50}, which is related to but different from the association and dissociation constants. If two ligands were present at the same time, more of the higher-affinity ligand would be bound to the available receptor binding sites. Binding affinity is most commonly determined using a radiolabeled ligand, known as a hot ligand. Competitive binding experiments involve binding-site competition between a hot ligand and a cold ligand (untagged ligand). Nonlabeled methods such as surface plasmon resonance and dual polarization interferometry can also quantify the affinity not only from concentration based assays, but also from the kinetics of association and dissociation.[66] Microscale thermophoresis (MST) is a method

DOI: 10.1021/acs.bioconjchem.5b00327
Bioconjugate Chem. 2015, 26, 1413−1438

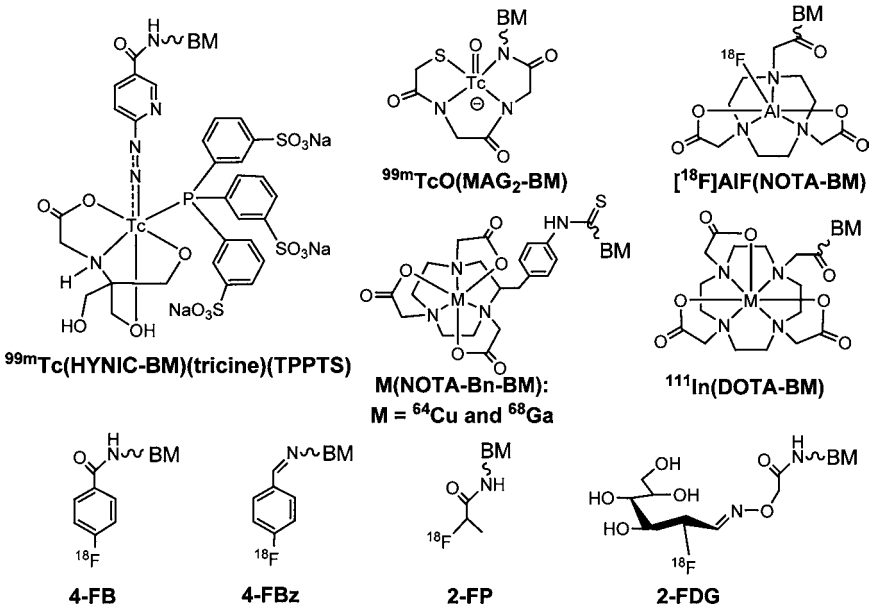

Figure 2. Examples of BFCs useful for radiolabeling of small biomolecules, such as cyclic RGD peptides. HYNIC and MAG_2 are useful for ^{99m}Tc-labeling. DOTA, NOTA, and their derivatives are better suited for chelation of ^{64}Cu, ^{68}Ga, and ^{111}In. For ^{18}F-labeling, 4-FB, 4-FBz, 2-FP, and 2-FDG are often used as prosthetic groups. The Al(NOTA) chelate is highly efficient for routine radiosynthesis of ^{18}F radiotracers using a kit formulation.

that allows the determination of binding affinity without any limitation to the ligand's molecular weight.[67]

Integrin-Targeted Radiotracer. Figure 1 shows the schematic illustration of an integrin-targeted radiotracer. A cyclic RGD peptide serves as the targeting biomolecule to carry an isotope to integrins expressed on tumor cells and activated endothelial cells of tumor neovasculature. BFC is a bifunctional coupling agent to attach the isotope to cyclic RGD peptide.[68] PKM is the pharmacokinetic modifying linker which is often used to improve the excretion kinetics of radiotracers.[68−70]

Radionuclide. The choice of radionuclide depends on the imaging modality (SPECT vs PET). More than 80% of the radiotracers for SPECT in nuclear medicine are ^{99m}Tc compounds due to the optimal nuclear properties of ^{99m}Tc and its easy availability at low cost.[68−70] The 6 h half-life is long enough to allow radiopharmacists to carry out radiosynthesis and for physicians to collect clinically useful images. At the same time, it is short enough to permit administration of 20−30 mCi of ^{99m}Tc without imposing a significant radiation dose to the cancer patient. The most clinically relevant PET isotopes are ^{18}F, ^{64}Cu, and ^{68}Ga. ^{18}F is a cyclotron-produced isotope. Despite its short half-life ($t_{1/2}$ = 110 min), the commercial availability of preparative modules makes ^{18}F radiotracers more accessible to clinicians. ^{64}Cu is another PET isotope to develop target-specific radiotracers. It has a half-life of 12.7 h and a β^+ emission (abundance: 18%; and E_{max} = 0.655 MeV). Despite poor nuclear properties, its long half-life makes it feasible to prepare, transport, and deliver ^{64}Cu radiotracers for clinical applications.[71] The breakthroughs in the production of ^{64}Cu with high specific activity have made it more available to research institutions without the on-site cyclotron facilities.[7,71] ^{64}Cu is a viable alternative to ^{18}F for research programs that wish to incorporate high resolution and sensitivity of PET, but cannot afford to maintain the expensive isotope production infrastructure.[71] ^{68}Ga is a generator-produced PET isotope with a half-life of 68 min. The ^{68}Ge−^{68}Ga generator can be used for more than a year, allowing PET studies without the on-site cyclotron. If the radiotracer is properly designed, ^{68}Ga can be as useful for PET as ^{99m}Tc for SPECT.[72] The ^{68}Ga-labeled somatostatin analogues have been studied for PET imaging of somatostatin-positive tumors in preclinical animal models and cancer patients.[72−75] Gallium chemistry and related nuclear medicine applications have been reviewed recently.[72]

Bifunctional Coupling Agent (BFC). The choice of BFC depends on radionuclide. Among various BFCs (Figure 2), HYNIC is of great interest due to its high ^{99m}Tc-labeling efficiency, the high solution stability of its ^{99m}Tc complexes, and the use of co-ligands to modify biodistribution properties of ^{99m}Tc radiotracers.[46,47,68−70] HYNIC and related radiochemistry have been reviewed.[70] In contrast, DOTA and NOTA derivatives (Figure 2) have been widely used for ^{68}Ga- and ^{64}Cu-labeling of biomolecules due to the high hydrophilicity and high stability of their ^{68}Ga/^{64}Cu chelates.[7,71,72] Because of the short half-life of ^{68}Ga ($t_{1/2}$ = 68 min), fast and efficient radiolabeling is important for ^{68}Ga radiotracers. Organic prosthetic groups (Figure 2: 4-FB, 4-FBz, 2-FP, and 2-FDG) are needed for ^{18}F-labeling.[76−89] Because of the aromatic rings, 4-FB, 4-FBz, and 2-FP groups often have relatively high lipophilicity, which might lead to more hepatobiliary excretion. The results from recent studies indicate that Al(NOTA) (Figure 2) is highly efficient for routine radiosynthesis of ^{18}F-labeled small biomolecule radiotracers using the kit formulation.[90−97] The Al(NOTA) chelate offers significant advantages over organic prosthetic groups (e.g., 4-FB, 4-FBz, and 2-FP) with respect to the ^{18}F-labeling efficiency and hydrophilicity, which is important for rapid renal excretion of ^{18}F radiotracers and minimization of their accumulation in normal organs, such as liver and lungs.

Integrins as Molecular Targets for Tumor Imaging. Tumors produce many angiogenic factors, which are able to activate endothelial cells in the established blood vessels and induce endothelial proliferation, migration, and new vessel formation (angiogenesis) through a series of sequential but partially overlapping steps. Angiogenesis is a requirement for tumor growth and metastasis.[98−101] The angiogenic process depends on the vascular endothelial cell migration and invasion,

DOI: 10.1021/acs.bioconjchem.5b00327
Bioconjugate Chem. 2015, 26, 1413−1438

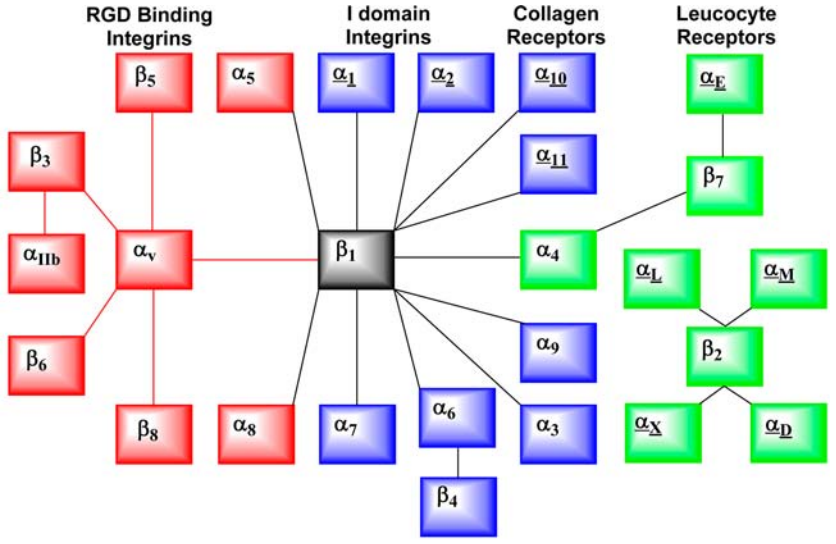

Integrins	Recognition Sequence	Natural Ligands
$\alpha_v\beta_1$, $\alpha_v\beta_3$, $\alpha_v\beta_5$, $\alpha_v\beta_6$, $\alpha_v\beta_8$, $\alpha_5\beta_1$, $\alpha_8\beta_1$, $\alpha_{IIb}\beta_3$	RGD	vitronectin, fibronectin, osteopontin, fibrinogen
$\alpha_4\beta_1$, $\alpha_9\beta_1$, $\alpha_4\beta_7$, $\alpha_E\beta_7$, $\alpha_L\beta_2$, $\alpha_M\beta_2$, $\alpha_X\beta_2$, $\alpha_D\beta_2$	LDV and related sequences	fibronectin, vascular cell adhesion molecule 1, mucosal addressin cell adhesion molecule 1, intercellular cell adhesion molecule 1
$\alpha_1\beta_1$, $\alpha_2\beta_1$, $\alpha_{10}\beta_1$, $\alpha_{11}\beta_1$	GFOGER	collagen, laminin
$\alpha_3\beta_1$, $\alpha_6\beta_1$, $\alpha_7\beta_1$, $\alpha_6\beta_4$	other	laminin

Figure 3. Top: Combinations of integrin subunits that form the 24 human receptors. Bottom: Natural integrin ligands and their corresponding recognition peptide sequences. Both the schematic illustration and the table were adapted from *J. Med. Chem.* **2014**, *57*, 6301−6315.

and is regulated by various cell adhesion receptors. Integrins are such a family of receptors that facilitate cellular adhesion to and migration on extracellular matrix proteins in the intercellular spaces and basement membranes, and regulate the entry and withdraw from the cell cycle. The integrin family comprises 24 transmembrane receptors (Figure 3).[98−101] Integrins possess redundancy in ligand recognition, adhesion, and signaling. Their main function is to integrate cell adhesion and interaction with the extracellular microenvironment with the intracellular signaling and cytoskeletal rearrangement through transmitting signals across the cell membrane upon ligand binding. Many integrins are crucial to tumor growth and metastasis. They also contribute to the pathological events such as thrombosis,[102] atherosclerosis,[103] infection caused by pathogenic microorganisms,[104,105] and immune dysfunction.[106] Among the 24 members of integrin family, the $\alpha_v\beta_3$ is studied most extensively for its role in tumor angiogenesis and metastasis.[98−101,107,108] It is not surprising that radiolabeled cyclic RGD peptides are often called "$\alpha_v\beta_3$-targeted" radiotracers in most of the current literature.[11−65]

The changes in the $\alpha_v\beta_3$ expression levels and activation state have been well-documented during tumor growth and metastasis.[98−101,107,108] The $\alpha_v\beta_3$ is expressed at relatively low levels on the epithelial cells and mature endothelial cells, but it is highly expressed in solid tumors, including osteosarcomas, glioblastoma, melanomas, and carcinomas of lung and breast.[107−124] Studies show that the $\alpha_v\beta_3$ is overexpressed on both tumor cells and activated endothelial cells of tumor neovasculature.[44,47,115] It is believed that the $\alpha_v\beta_3$ on endothelial cells modulate the cell adhesion and migration during tumor angiogenesis, while the $\alpha_v\beta_3$ on carcinoma cells potentiate metastasis by facilitating the invasion and movement of tumor cells across blood vessels.[119−124] It has also been shown that the $\alpha_v\beta_3$ expression levels correlate well with the metastatic potential and aggressiveness of solid tumors.[106−108,122−124] The $\alpha_v\beta_3$ is an important biological target for development of antiangiogenic drugs,[125−135] and molecular imaging probes for diagnosis of $\alpha_v\beta_3$-positive tumors.[11−65]

Cyclic RGD Peptides as Targeting Biomolecules. The $\alpha_v\beta_3$ is a receptor for extracellular matrix proteins with the exposed RGD tripeptide sequence. Theoretically, both linear and cyclic RGD peptides can be used as targeting biomolecules to develop $\alpha_v\beta_3$-targeted radiotracers. The drawback associated with the linear RGD peptides is their low binding affinity (IC_{50} > 100 nM), lack of specificity ($\alpha_v\beta_3$ vs $\alpha_{IIb}\beta_3$, $\alpha_v\beta_5$, $\alpha_5\beta_1$, $\alpha_6\beta_4$, $\alpha_4\beta_1$, or $\alpha_v\beta_6$), and rapid degradation by proteases in serum.[130,134] It was shown that cyclization of RGD peptides via linkers, such as S−S disulfide, thioether, and aromatic rings, leads to the increased integrin binding affinity.[125−134] The integrin selectivity ($\alpha_v\beta_3$ vs $\alpha_{IIb}\beta_3$) could be achieved by altering the cyclic RGD peptide backbone (Figure 4). Incorporation of the RGD tripeptide sequence into a cyclic pentapeptide (Figure 4: c(RGDfV) and EMD121974 or Cilengitide) significantly increases the binding affinity and selectivity of $\alpha_v\beta_3/\alpha_v\beta_5$ over $\alpha_{IIb}\beta_3$.[128−134] Many cyclic RGD peptides have been evaluated as $\alpha_v\beta_3/\alpha_v\beta_5$ antagonists for treatment of cancer. The results from

DOI: 10.1021/acs.bioconjchem.5b00327
Bioconjugate Chem. 2015, 26, 1413−1438

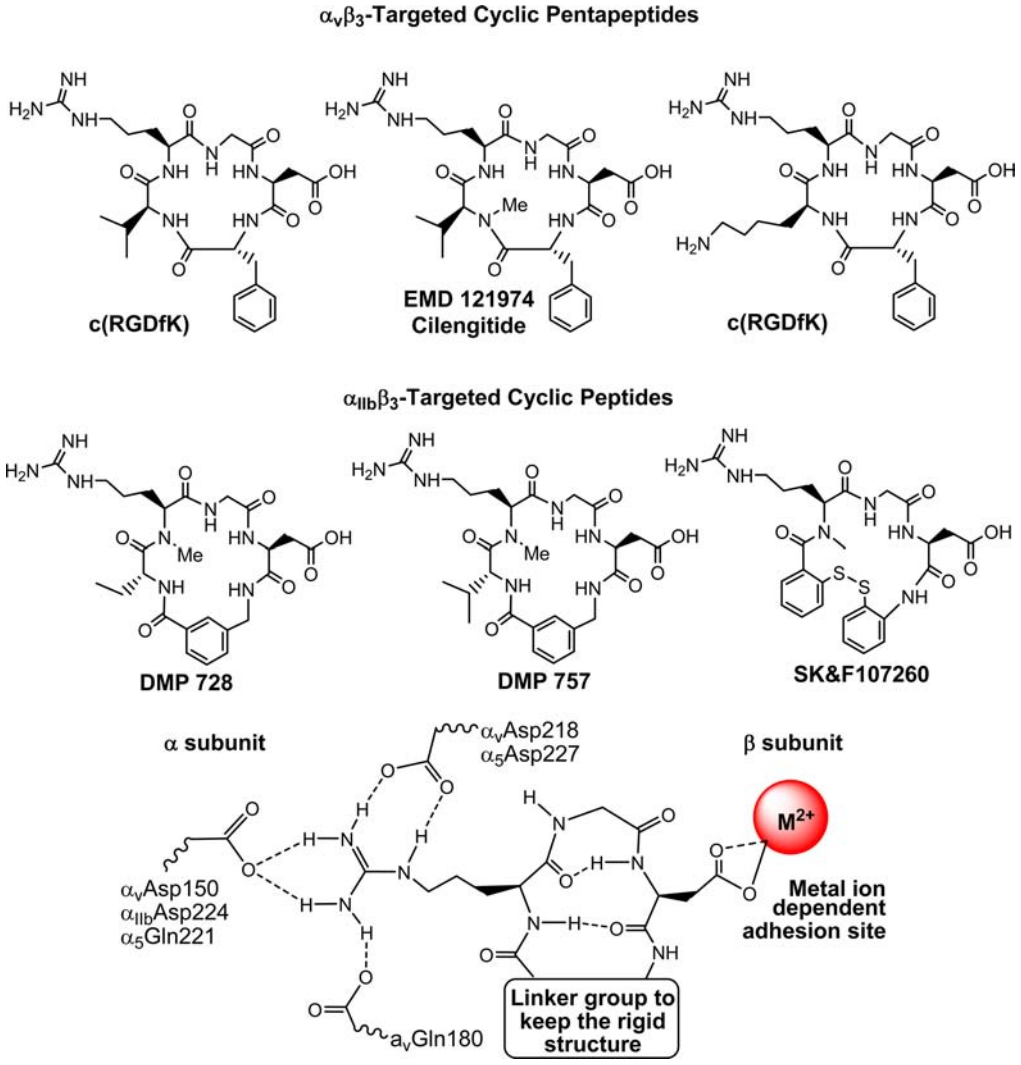

Figure 4. Examples of cyclic RGD peptides and key features at the binding site between the cyclic RGD peptide and integrins (particularly $\alpha_v\beta_3$, $\alpha_v\beta_5$, and $\alpha_{IIb}\beta_3$). The integrin selectivity can be achieved by altering the linker group in the cyclic peptide backbone. Cyclic pentapeptides are highly selective for $\alpha_v\beta_3$ and $\alpha_v\beta_5$ whereas the cyclic peptides with rigid aromatic rings show very high selectivity for $\alpha_{IIB}\beta_3$ over $\alpha_v\beta_3$, $\alpha_v\beta_5$, and $\alpha_5\beta_1$.

structure−activity studies indicate that the amino acid residue in position 5 has little impact on the $\alpha_v\beta_3/\alpha_v\beta_5$ binding affinity.[128−134] The valine (V) residue in c(RGDfV) can be replaced by lysine (K) or glutamic acid (E) to afford c(RGDfK) and c(RGDfE), respectively, without significantly changing their $\alpha_v\beta_3/\alpha_v\beta_5$ binding affinity. Cilengitide is currently under phase III clinical investigations as an "orphan drug" for treatment of glioblastoma and other cancer types either as stand-alone or in combination with radiation therapy.[135−142] It seems that the $\alpha_{IIB}\beta_3$ is less sensitive to variations in the peptide backbone and can accommodate a larger distance than both $\alpha_v\beta_3$ and $\alpha_v\beta_5$.[66,129] The addition of a rigid aromatic ring into a cyclic peptide structure (Figure 4: DMP728 and DMP757) enhance the binding affinity and selectivity of $\alpha_{IIB}\beta_3$ over $\alpha_v\beta_3/\alpha_v\beta_5$. DMP728 and DMP757 were originally developed by DuPont Pharma as antithrombosis agents.[143−145] We have been using the ^{99m}Tc-labeled DMP757 derivatives as SPECT radiotracers for thrombosis imaging.[146−154]

Figure 5 displays examples of monomeric cyclic RGD peptides. Among the radiotracers evaluated in various preclinical tumor-bearing animal models, ^{18}F-Galacto-RGD was the first PET radiotracer under clinical investigation for visualizing the $\alpha_v\beta_3$ expression in cancer patients.[155−158] [^{18}F]AH111585 is another $\alpha_v\beta_3$-targeted PET radiotracer under clinical evaluation for tumor imaging.[159] The imaging studies in cancer patients showed that there was sufficient $\alpha_v\beta_3$ expression for PET imaging, and the tumor uptake of ^{18}F-Galacto-RGD correlates well with the $\alpha_v\beta_3$ expression level.[157,158] However, the radiotracers derived from monomeric cyclic RGD peptides all have relatively low tumor uptake and T/B ratios because of their low $\alpha_v\beta_3$ binding affinity and fast dissociation kinetics.

It is important to note that cyclic RGD peptides bind not only $\alpha_v\beta_3$, but also $\alpha_v\beta_5$, $\alpha_5\beta_1$, $\alpha_6\beta_4$, $\alpha_4\beta_1$, and $\alpha_v\beta_6$ integrins regardless of their multiplicity because they all share similar features at the RGD-binding sites (Figure 4). While $\alpha_v\beta_3$ plays a pivotal role in tumor growth, progression and metastasis, $\alpha_{IIB}\beta_3$ is critical for platelet aggregation during thrombosis formation. It was believed that the interaction between $\alpha_v\beta_3$ and $\alpha_{IIb}\beta_3$ facilitates the adhesion of tumor cells to tumor vasculature, which often leads to metastasis.[160,161] The $\alpha_v\beta_5$ is very similar to $\alpha_v\beta_3$ in the ligand binding region (Figure 4), and they share a similar expression pattern and biological function. Both $\alpha_v\beta_5$ and $\alpha_v\beta_3$ are highly expressed on the activated endothelial cells

DOI: 10.1021/acs.bioconjchem.5b00327
Bioconjugate Chem. 2015, 26, 1413−1438

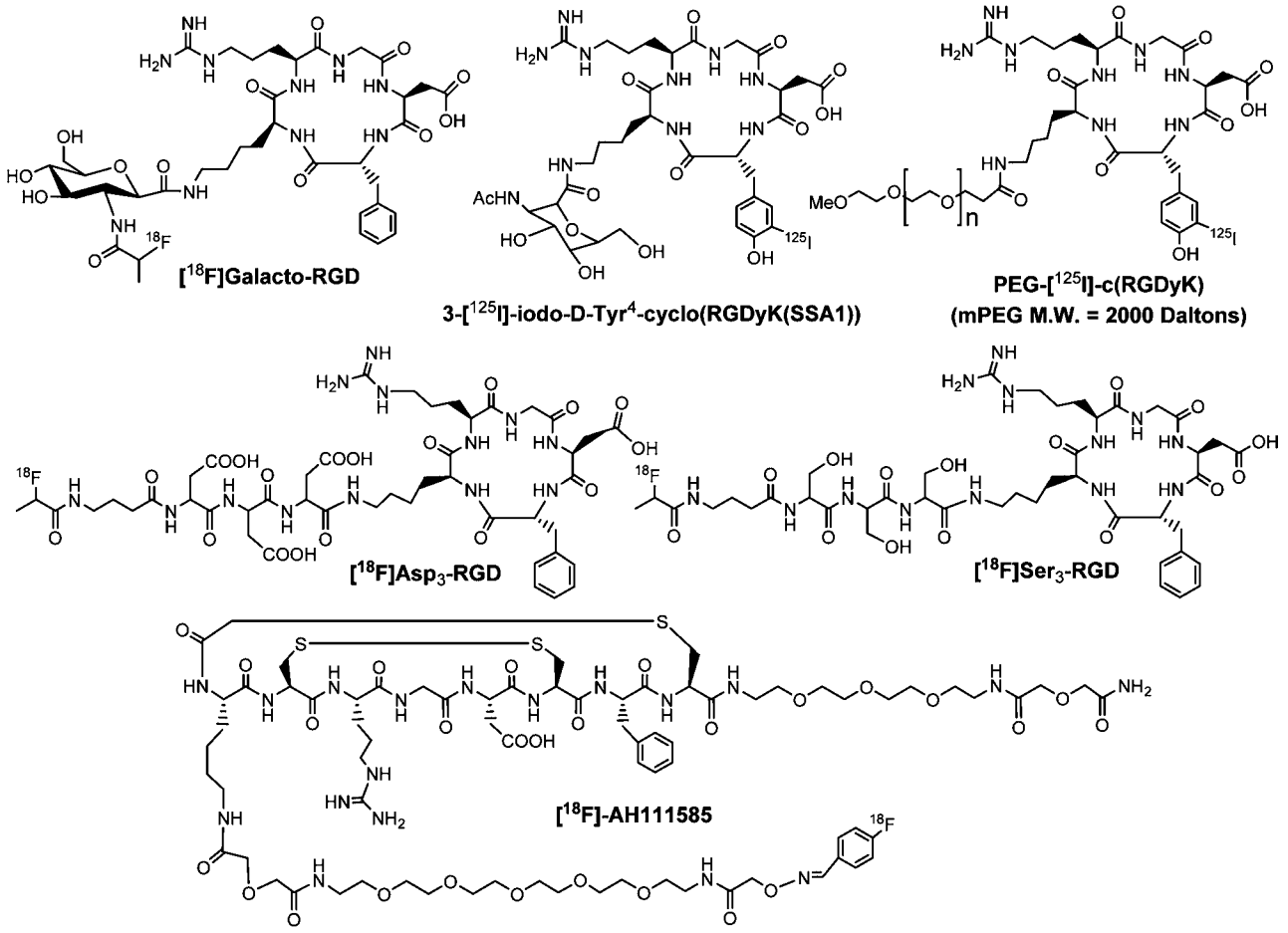

Figure 5. Examples of the radiolabeled monomeric cyclic RGD peptides as radiotracers. The D_3 (Asp-Asp-Asp), S_3 (Ser-Ser-Ser), PEG (polyethylene glycol), and sugar linkers are used to enhance radiotracer excretion kinetics from noncancerous organs. [^{18}F]Galacto-RGD was the first PET radiotracer under clinical investigation for visualization of $\alpha_v\beta_3$ expression in cancer patients. [^{18}F]AH111585 was developed as a new PET radiotracer for tumor imaging.

and have similar roles in tumor angiogenesis, promoting angiogenic response to growth factors. The $\alpha_v\beta_5$ is overexpressed on many tumor types in both cell lines and clinical material.[162] A number of tumors coexpress $\alpha_v\beta_3$ and $\alpha_v\beta_5$,[163−169] because they both engage the same extracellular matrix ligands and activate cell signaling pathways to promote tumor progression.[168,169] It was reported that the expression of $\alpha_v\beta_3$, $\alpha_v\beta_5$, $\alpha_5\beta_1$, $\alpha_6\beta_4$, $\alpha_4\beta_1$, and $\alpha_v\beta_6$ on the tumor cells is well correlated with the tumor progression.[98,164,165] Structures of other RGD-binding integrins (e.g., $\alpha_v\beta_6$, $\alpha_v\beta_8$, $\alpha_v\beta_1$, and $\alpha_8\beta_1$) have not yet been studied in details. However, it is well-known that the $\alpha_4\beta_1$, $\alpha_9\beta_1$, $\alpha_4\beta_7$, $\alpha_E\beta_7$, $\alpha_L\beta_2$, $\alpha_M\beta_2$, $\alpha_X\beta_2$, and $\alpha_D\beta_2$ integrins all recognize the LDV, LDT, and IDS tripeptide sequences.[98] In contrast, the collagen and laminin-binding integrins ($\alpha_1\beta_1$, $\alpha_2\beta_1$, $\alpha_{10}\beta_1$, and $\alpha_{11}\beta_1$) recognize the GFOGER hexapeptide sequence.[169]

There has been a continuing debate on whether one should separate $\alpha_v\beta_3$ from $\alpha_v\beta_5$, $\alpha_5\beta_1$, $\alpha_6\beta_4$, $\alpha_4\beta_1$, and $\alpha_v\beta_6$. The answer to this question lies in the purpose of PET or SPECT imaging studies. If the purpose is to detect the presence of tumor or to distinguish between the benign and malignant tumors, there will be no need to separate them. The presence of multiple integrins results in a larger "receptor population". Actually, the capability of radiolabeled cyclic RGD peptides to target multiple integrins is expected to improve their tumor uptake because of the larger receptor population compared to $\alpha_v\beta_3$ alone. Studies on the compounds highly active against $\alpha_v\beta_3$ reveal that they also possess similar activity against $\alpha_v\beta_5$.[170] Dual antagonists have been deliberately prepared and were found to have very similar affinity for $\alpha_v\beta_3$ and $\alpha_v\beta_5$.[170,171] As long as the biomolecule contains one or more RGD tripeptide sequence, it will bind $\alpha_v\beta_3$, $\alpha_v\beta_5$, $\alpha_5\beta_1$, $\alpha_6\beta_4$, $\alpha_4\beta_1$, and $\alpha_v\beta_6$ regardless of peptide multiplicity. If the purpose of PET or SPECT study is to screen the appropriate patients for a specific therapy with $\alpha_v\beta_3$ antibodies or small-molecule $\alpha_v\beta_3$ antagonists, the separation of $\alpha_v\beta_3$ from $\alpha_v\beta_5$, $\alpha_5\beta_1$, $\alpha_6\beta_4$, $\alpha_4\beta_1$, and $\alpha_v\beta_6$ may become necessary because the $\alpha_v\beta_3$-specificity is more important in this situation. However, radiolabeled cyclic RGD peptides may still be useful for this purpose if the expression of $\alpha_v\beta_3$ is linearly correlated to the expression levels of $\alpha_v\beta_5$, $\alpha_5\beta_1$, $\alpha_6\beta_4$, $\alpha_4\beta_1$, and/or $\alpha_v\beta_6$.

MAXIMIZING BINDING AFFINITY VIA MULTIMERIZATION

Multimerization of Cyclic RGD Peptides. Multivalent interactions have been used in such a way that the weak interactions may become biologically relevant.[172−174] The multivalence concept has been used to develop $\alpha_v\beta_3$-targted radiotracers.[11−65] It is believed that multimeric RGD peptides could provide more potent antagonists with better tumor-targeting capability. RGD_2 (Figure 6) was the first cyclic RGD dimer for development of diagnostic (^{99m}Tc and ^{64}Cu) and

DOI: 10.1021/acs.bioconjchem.5b00327
Bioconjugate Chem. 2015, 26, 1413−1438

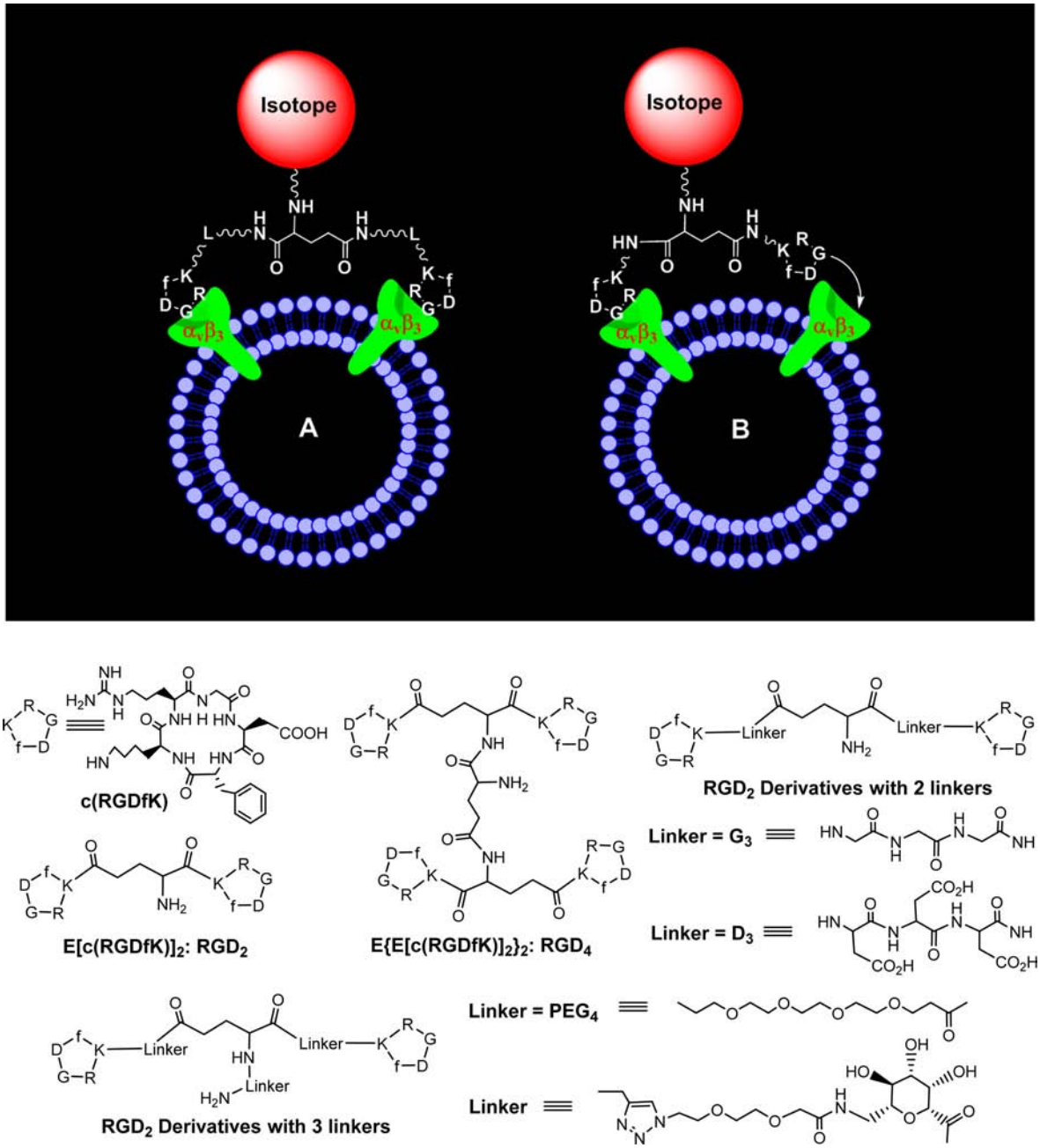

Figure 6. Top: Schematic illustration of the interactions between a dimeric cyclic RGD peptide and $\alpha_v\beta_3$. (A) The distance between two RGD motifs is long due to the presence of two linkers (L). As a result, the cyclic RGD dimer is able to bind $\alpha_v\beta_3$ in a "bivalent" fashion. (B) The distance between two RGD motifs is not long enough for simultaneous $\alpha_v\beta_3$ binding. However, the RGD concentration is "locally enriched" in the vicinity of neighboring $\alpha_v\beta_3$ sites once the first RGD motif is bound. In both cases, the end-result would be higher $\alpha_v\beta_3$ binding affinity for dimeric cyclic RGD peptides. Bottom: Examples of cyclic RGD dimers and tetramers for development of $\alpha_v\beta_3$-targeted radiotracers. The D_3, G_3, PEG_2, PEG_4, and sugar linkers are used to increase the distance between two cyclic RGD motifs and to improve radiotracer excretion kinetics from noncancerous organs.

therapeutic (^{90}Y and ^{177}Lu) radiotracers.[175−179] RGD_4 (Figure 6) was also used to develop SPECT and PET radiotracers.[19,21,30] The in vitro assays and biodistribution data clearly showed that the radiolabeled dimeric and tetrameric cyclic RGD peptides have higher $\alpha_v\beta_3$ binding affinity and better tumor uptake than their corresponding monomeric analogues.[19,21,30,34−50]

Bivalency and Locally Enhanced RGD Concentration. Figure 6 illustrates the interactions between a dimeric RGD peptide and $\alpha_v\beta_3$. Two important factors (Figure 6A: bivalency and enhanced RGD concentration) contribute to the high $\alpha_v\beta_3$ binding affinity of multimeric cyclic RGD peptides (Table 1).[52,55,61] The concentration factor exists in all multimeric cyclic RGD peptides regardless of the linker length between two RGD motifs. The key to achieving bivalency is the distance between two cyclic RGD motifs. Given the short distance (six bonds excluding the side-arms of K-residues) between two RGD motifs in RGD_2 it is unlikely that they bind to two adjacent $\alpha_v\beta_3$ sites simultaneously. However, the binding of one RGD motif to $\alpha_v\beta_3$ will increase the local concentration of a second RGD motif in the vicinity of neighboring $\alpha_v\beta_3$ sites (Figure 6A). The concentration factor may explain the higher

DOI: 10.1021/acs.bioconjchem.5b00327
Bioconjugate Chem. 2015, 26, 1413−1438

Table 1. IC_{50} Values of Selected Cyclic Peptides and Their Corresponding DOTA, FITC, HYNIC, and NOTA Conjugates

peptide/conjugate	IC_{50} (nM)[a]	radiotracer	ref
c(RGDyK)	458 ± 45		34, 35
HYNIC-G-RGD	358 ± 8	^{99m}Tc-G-RGD	34
HYNIC-P-RGD	452 ± 11	^{99m}Tc−P-RGD	35
HYNIC-RGD_2	112 ± 21	^{99m}Tc-RGD_2	35
HYNIC-P-RGD_2	84 ± 7	^{99m}Tc−P-RGD_2	35
HYNIC-2G-RGD_2	60 ± 4	^{99m}Tc-2G-RGD_2	34
HYNIC-2P-RGD_2	52 ± 7	^{99m}Tc-2P-RGD_2	35
HYNIC-P2D-RGD_2	61 ± 2	^{99m}Tc−P2D-RGD_2	49
HYNIC-P2G-RGD_2	62 ± 5	^{99m}Tc−P2G-RGD_2	49
HYNIC-3G-RGD_2	59 ± 3	^{99m}Tc-3G-RGD_2	34
HYNIC-3P-RGD_2	60 ± 3	^{99m}Tc-3P-RGD_2	35
HYNIC-Galacto-RGD_2	29 ± 5	^{99m}Tc-Galacto-RGD_2	48
HYNIC-RGD_4	7 ± 2	^{99m}Tc-RGD_4	35
DOTA-RGD_2	102 ± 5	^{64}Cu-RGD_2/^{111}In-RGD_2	33, 39, 41, 42
DOTA-3G-RGD_2	74 ± 3	^{64}Cu-3G-RGD_2/^{111}In-3G-RGD_2	37, 39, 41
DOTA-3P-RGD_2	62 ± 6	^{64}Cu-3P-RGD_2/^{111}In-3P-RGD_2	37, 39, 42
DOTA-3P-RGK_2	596 ± 48	^{111}In-Galacto-RGD_2	50
DOTA-Galacto-RGD_2	27 ± 2	^{111}In-Galacto-RGD_2	50
DOTA-RGD_4	10 ± 2	^{64}Cu-RGD_4/^{111}In-RGD_4	20
NOTA-RGD_2	100 ± 3	^{68}Ga(NOTA-RGD_2)	23
NOTA-2G_3-RGD_2	66 ± 4	^{68}Ga(NOTA-2G-RGD_2)	23
NOTA-2P-RGD_2	54 ± 2	^{68}Ga(NOTA-2P-RGD_2)	23
FITC-RGD_2	89 ± 17		183
FITC-3P-RGD_2	32 ± 7		183
FITC-Galacto-RGD_2	28 ± 8		183
FITC-3P-RGK_2	589 ± 73		183

[a] IC_{50} values depend largely on the radioligand and tumor cell lines. To maintain consistency and reproducibility, U87MG glioma cells (high $\alpha_v\beta_3$ and $\alpha_v\beta_5$ expression) have been used as the "host cells" and ^{125}I-echistatin as the radioligand. Since the whole-cell displacement assay is operator-dependent, caution should be taken when comparing their IC_{50} values reported in the literature.

tumor uptake of radiolabeled RGD_2 than that of its monomeric derivatives (Table 1).[175−179] The distance between two cyclic RGD motifs is 38 bonds in 3P-RGD_2, and 26 bonds 3G-RGD_2, which are definitely long enough for 3P-RGD_2 and 3G-RGD_2 to achieve bivalency. As a result, HYNIC-3P-RGD_2 (IC_{50} = 60 ± 3 nM) and HYNIC-3G-RGD_2 (IC_{50} = 59 ± 3 nM) have higher $\alpha_v\beta_3$ binding affinity than HYNIC-P-RGD_2 (IC_{50} = 89 ± 7 nM).[34,35] ^{99m}Tc-3P-RGD_2 and ^{99m}Tc-3G-RGD_2 had higher tumor uptake than ^{99m}Tc-P-RGD_2 (Figure 7). The concentration factor is more likely responsible for the higher $\alpha_v\beta_3$ binding affinity of HYNIC-RGD_4 (IC_{50} = 7 ± 2 nM) than that of HYNIC-3P-RGD_2 and HYNIC-3G-RGD_2. The fact that the tumor uptake of ^{99m}Tc-3G-RGD_2 and ^{99m}Tc-3P-RGD_2 is comparable to that of ^{99m}Tc-RGD_4 (Figure 7) within experimental error suggests that multimeric cyclic RGD peptides are not necessarily multivalent in binding to integrins, and the contribution from the concentration factor is not as much as that from the bivalency factor.[39,41] In addition, the capability of a multimeric cyclic RGD peptide to achieve bivalency also depends on the $\alpha_v\beta_3$ density in tumor tissues. If the tumor $\alpha_v\beta_3$ density is high, the distance between two neighboring $\alpha_v\beta_3$ sites will be short. As a result, it is easier for the multimeric cyclic RGD peptide to achieve bivalency. If the tumor $\alpha_v\beta_3$ density is low, the distance between two neighboring $\alpha_v\beta_3$ sites will be long. In this case, it will be much more difficult for the same multimeric cyclic RGD peptide to achieve simultaneous $\alpha_v\beta_3$ binding.

Multimerization on Radiotracer Tumor Retention Time. We examined the impact of multiplicity on the retention time of ^{111}In-labeled cyclic RGD peptide DOTA conjugates (Figure 8) in the U87MG tumors.[39,41,42] It was found that the glioma uptake (% ID/g at <24 h p.i.) follow the general ranking order of ^{111}In-6G-RGD_4 ~ ^{111}In-6P-RGD_4 ~ ^{111}In-3P-RGD_2 ≫ ^{111}In-P-RGD_2 > ^{111}In-P-RGD (Figure 9). Multimerization significantly enhances the radiotracer tumor uptake. The tumor retention times follow the ranking order of ^{111}In-6G-RGD_4 ($T_{1/2}$ > 72 h) > ^{111}In-6P-RGD_4 ($T_{1/2}$ ~ 35 h) > ^{111}In-3P-RGD_2 > ($T_{1/2}$ ~ 30 h) > ^{111}In-P-RGD_2 ($T_{1/2}$ ~ 24 h) > ^{111}In-P-RGD ($T_{1/2}$ ~ 10 h).[41] As a result of the increased peptide multiplicity, the tumor retention time of ^{111}In-labeled cyclic RGD peptides increases and their dissociation rate from the tumor tissue decreases. The biodistribution data were consistent with the results from the whole-body planar imaging studies.[39,41] The bivalency factor most likely contributes to the higher tumor uptake and longer tumor retention time of ^{111}In-3P-RGD_2 than that of ^{111}In-P-RGD_2. ^{111}In-3P-RGD_2 and ^{111}In-

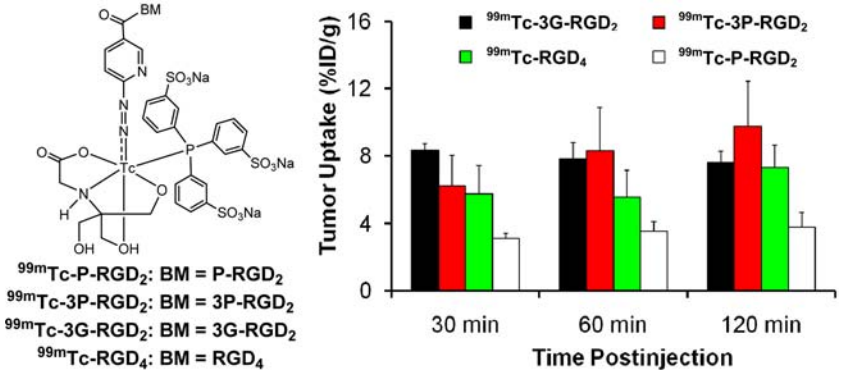

Figure 7. Direct comparison of tumor uptake for ^{99m}Tc-P-RGD_2, ^{99m}Tc-3G-RGD_2, ^{99m}Tc-3P-RGD_2, and ^{99m}Tc-RGD_4 in athymic nude mice bearing the MDA-MB-435 human breast cancer xenografts. The biodistribution data were from refs 30, 34, and 35.

DOI: 10.1021/acs.bioconjchem.5b00327
Bioconjugate Chem. 2015, 26, 1413−1438

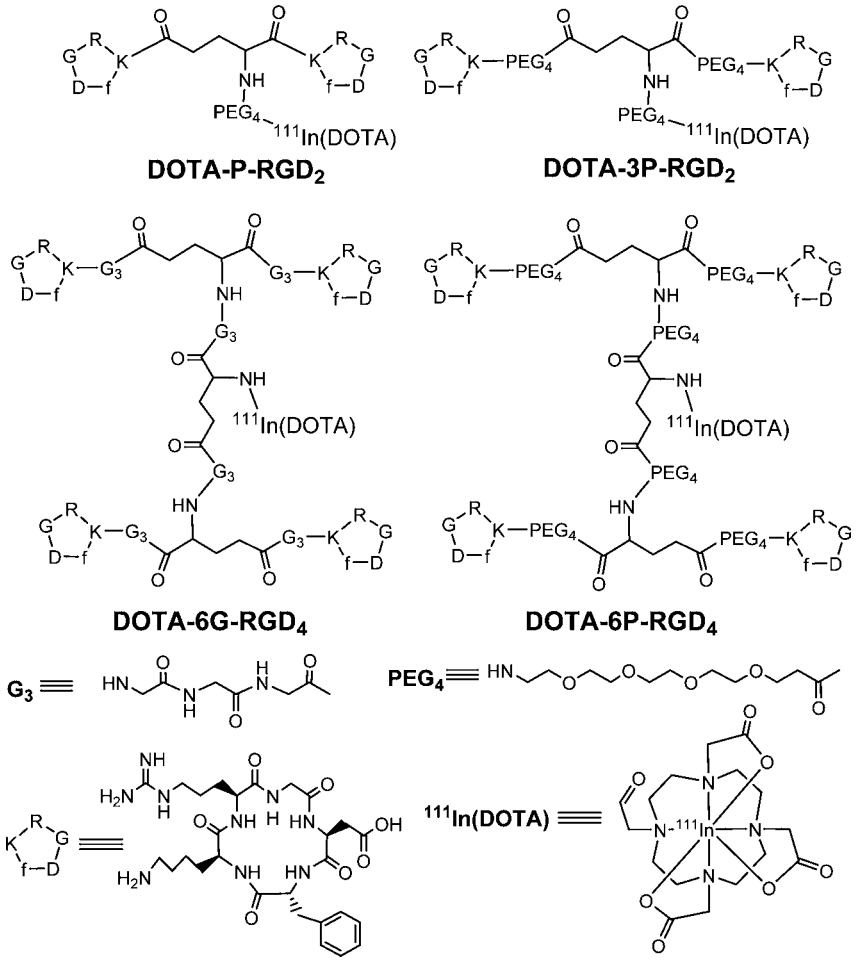

Figure 8. Chemdraw structures of ^{111}In-labeled cyclic RGD peptide DOTA-conjugates.

6P-RGD$_4$ share very similar (not identical) glioma tumor uptake values at <24 h p.i. Even though ^{111}In-6P-RGD$_6$ has a longer tumor retention time (as indicated by its higher tumor uptake at 72 h p.i.) than ^{111}In-3P-RGD$_2$, the tumor/liver ratios of ^{111}In-3P-RGD$_2$ are better than those of ^{111}In-6P-RGD$_4$.[39,41] There is always a subtle balance between peptide multiplicity and tumor/background ratios. The combination of high tumor uptake and high tumor/liver ratios makes ^{111}In-3P-RGD$_2$ better suited for imaging than ^{111}In-P-RGD, ^{111}In-P-RGD$_2$, and ^{111}In-6P-RGD$_4$.

Impact of Linker Groups. As illustrated in Figure 6, the linker groups are used for two purposes: increasing the distance between two RGD motifs so that they are able to the $\alpha_v\beta_3$ in a bivalent fashion, and improving the radiotracer excretion kinetics. Different linkers (Figure 6) have been proposed to increase the distance between two RGD motifs and improve pharmacokinetics of radiotracers.[38−42,47−50] The results from in vitro and in vivo assays showed that the linkers (G_3 vs D_3 and PEG_4 or PEG_4 vs SAA, 1,2,3-triazole, and PEG_2 moieties) have little impact on the $\alpha_v\beta_3$ binding affinity of HYNIC-conjugated dimeric cyclic RGD peptides (Table 1) as long as they are long enough for bivalency. However, the overall molecular charges may have significant impact on the radiotracer uptake in both tumors and normal organs. For example, HYNIC-3G-RGD$_2$ and HYNIC-3P-RGD$_2$ share almost identical $\alpha_v\beta_3$ binding affinities (Table 1). Since the G_3 and PEG_4 linkers are neutral, their corresponding radiotracers ^{99m}Tc-3G-RGD$_2$ and ^{99m}Tc-3P-RGD$_2$ have very similar glioma tumor uptake (Figure 7) and excretion kinetics from normal organs.[34,35] Similar comparison can be made between ^{99m}Tc-3P-RGD$_2$ and ^{99m}Tc-Galactor-RGD$_2$.[48] In contrast, the D_3 linker is triply charged under physiological conditions. Even though HYNIC-P2D-RGD$_2$ and HYNIC-P2G-RGD$_2$ share almost identical $\alpha_v\beta_3$ binding affinity,[49] the tumor uptake of ^{99m}Tc-P2D-RGD$_2$ (2.20 ± 0.42, 2.85 ± 0.55, 3.11 ± 0.47, and 2.45 ± 0.90%ID/g at 5, 30, 60, and 120 min p.i., respectively) was significantly lower (p < 0.01) than that of ^{99m}Tc-P2G-RGD$_2$ (9.27 ± 0.72, 8.85 ± 0.67, 8.17 ± 1.10, and 7.82 ± 0.76%ID/g at 5, 30, 60, and 120 min p.i., respectively) over the 2 h study period.[49] In contrast, ^{99m}Tc-P2G-RGD$_2$ and ^{99m}Tc-3P-RGD$_2$ shared similar tumor uptake values (7.82−9.27%ID/g for ^{99m}Tc-P2G-RGD$_2$; and 7.24−8.72%ID/g for ^{99m}Tc-3P-RGD$_2$).[49] However, ^{99m}Tc-P2D-RGD$_2$ had intestinal uptake values of 5.86 ± 1.37, 6.58 ± 0.88, 7.08 ± 0.92, and 4.74 ± 0.33%ID/g at 5, 30, 60, and 120 min p.i., respectively, which were much lower than those of ^{99m}Tc-P2G-RGD$_2$ (11.72 ± 2.01, 9.27 ± 1.15, 6.17 ± 1.55, and 4.74 ± 1.09%ID/g at 5, 30, 60, and 120 min p.i., respectively) over the 2 h study period. Therefore, the linker groups between the two cyclic RGD moieties have a significant impact on the blood clearance, tumor uptake, and biodistribution properties of ^{99m}Tc-labeled dimeric cyclic RGD peptides.

Impact of ^{99m}Tc Chelates. Figure 10 compares the 60 min biodistribution data of ^{99m}Tc-3P-RGD$_2$, ^{99m}Tc-3P-RGD$_2$-A, and ^{99m}Tc-3P-RGD$_2$-B in the U87MG glioma model.[46,47] It was found that replacing the highly charged and bulky [^{99m}Tc-

DOI: 10.1021/acs.bioconjchem.5b00327
Bioconjugate Chem. 2015, 26, 1413−1438

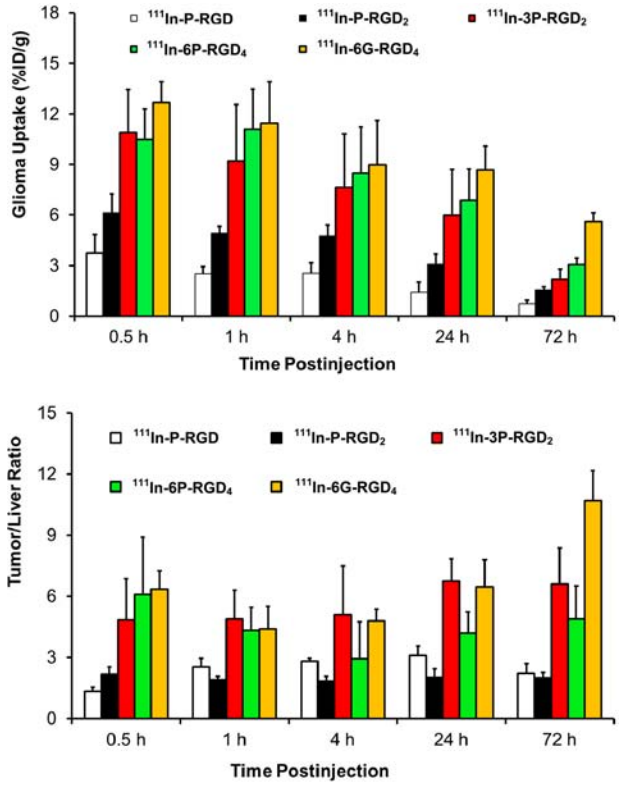

Figure 9. Comparison of the glioma uptake (Top) and tumor/liver ratios (Bottom) of ^{111}In-labeled cyclic RGD peptides in athymic nude mice bearing U87MG glioma xenografts at 0.5, 1, 4, 24, and 72 h after administration of ^{111}In radiotracer. The biodistribution data were from refs 41 and 42.

(HYNIC) (tricine) (TPPTS)] (MW ~ 970 Da) with a smaller [^{99m}Tc(HYNIC-K(NIC)) (tricine)] (MW ~ 650 Da) or [^{99m}Tc(K(HYNIC)$_2$) (tricine)] (MW ~ 670 Da) had little impact on the tumor uptake,[46,47] suggesting that changing the ^{99m}Tc chelates had no adverse effect on their tumor-targeting capability. However, the change in ^{99m}Tc chelates resulted in significant uptake differences in normal organs, (e.g., intestines, kidneys, lungs, and spleen).[46,47] Since [^{99m}Tc(HYNIC-K(NIC)) (tricine)] is structurally similar to [^{99m}Tc(K(HYNIC)$_2$) (tricine)] (Figure 10), it was not surprising that ^{99m}Tc-3P-RGD$_2$-A and ^{99m}Tc-3P-RGD$_2$-B shared almost identical biodistribution properties.[47] A major advantage of using K(HYNIC)$_2$ and HYNIC-K(NIC) as BFCs is the use of $SnCl_2$ as a reducing agent during ^{99m}Tc-labeling because TPPTS can easily reduce the S−S disulfide bond, which is often important for small biomolecules to maintain their biological activity and tumor-targeting capability. The disadvantage of K(HYNIC)$_2$ and HYNIC-K(NIC) is that there are more than two isomers in [^{99m}Tc(HYNIC-K(NIC)) (tricine)] and [^{99m}Tc(K(HYNIC)$_2$) (tricine)].[46,47]

Impact of Radiometal Chelates. ^{111}In-3P-RGD$_2$ and ^{64}Cu-3P-RGD$_2$ share the same DOTA-3P-RGD$_2$ conjugate. In spite of the difference in their structures and overall molecular charge, the tumor uptake of ^{111}In-3P-RGD$_2$ (10.89 ± 2.55 and 7.65 ± 3.17%ID/g at 30 and 240 min p.i., respectively) was very close to that of ^{64}Cu-3P-RGD$_2$ (8.23 ± 1.97 and 6.43 ± 1.22%ID/g at 30 and 240 min p.i., respectively).[37,39−42] They also shared very similar uptake in normal organs. For example, the kidney uptake of ^{111}In-3P-RGD$_2$ was 5.80 ± 0.95 at 30 min p.i. and 2.78 ± 0.20%ID/g at 240 min p.i., and was comparable to that of ^{64}Cu-3P-RGD$_2$ (6.59 ± 0.93%ID/g at 30 min p.i. and 2.81 ± 0.36% ID/g at 240 min p.i.). The liver uptake of ^{111}In-3P-RGD$_2$ is 2.52 ± 0.57%ID/g at 30 min and 1.61 ± 0.06%ID/

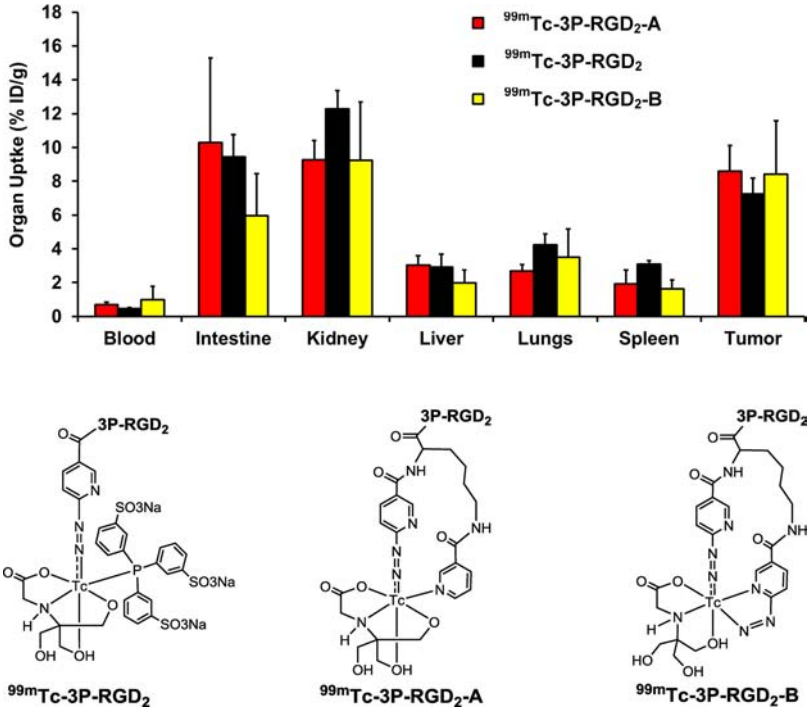

Figure 10. Direct comparison of the 60 min biodistribution data for ^{99m}Tc-3P-RGD$_2$, ^{99m}Tc-3P-RGD$_2$-A, and ^{99m}Tc-3P-RGD$_2$-B in the athymic nude mice bearing U87MG human glioma xenografts to show the impact of ^{99m}Tc chelates on biodistribution properties of ^{99m}Tc radiotracers. The biodistribution data were from refs 46 and 47.

DOI: 10.1021/acs.bioconjchem.5b00327
Bioconjugate Chem. 2015, 26, 1413−1438

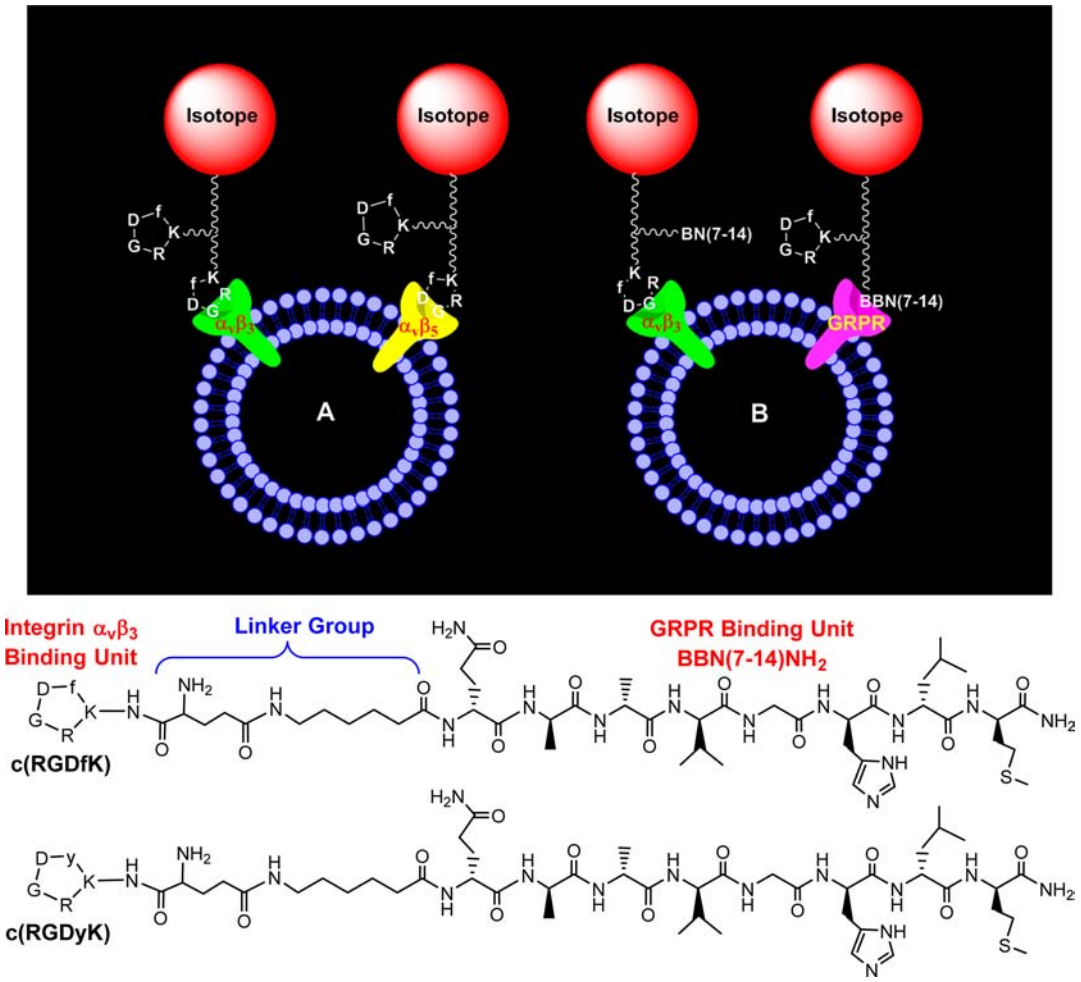

Figure 11. (A) Schematic presentation of a dimeric cyclic RGD peptide targeting two or more integrins (e.g., $\alpha_v\beta_3$, $\alpha_v\beta_5$, $\alpha_5\beta_1$, $\alpha_6\beta_4$, $\alpha_4\beta_1$, and $\alpha_v\beta_6$). (B) Schematic illustration of a bifunctional peptide targeting two different receptors (e.g., $\alpha_v\beta_3$ and GRPR). By targeting two different receptors, the radiotracer will have more opportunities to localize in tumor due to the increased receptor population. The two targeted receptors (e.g., $\alpha_v\beta_3/\alpha_v\beta_5$ or $\alpha_v\beta_3$/GRPR) must be colocalized and the distance between them must be short for the bifunctional radiotracer to achieve simultaneous receptor binding. Bottom: Examples of bifunctional peptides containing c(RGDfK)/c(RGDyK) and Aca-BBN(7−14)NH_2 (ε-aminocaproic acid-Gln-Trp-Ala-Val-Gly-His-Leu-Met-NH_2).

g at 240 min p.i., while ^{64}Cu-3P-RGD_2 has liver uptake of 2.80 ± 0.35%ID/g at 30 min p.i. and 1.87 ± 0.51%ID/g at 240 min p.i.[37,39−42] Changing from ^{111}In(DOTA) to ^{64}Cu(DOTA) has minimal impact on the tumor uptake and excretion kinetics of the corresponding radiotracers. A similar conclusion can be made by comparing biodistribution properties of ^{64}Cu-3P-RGD_2 and ^{111}In-3G-RGD_2.[37,41,42]

MAXIMIZING RADIOTRACER UPTAKE BY TARGETING MULTIPLE RECEPTORS

Both receptor binding affinity and receptor population are important for the tumor selectivity and tumor uptake of radiolabeled cyclic RGD peptides. There are two general approaches to maximize the "receptor population". The first approach (Figure 11A) involves use of the same cyclic RGD peptide (monomeric and multimeric) to target two or more integrins (particularly $\alpha_v\beta_3$ and $\alpha_v\beta_5$) overexpressed on both tumor cells and activated endothelial cells of tumor neovasculature. Radiolabeled multimeric cyclic RGD peptides have advantages over those targeting only $\alpha_v\beta_3$ or $\alpha_v\beta_5$ because of their capability to target multiple integrins (e.g., $\alpha_v\beta_3$, $\alpha_v\beta_5$, $\alpha_5\beta_1$, $\alpha_6\beta_4$, $\alpha_4\beta_1$, and $\alpha_v\beta_6$). Another approach involves the use of a bifunctional peptide (Figure 11B) that is able to target two different receptors, such as $\alpha_v\beta_3$ and gastrin-releasing peptide receptor (GRPR). By targeting two different receptors, the "bifunctional" radiotracers will have more opportunities to localize in the tumor tissue (including the tumor cells and tumor neovasculature) and are expected to have a slower dissociation rate from the tumor.

Bivalent heterodimers containing BBN(7−14) and c(RGDfK) or c(RGDyK) (Figure 11) have been used to target the $\alpha_v\beta_3$ and GRPR simultaneously.[180−182] The xenografted PC-3 and MDA-MB-435 tumor-bearing animal models were used to evaluate their tumor-targeting capability. However, there is lack of concrete in vivo evidence to prove if c(RGDfK)-BBN(7−14) and c(RGDyK)-BBN(7−14) are indeed "bivalent", and whether there is a "synergetic effect" between the cyclic RGD and BBN(7−14) peptides. It is also unknown which receptor binding unit actually contributes to the tumor uptake of "bifunctional radiotracers". Since the PC-3 tumors have low $\alpha_v\beta_3$ expression and the MDA-MB-435 tumors have little or no expression of GRPR,[40,47,181,182] the xenografted PC-3 and MDA-MB-435 tumor-bearing models are not appropriate to prove the concept of "bivalent heterodimers" because the

DOI: 10.1021/acs.bioconjchem.5b00327
Bioconjugate Chem. 2015, 26, 1413−1438

Chart 2. Schematic Illustration of Blocking Experiments

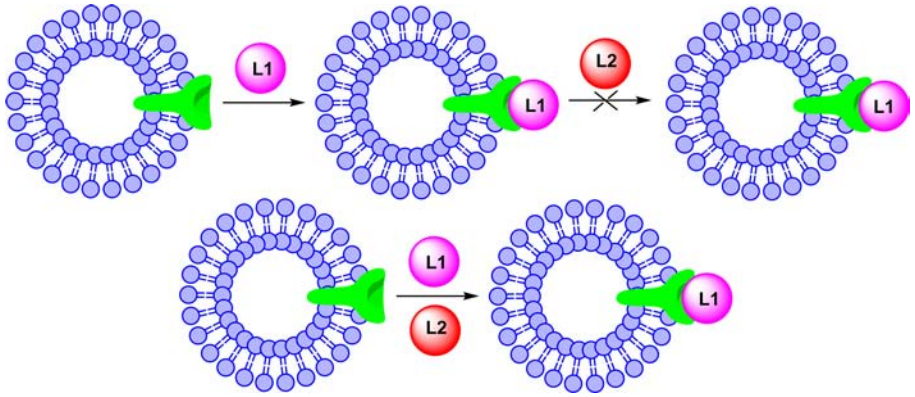

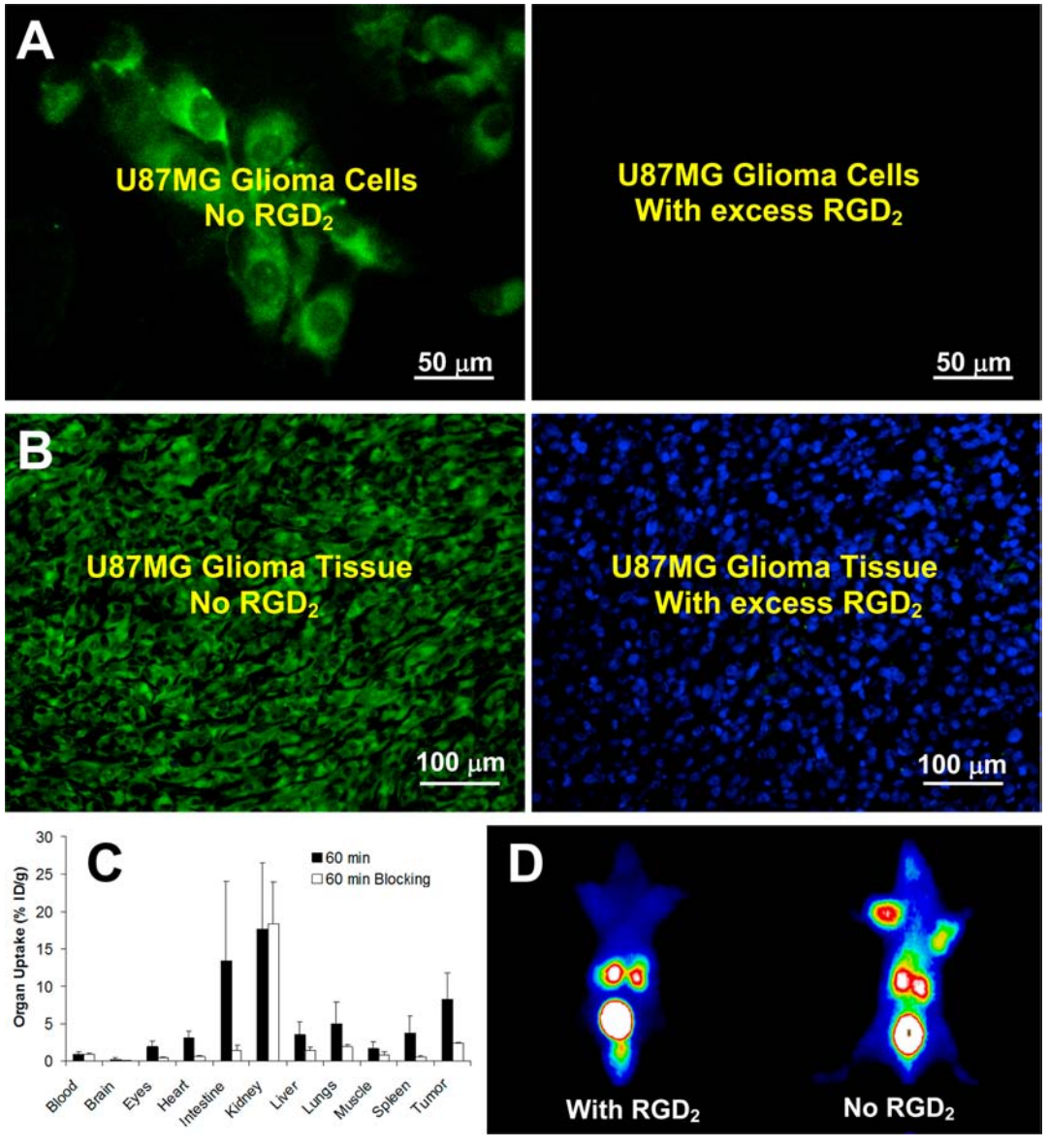

Figure 12. (A) Selected microscopic images (magnification 400×) of living U87MG glioma cells stained with FITC-Galacto-RGD_2 in the absence (left) and presence (right) of excess RGD_2. (B) Microscopic images (Magnification 200×) of a tumor slice stained with FITC-Galacto-RGD_2 in the absence (left) and presence (right) of excess RGD_2. The cellular and tumor staining data were from ref 183. (C) Comparison of organ uptake (%ID/g) for ^{99m}Tc-2P-RGD_2 in the absence or presence of excess RGD_2 at 60 min p.i. (D) 60 min planar images of the tumor-bearing mice administered with ^{99m}Tc-3P-RGD_2 in the absence/presence of RGD_2. Co-injection of excess RGD_2 resulted in significant reduction in the uptake of ^{99m}Tc-3P-RGD_2 in both tumor and normal organs. The biodistribution and imaging data were obtained from ref 35.

DOI: 10.1021/acs.bioconjchem.5b00327
Bioconjugate Chem. 2015, 26, 1413−1438

$\alpha_v\beta_3$ and GRPR receptors must be colocalized and the distance between them must be short in order for the bifunctional radiotracer to achieve bivalency. Otherwise, it is very difficult to observe the "synergetic effect" even if they are able to target individual receptors.

IMPORTANT BIOLOGICAL ASSAYS

Integrin Binding Assays. The integrin binding affinity of a cyclic RGD peptide can be determined using the immobilized $\alpha_v\beta_3$ assay or the whole-cell competitive displacement assay with ^{125}I-echistatin or ^{125}I-c(RGDyK) as the radioligand. The immobilized $\alpha_v\beta_3$ assay can provide the $\alpha_v\beta_3$ binding affinity of a cyclic RGD peptide with high specificity and selectivity. However, the IC_{50} (the concentration to achieve 50% displacement of the radioligand or fluorescent probe) values from the immobilized $\alpha_v\beta_3$ assays do not reflect the contributions from its binding to other integrins (namely, $\alpha_v\beta_5$, $\alpha_5\beta_1$, $\alpha_6\beta_4$, $\alpha_4\beta_1$, and $\alpha_v\beta_6$), and are not reliable to predict the tumor uptake of radiolabeled cyclic RGD peptides since the $\alpha_v\beta_3$ density would never be as high as that used in the immobilized $\alpha_v\beta_3$ assay. In contrast, the whole-cell displacement assay will provide a measure of the capability of a specific cyclic RGD peptide in binding to all integrins ($\alpha_v\beta_3$, $\alpha_v\beta_5$, $\alpha_5\beta_1$, $\alpha_6\beta_4$, $\alpha_4\beta_1$, and $\alpha_v\beta_6$) on tumor cells. However, the IC_{50} values depends largely on the radioligand (^{125}I-c(RGDyK) vs ^{125}I-echistatin) and tumor cell lines (U87MG vs MDA-MB-435) used in this assay. The IC_{50} values using ^{125}I-echistatin as the radioligand are much higher than those with ^{125}I-c(RGDyK) because of the higher integrin binding affinity of ^{125}I-echistatin. To keep the consistency and reproducibility, we have been using U87MG glioma cells (high $\alpha_v\beta_3$ and $\alpha_v\beta_5$ expression) as the "host cells" and ^{125}I-echistatin as the radioligand.[34−50] Since the whole-cell displacement assay is operator-dependent, caution should be taken when comparing their IC_{50} values with those reported in the literature. Whenever possible, a "control compound", such as c(RGDfK) or c(RGDyK), should be used in each experiment.

Blocking Experiments to Demonstrate Integrin Specificity. Blocking experiment (Chart 2) is commonly used to demonstrate the $\alpha_v\beta_3$ specificity of radiolabeled cyclic RGD peptides with a known $\alpha_v\beta_3$ antagonist (e.g., c(RGDfK) or RGD_2) as the blocking agent. The blocking experiment is often performed using the in vitro tissue (Figure 12A) and cellular (Figure 12B) IHC staining assays, or by ex-vivo biodistribution (Figure 12C) and/or in vivo imaging (Figure 12D). The blocking agent can be administered before injection of the radiotracer or coadministered with the radiotracer. Co-injection of excess blocking agent (e.g., c(RGDfK) or RGD_2) will result in partial or complete blockage of the radiotracer tumor uptake (Figure 12C). There is also a significant reduction in radiotracer uptake in the $\alpha_v\beta_3$-positive organs (e.g., eyes, intestine, kidneys, lungs, liver, muscle and spleen).[41]

Nonsense Peptide to Demonstrate RGD Specificity. There are several ways to determine the RGD-specificity of cyclic RGD peptides. These include (1) in vitro $\alpha_v\beta_3$ binding assay, (2) tissue or cellular IHC staining assay, (3) PET or SPECT imaging, and (4) ex vivo biodistribution. In all cases, a "nonsense peptide" with the "scrambled sequence" will be used for comparison purposes. For example, 3P-RGK_2 is a nonsense peptide with the chemical composition identical to that of 3P-RGD_2. The $\alpha_v\beta_3$ binding affinity of DOTA-3P-RGK_2 (IC_{50} = 596 ± 48 nM) was >20× lower than that of DOTA-3P-RGD_2 (IC_{50} = 29 ± 4 nM). Similar results were also observed with FITC-3P-RGK_2 (IC_{50} = 589 ± 73 nM) and FITC-3P-RGD_2 (IC_{50} = 32 ± 7 nM). Due to the low $\alpha_v\beta_3$ affinity of DOTA-3P-RGK_2,[41,42] ^{111}In-3P-RGK_2 had much lower uptake than ^{111}In-3P-RGD_2 in tumors and the $\alpha_v\beta_3$-positive organs, such as intestine, liver, lungs, and spleen (Figure 13A).[41,42] The

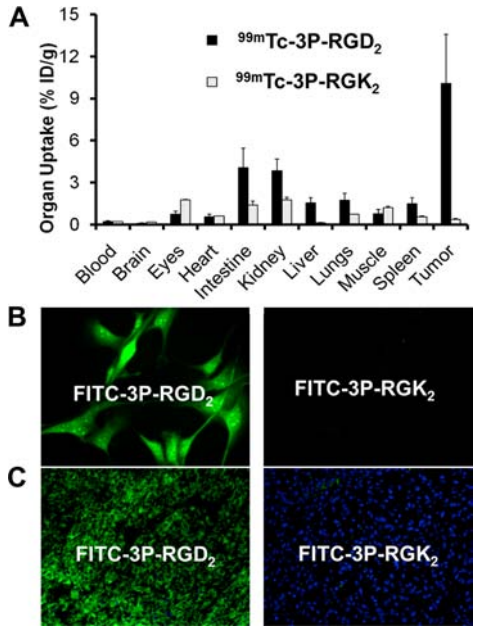

Figure 13. (A) Comparison of the 60 min biodistribution data of ^{99m}Tc-3P-RGD_2 and ^{99m}Tc-3P-RGK_2 in athymic nude mice bearing U87MG glioma xenografts. The low tumor uptake of ^{99m}Tc-3P-RGK_2 indicates that the $\alpha_v\beta_3$-binding of radiolabeled dimeric cyclic peptides are RGD-specific. (B) Selected microscopic images (magnification 400×) of the acetone-fixed U87MG glioma cells stained with FITC-3P-RGD_2 and FITC-3P-RGK_2. (C) Microscopic images (magnification 200×) of the xenografted U87MG glioma tissue stained with FITC-3P-RGD_2 and FITC-3P-RGK_2. Blue color indicates the presence of nuclei stained with DAPI. The cellular and tissue staining data were from ref 183.

U87MG glioma cells (Figure 13B) and tumor tissue (Figure 13C) could be stained with FITC-3P-RGD_2, but not with FITC-3P-RGK_2 under the same conditions.[183] These results clearly show that the radiotracer uptake in tumors indeed is RGD-specific. It must be noted that using the "scrambled" peptides (e.g., 3P-RGK_2) can significantly reduce the $\alpha_v\beta_3$ binding affinity, but this may not totally eliminate their capability for $\alpha_v\beta_3$ binding because the $\alpha_v\beta_3$ binding involves all three amino acid residues (Figure 4) in order to achieve maximal binding capability. Even if the $\alpha_v\beta_3$ binding capability can be totally eliminated, the scrambled peptides can still bind to other integrins ($\alpha_v\beta_5$, $\alpha_5\beta_1$, $\alpha_6\beta_4$, $\alpha_4\beta_1$, and $\alpha_v\beta_6$) with low affinity.

Pharmacokinetics and Metabolism. Pharmacokinetics describes how the body affects a specific drug after administration through the mechanisms of absorption and distribution, as well as the chemical changes of drug substance in the body. There are two important biological interactions (Chart 3: receptor binding and protein binding) once the radiotracer is injected into blood circulation. Receptor binding is necessary for the radiotracer to localize in tumor selectively. Higher binding affinity will lead to greater radiotracer tumor uptake.[49] Protein bonding is generally detrimental because it will reduce the number of radiotracer molecules available for

DOI: 10.1021/acs.bioconjchem.5b00327
Bioconjugate Chem. 2015, 26, 1413−1438

Chart 3. Schematic Illustration of Biological Interactions, Elimination Routes, and Metabolism of Target-Specific Radiotracers

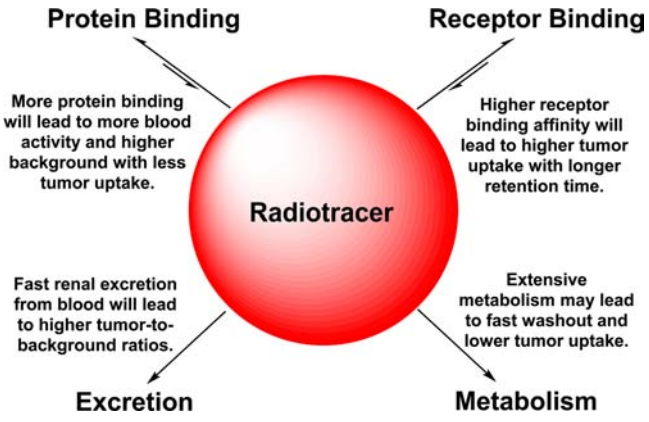

receptor binding, and result in more blood radioactivity (Chart 3).[49] Therefore, the protein bonding should be minimized. In addition, hydrophilic radiotracers tend to fast renal excretion, which will lead to lower background radioactivity in the blood pool and normal organs (such as liver, lungs, and muscle) with better T/B ratios. In contrast, lipophilic radiotracers tend to excreted through the hepatobiliary route with a higher degree of metabolism. High metabolic instability may result in lower tumor uptake, and higher background activity if the metabolite has longer body retention, which will definitely lead to poorer target-to-background ratios.

The tumor uptake and distribution properties of are normally determined by biodistribution at different time points after administration of the radiotracer. Even though PET has the capacity to quantify absolute radioactivity, the CT component must be included and coregistered during image acquisition and data processing. Otherwise, it would be very difficult to determine the volume and radioactivity concentration in each organ. Both PET and SPECT have the capability to determine the tumor uptake and washout kinetics via dynamic planar imaging. The tumor uptake is often expressed as the percentage of initial uptake. The blood clearance kinetics of a radiotracer can be measured by collecting blood samples at specific time points over a specific period of time.[49] The blood radioactivity usually expressed as the percentage of its initial radioactivity will be plotted against time. The most important parameter for kinetic studies is the rate of changes in the radiotracer organ uptake. The metabolic stability is determined by analyzing both urine and feces samples at a specified time point. In certain situations, tissue samples are harvested to determine the in vivo stability of radiotracers in the tumor, kidneys, liver, and lungs. It is important to note that the radiotracer uptake in a specific organ represents only a small portion of the total radioactivity injected into each animal. A major portion of the injected radiotracer and its metabolites has been excreted via both renal and hepatobiliary routes. Thus, the assays of radioactivity in urine and feces samples are more reliable for determination of the metabolic stability of the radiotracer.

MONITORING TUMOR RESPONSE TO ANTIANGIOGENIC THERAPY

Clinical Need for Biomarkers to Monitor Antiangiogenic Therapy. Inhibiting angiogenesis is a promising strategy for cancer therapy. As antiangiogenic therapies have become a common practice in clinics, finding suitable biomarkers for modulation of the tumor vasculature has become important. An ideal biomarker for monitoring antiangiogenic therapy should have the capacity to track biological changes in the tumor vasculature during and after antiangiogenic treatment. Microvessel density has been proposed as the prognostic indicator of the progression, overall survival, and disease-free survival in cancer patients. Evaluation of microvessel density is often performed by immunostaining endothelial cells in the tumor tissues and counting the number of vessels. However, this approach is not practical for routine monitoring of antiangiogenic therapy mainly due to invasive nature of the biopsy procedure. DCE-MRI were used to measure the tumor perfusion properties;[184−187] but it is technically challenging and standardization is very complicated. The MRI techniques have little or no capability to monitor biological changes in the tumor vasculature during and after antiangiogenic treatment. ^{18}F-FDG PET has been used to monitor the antiangiogenic linifanib therapy by determining the reduced metabolic activity in the treated tumors.[188] However, glucose metabolism may not be an ideal biomarker for monitoring antiangiogenic therapy because most of the metabolic activities take place in tumor cells rather than tumor vasculature.

Linear Relationship between Tumor Uptake and $\alpha_v\beta_3$ Expression. It is well-established that the total $\alpha_v\beta_3$ expression on both tumor cells and activated endothelial cells of the tumor neovasculature contributes to the tumor uptake of a $\alpha_v\beta_3$-targeted radiotracer regardless of peptide multiplicity.[44,115] If the $\alpha_v\beta_3$-targeted radiotracer is used for accurate measurement of $\alpha_v\beta_3$ expression, there must be a linear relationship between its tumor uptake and $\alpha_v\beta_3$ expression levels. However, there were a few reports to describe this relationship in the literature.[20,155−158] ^{99m}Tc-3P-RGD$_2$ was studied for its capability to monitor the $\alpha_v\beta_3$ expression levels.[44] IHC was performed to determine the β_3 levels in the xenografted U87MG, MDA-MB-435, A549, HT29, and PC-3 tumors.[44] An excellent relationship (Figure 14A) was observed between the tumor uptake of ^{99m}Tc-3P-RGD$_2$ and the $\alpha_v\beta_3$ expression levels.[44] There is also an excellent relationship between its tumor uptake and CD31 expression levels (Figure 14B). These linear relationships suggest that ^{99m}Tc-3P-RGD$_2$ is useful for monitoring the $\alpha_v\beta_3$ and CD31 expression in cancer patients, to select most appropriate cancer patients who will benefit most from antiangiogenic therapy, and to monitor the tumor response to the antiangiogenic treatment.

Monitoring Antiangiogenic Therapy with $\alpha_v\beta_3$-Targeted Radiotracers. The cross-talk between integrins and receptor tyrosine kinases (e.g., VEGFR and PDGFR) is crucial for many cellular functions.[189−194] The $\alpha_v\beta_3$ and PDGFR-β colocalize and PDGFR activation increases the endothelial cell migration and proliferation. The functional association between $\alpha_v\beta_3$ and VEGFR2/PDGFR is of reciprocal nature since each is able to promote the activation of its counterpart. This mutually beneficial relationship provides the conceptual basis to use radiolabeled cyclic RGD peptides for monitoring antiangiogenic therapy.[195−198] It was reported that the tumor uptake of [^{18}F]AH111585 was significantly reduced 2 days after sunitinib treatment, and [^{18}F]AH111585 was better than ^{18}F-FDG for monitoring angiogenesis therapy.[196] ^{64}Cu-DOTA-RGD was used to monitor dasatinib therapy.[198] It was found that dasatinib treatment significantly reduced the ^{64}Cu-DOTA-RGD uptake in treated tumors. A significant challenge for ^{18}F PET radiotracers, such as [^{18}F]-Galacto-RGD and [^{18}F]AH111585,

DOI: 10.1021/acs.bioconjchem.5b00327
Bioconjugate Chem. 2015, 26, 1413−1438

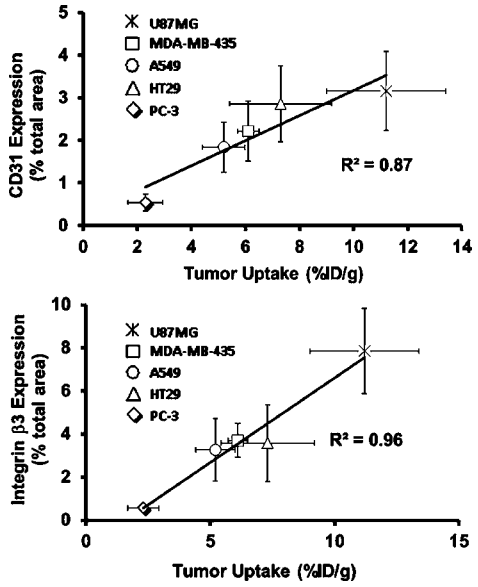

Figure 14. Relationship between the tumor uptake (%ID/g: radioactivity density) and relative β_3 (top) CD31 (bottom) expression levels (fluorescence density) in five different xenografted tumors (U87MG, MDA-MB-435, A549, HT29, and PC-3). The total β_3 expression was represented by the percentage of red area over total area in each slice of tumor tissue. Each data point was derived from at least 15 different areas of same tissue (100× magnification). The experimental data were from ref 40.

to assume widespread clinical utility is their poor availability at high cost.

^{99m}Tc-3P-RGD$_2$ was used to monitor the tumor response to linifanib treatment.[199,200] Linifanib is a multitargeted receptor tyrosine kinase inhibitor targeting VEGF and PDGF receptors.[201−206] It was found that there was a significant decrease in tumor uptake and T/M ratios in the xenografted U87MG model while no significant changes in tumor uptake of ^{99m}Tc-3P-RGD$_2$ were seen in the PC-3 model after linifanib therapy.[199] The uptake changes in MDA-MB-435 tumors were between those observed in the U87MG and PC-3 models (Figure 15).[200] This is consistent with the $\alpha_v\beta_3$ expression levels on three xenografted tumors.[44,47] Highly vascularized U87MG tumors with high levels of $\alpha_v\beta_3$ and CD31 have better response to linifanib therapy than poorly vascularized PC-3 tumors with low levels of $\alpha_v\beta_3$ and CD31 (Figure 15). Thus, ^{99m}Tc-3P-RGD$_2$ has the potential as the pretreatment screening tool to select appropriate patients who will benefit most the antiangiogenic treatment. If the tumor in a cancer patient has a high $\alpha_v\beta_3$ expression, as indicated by high tumor uptake of ^{99m}Tc-3P-RGD$_2$ in SPECT/CT images at the time of diagnosis, antiangiogenic therapy would more likely be effective. If the tumor has little $\alpha_v\beta_3$ expression, as indicated by the low tumor uptake of ^{99m}Tc-3P-RGD$_2$, antiangiogenic therapy would not be effective regardless of the amount of antiangiogenic drug administered into each patient.

■ MONITORING TUMOR METASTASIS

Recently, we used ^{99m}Tc-3P-RGD$_2$ for noninvasive monitoring of tumor growth and progression of breast cancer metastasis.[207,208] As illustrated in Figure 16A, there were no metastatic tumors detectable in the lungs at week 4 after tumor cell inoculation. By week 6, small lesions started to appear in the mediastinum and lungs. At week 8, SPECT/CT images revealed many metastatic tumors in both lungs. Figure 16B compares the %ID (left) and %ID/cm^3 (right) uptake values of ^{99m}Tc-3P-RGD$_2$ in the lungs. Even though the lung uptake of ^{99m}Tc-3P-RGD$_2$ (0.41 ± 0.05%ID) at week 4 was slightly higher than that in the control animals (0.36 ± 0.06%ID), this difference was not significant ($p > 0.05$) within experimental error. At week 6, the tumor burden in the lungs became significant (Figure 16B). The lung uptake of ^{99m}Tc-3P-RGD$_2$ was higher (0.89 ± 0.12%ID; $p < 0.01$) than that in the control group.[208] By week 8, the lung uptake of ^{99m}Tc-3P-RGD$_2$ increased to 1.40 ± 0.42%ID. In all cases, the lung size remained relatively unchanged (1.21−1.32 cm^3) during the eight-week study period. It is clear that ^{99m}Tc-3P-RGD$_2$ SPECT is an excellent molecular imaging tool to monitor the tumor micrometastasis and metastatic tumor burden in a noninvasive fashion.

Clinical Experiences with ^{99m}Tc-3P-RGD$_2$. ^{99m}Tc-3P-RGD$_2$ is under clinical investigation as a new radiotracer for tumor imaging. In the first in-human study, ^{99m}Tc-3P-RGD$_2$ was investigated for its capability to differentiate solitary pulmonary nodules (SPNs).[209] Among the 21 patients with SPNs, 15 (71%) were diagnosed as malignant and 6 (29%) were benign. The sensitivities for CT and ^{99m}Tc-3P-RGD$_2$ SPECT were 80% and 100%, respectively. All SPNs undetected by CT can be accurately diagnosed by ^{99m}Tc-3P-RGD$_2$ SPECT. These results demonstrated the utility of ^{99m}Tc-3P-RGD$_2$ SPECT in differentiating SPNs.[209] A multicenter study was performed in 70 patients with suspected lung cancer.[210] It was found that ^{99m}Tc-3P-RGD$_2$ SPECT was effective in detecting lung malignancies. Planar imaging and chest SPECT are complementary for detection of primary tumors and metastasis.[210] In a recently study, ^{99m}Tc-3P-RGD$_2$ SPECT was used to detect the radioactive iodine-refractory differentiated thyroid carcinoma (DTC).[211] It was found that ^{99m}Tc-3P-RGD$_2$ SPECT was able to identify all the DTC lesions. There was a significant correlation between the T/B ratios and growth rates of DTC lesions. It was concluded that ^{99m}Tc-3P-RGD$_2$ SPECT is useful for the diagnosis of DTC lesions.[211] ^{99m}Tc-3P-RGD$_2$ SPECT was also evaluated for its capability to assess the breast cancer lessons.[212] It was found that the mean target/nontarget ratio of ^{99m}Tc-3P-RGD$_2$ in malignant lesions was significantly higher than that in benign lesions (3.54 ± 1.51 vs 1.83 ± 0.98, $p < 0.001$). The sensitivity, specificity, and accuracy of ^{99m}Tc-3P-RGD$_2$ were 89.3%, 90.9%, and 89.7%, respectively, with the target/nontarget cutoff value of 2.40.[213] The mean target/nontarget ratio of ^{99m}Tc-MIBI in malignant lesions was also significantly higher than that in the benign lesions (2.86 ± 0.99 vs 1.51 ± 0.61, $p < 0.001$). The sensitivity, specificity, and accuracy of ^{99m}Tc-MIBI were 87.5%, 72.7%, and 82.1%, respectively, with the target/nontarget cutoff value of 1.45. The area under the curve for ^{99m}Tc-3P-RGD$_2$ was higher than that for ^{99m}Tc-MIBI, but this difference was not statistically significant, most likely because of the limited number of patients.

Clinical Experiences with ^{18}F-Alfatide-I. [^{18}F]AlF-(NOTA-P-RGD$_2$) (denoted as ^{18}F-Alfatide-I) is the ^{18}F-labeled cyclic RGD dimer P-RGD$_2$, the ^{99m}Tc and ^{111}In analogues of which have been evaluated as SPECT radiotracers for tumor imaging.[38,41] The Al(NOTA) chelate was the platform used for ^{18}F-labeling of P-RGD$_2$ to avoid the multistep and time-consuming radiosynthesis.[214] Under optimized conditions, ^{18}F-Alfatide-I was prepared in high yield (~42%) with >95%

DOI: 10.1021/acs.bioconjchem.5b00327
Bioconjugate Chem. 2015, 26, 1413−1438

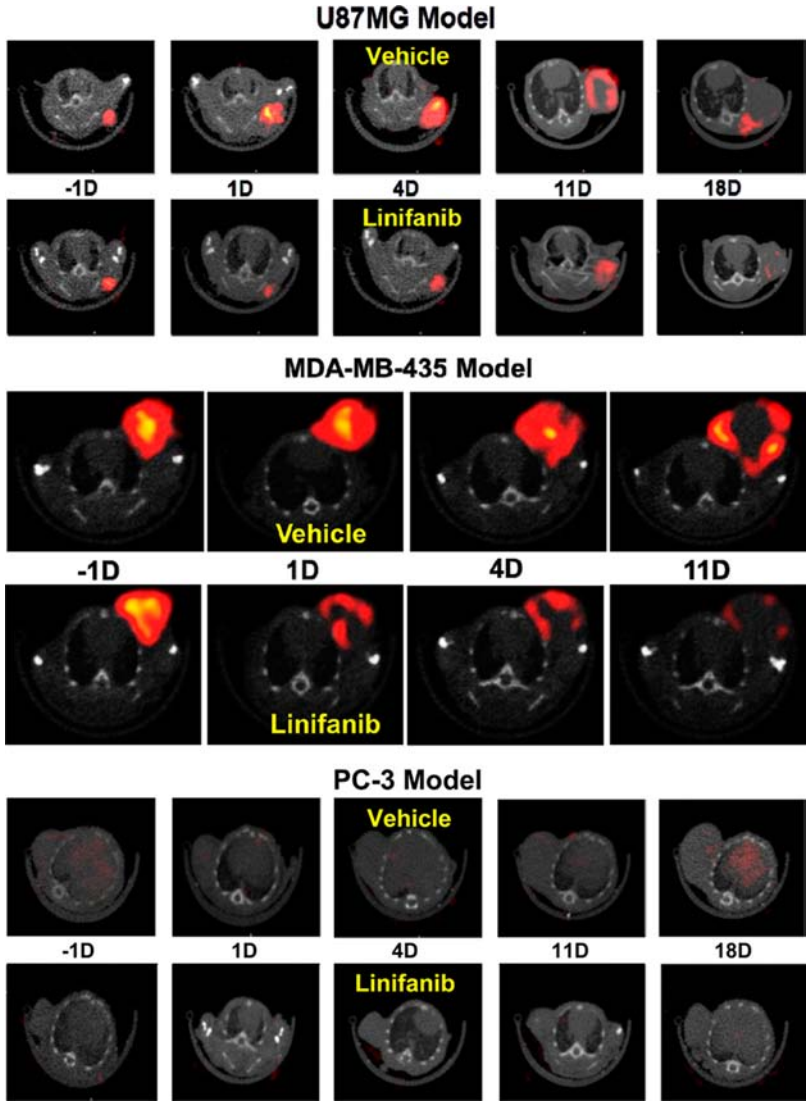

Figure 15. Transverse views of representative SPECT/CT images for athymic nude mice bearing U87MG glioma (top), MDA-MB-435 breast cancer (middle), and PC-3 prostate (bottom) cancer xenografts at −1, 1, 4, 11, and 18 days for the vehicle and linifanib-treated groups. The imaging data were from refs 199 and 217.

radiochemical purity. However, chromatographic purification is still needed after ^{18}F-labeling. It took about 20 min to complete both radiosynthesis and postlabeling filtration. Nine patients with lung cancer were examined with ^{18}F-Alfatide-I PET, and 1 tuberculosis patient was also investigated using ^{18}F-Alfatide-I and ^{18}F-FDG PET. It was found that ^{18}F-Alfatide-I PET could identify all the tumors with the mean uptake of 2.90 ± 0.10. The tumor/muscle and tumor/blood ratios were 5.87 ± 2.02 and 2.71 ± 0.92, respectively. It was concluded that ^{18}F-Alfatide-I PET allows specific imaging of the $\alpha_v\beta_3$ expression in lung cancer patients.[214] ^{18}F-Alfatide-I was also compared to ^{18}F-FDG in detection of DTC lymph node metastasis.[215] Twenty DTC patients with presumptive lymph node metastasis were examined with ^{18}F-Alfatide-I and ^{18}F-FDG PET/CT. Sixteen patients were evaluated by cytology results. A total of 39 presumptive lymph node metastases were clearly visualized on PET/CT images, and 35 lesions were confirmed as malignant tumor by biopsy and other clinical findings. It was also found that 15 DTC lesions with the diameter >1.5 cm had higher ^{18}F-Alfatide-I uptake than the lesions <1.5 cm. Although most DTC lymph node metastases showed abnormal uptake of ^{18}F-Alfatide-I, its diagnostic value was not as good as that of ^{18}F-FDG.[215]

Clinical Experiences with ^{18}F-Alfatide-II. [^{18}F]AlF-(NOTA-2P-RGD$_2$) (denoted as ^{18}F-Alfatide-II) is another ^{18}F-labeled dimeric cyclic RGD peptide 2P-RGD$_2$, which was first developed by Dr. Liu's group at Purdue University for preparation of ^{99m}Tc-2P-RGD$_2$.[35,41] Dr. Chen's group at the National Institute of Biomedical Imaging and Bioengineering (NIBIB) recently reported the use of ^{18}F-Alfatide-II and ^{18}F-FDG for monitoring the tumor responses to doxorubicin therapy in xenografted U87MG and MDA-MB-435 models.[216] It was found that there were substantial differences in the ^{18}F-Alfatide-II binding potential and ^{18}F-FDG influx rate 3 days after doxorubicin treatment.[216] It was also found that injection of [^{18}F]Alfatide-II was well tolerated in all healthy volunteers.[217] ^{18}F-Alfatide-II showed rapid clearance from the blood pool and kidneys. Nine patients with 20 brain metastatic lesions identified by MRI and/or CT were enrolled in this study. All 20 brain lesions were visualized by ^{18}F-Alfatide-II PET, while only 10 lesions were visualized by ^{18}F-FDG, and 13 by CT.[217] It was

DOI: 10.1021/acs.bioconjchem.5b00327
Bioconjugate Chem. 2015, 26, 1413−1438

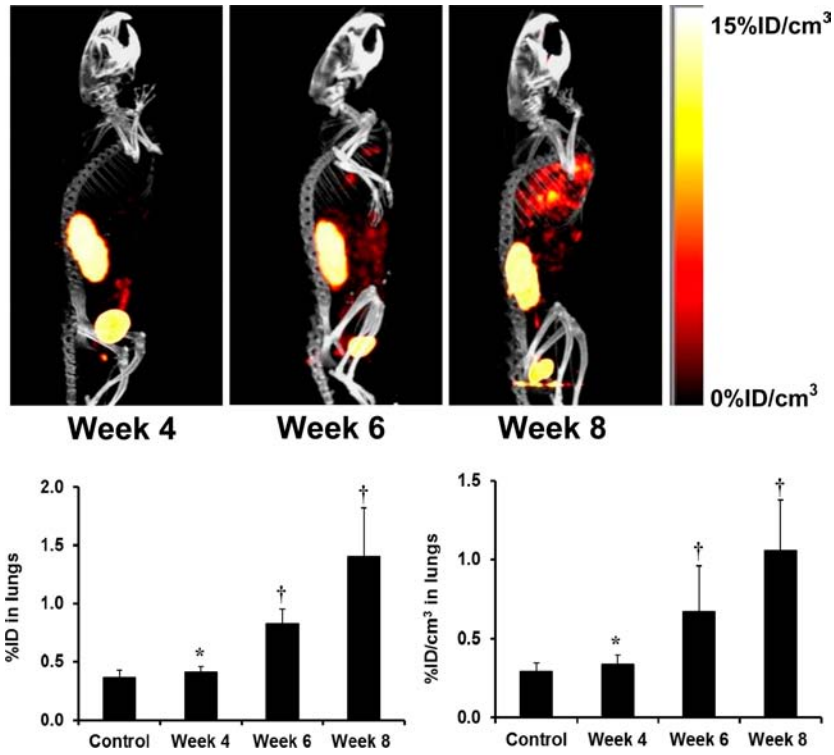

Figure 16. Top: 3D views of SPECT/CT images of an athymic nude mouse at week 4, 6, and 8 after tail-vein injection of 1.0×10^6 MDA-MB-231 cells. Bottom: %ID (left) and %ID/cm^3 (right) uptake values of ^{99m}Tc-3P-RGD$_2$ in the lungs obtained from SPECT/CT quantification in the athymic nude mice (n = 8) at week 4, 6, and 8 after tail-vein injection of 1.0×10^6 MDA-MB-231 cells. Normal animals (n = 4) were used in the control group. †: $p < 0.05$, significantly different from the control group; *: $p > 0.05$, no significant difference from the control group. The imaging and SPECT quantification data were from ref 200.

concluded that ^{18}F-Alfatide-II is a valuable biomarker of angiogenesis in finding brain metastases of different cancers.

NEW OPPORTUNITIES AND CHALLENGES

Advantages of Multimeric Cyclic RGD Peptides. Tumor imaging with radiolabeled cyclic RGD peptides depends on their $\alpha_v\beta_3$ binding affinity and the total $\alpha_v\beta_3$ population. The advantage of multimeric cyclic RGD peptides is their higher $\alpha_v\beta_3$ binding affinity than that of their monomeric analogues, and their capability to target multiple integrins in tumor tissues. The multi-integrin targeting capability may contribute to the fact that they are able to localize in human carcinomas of different origin. Our studies show that radiolabeled tetrameric cyclic RGD peptides have higher uptake than their dimeric analogues in both tumors and $\alpha_v\beta_3$-positive organs.[33,50] High tumor uptake is important for the sensitivity, but their potential as tumor imaging agents will rely upon the contrast between tumor and normal tissues. There is always a subtle balance between the tumor uptake and T/B ratios.

Other Applications and Limitations. The success of radiolabeled cyclic RGD peptides as PET or SPECT radiotracers can be attributed to their capability to target a large population of cancer patients with carcinomas of breast, lung, and prostate. It is important to note that $\alpha_v\beta_3$ is also overexpressed on activated endothelial cells during wound healing and post-infarct remodeling, in rheumatoid arthritis and atherosclerotic plaque.[218−221] Thus, $\alpha_v\beta_3$ is a biomarker for inflammation and angiogenesis.[221] The $\alpha_v\beta_3$-targeted radiotracers have been used for imaging myocardial angiogenesis,[222,223] inflammatory diseases,[224] hindlimb ischemia,[225] and plaque vulnerability.[226,227] It was reported that the ^{111}In-labeled $\alpha_v\beta_3$ antagonist was able to image angiogenesis after myocardial infarction.[222] ^{18}F-Galacto-RGD has been used to distinguish between the acute and chronic phases of T-cell mediated immune responses,[228] and to image the $\alpha_v\beta_3$ expression in human carotid atherosclerosis.[229] These promising results suggest that $\alpha_v\beta_3$-targeted radiotracers might be valuable for imaging angiogenesis after ischemic injury, myocardial infarction, and inflammation. These broad applications of $\alpha_v\beta_3$-targeted radiotracers also raise significant questions related to their tumor specificity. It important to note that radiolabeled RGD peptides are $\alpha_v\beta_3$-targeted radiotracers. As long as the diseased tissue has the $\alpha_v\beta_3$ overexpression, it will have radiotracer uptake. In this situation, the differentiation between tumors and other diseased tissues will depend on their difference in $\alpha_v\beta_3$ expression levels. For example, the mean T/B ratio of ^{99m}Tc-3P-RGD$_2$ in malignant breast cancer lesions was 3.54 ± 1.51, which was significantly ($p < 0.001$) higher than that in the inflammatory benign lesions (1.83 ± 0.98).[213] In this respect, radiolabeled cyclic RGD peptides are very similar to ^{18}F-FDG since the metabolic activity is elevated during tumor growth, wound healing, post-infarct remodeling, and in rheumatoid arthritis and atherosclerotic plaque.

Integrin $\alpha_v\beta_3$ Expression Heterogeneity. Because of variations in the tumor vasculature, different tumor tissues often have a large difference in $\alpha_v\beta_3$ expression levels. Recently, we evaluated FITC-labeled dimeric RGD peptides (e.g., FITC-Galacto-RGD$_2$) for their potential as fluorescent probes to quantify the total $\alpha_v\beta_3$ expression levels in both the xenografted tumors and human carcinoma tissues.[183] It was found that the total $\alpha_v\beta_3$ levels followed a general order of colon cancer > pancreatic cancer > lung adenocarcinoma ≈ squamous cell lung

DOI: 10.1021/acs.bioconjchem.5b00327
Bioconjugate Chem. 2015, 26, 1413−1438

cancer ≫ gastric cancer ≈ esophageal cancer. The same conclusion was also made using the fluorescence-labeled integrin β_3 antibody. For the xenografted tumors (cancer cells of human origin and tumor vasculature of murine origin), the $\alpha_v\beta_3$ expression levels followed the general trend of U87MG (high $\alpha_v\beta_3$ expression on both glioma cells and tumor vasculature) > MDA-MB-435 (moderately high $\alpha_v\beta_3$ expression on breast tumor cells and tumor vasculature) ∼ A549 (moderately high $\alpha_v\beta_3$ expression on lung tumor cells and tumor vasculature) ∼ HT29 (high $\alpha_v\beta_3$ expression on the tumor vasculature, but low $\alpha_v\beta_3$ expression on tumor cells) > PC-3 (low $\alpha_v\beta_3$ expression on both prostate cancer cells and tumor vasculature).[44,46,183] It has been estimated that the percentage of contribution from the tumor neovasculature to the total $\alpha_v\beta_3$ expression level and tumor uptake of ^{99m}Tc-3P-RGD$_2$ is ∼60% in the xenografted U87MG glioma model.[199] In the case of the xenografted HT29 tumors, the main contribution to the tumor uptake of ^{99m}Tc-3P-RGD$_2$ is from the $\alpha_v\beta_3$ on neovasculature.[44,46] Furthermore, the $\alpha_v\beta_3$ expression level may change with tumor metastatic status. For example, the $\alpha_v\beta_3$ expression level may be low in primary tumors. However, it could be very high once the $\alpha_v\beta_3$ is activated and the tumor becomes highly metastatic. Therefore, caution must be taken in generalizing the $\alpha_v\beta_3$-expression levels in different cancer types.

Comparison with ^{18}F-FDG. ^{18}F-FDG is the gold-standard in diagnostic oncology. It is not surprising that ^{18}F-FDG is often utilized as the positive control in evaluations of $\alpha_v\beta_3$-targeted radiotracers. However, this comparison may not be fair because they are targeting two different biological processes. ^{18}F-FDG is used to detect the metabolic activity while the RGD-based radiotracers target tumor $\alpha_v\beta_3$ expression. Clinical data from cancer patients suggest that perfusion, $\alpha_v\beta_3$ expression and glucose metabolism in active tumor areas are independent variables of the tumor biology.[230,231] There is no direct relationship between the tumor metabolism and $\alpha_v\beta_3$ expression.[230,231] Molecular imaging with ^{18}F-FDG and $\alpha_v\beta_3$-targeted radiotracers can provide complementary information and might help to evaluate both tumor metabolism and angiogenesis in vivo in its full complexity.

Challenges in Radiotracer Development. The discovery of highly novel targeting biomolecules (such as multimeric cyclic RGD peptides) requires intensive efforts from researchers and resources from their institutions. It is easy to use known cyclic RGD peptides from the literature to develop $\alpha_v\beta_3$-targeted radiotracers by simply changing the radioisotope (^{99m}Tc vs ^{18}F or ^{68}Ga) or radiometal chelate. However, the novelty of radiotracers developed from this approach is highly questionable. No industrial partners would commit millions of dollars to develop a new radiotracer without the intellectual proprietary position for commercialization. It must be emphasized that discovery of new multimeric cyclic RGD peptides is only the first step of a long process of radiotracer development. For diagnostic radiopharmaceuticals, the development times are generally 8−10 years and the total development costs are between $100 million and $200 million.[232] For research purposes, it is common to use postlabeling chromatography to improve radiotracer purity and specific activity before being used for preclinical animal studies. In clinical settings, chromatographic purification is not practical. Thus, development of efficient radiolabeling techniques is very important regardless of radioisotope. HYNIC and MAG$_2$ are useful for routine ^{99m}Tc-labeling of small biomolecules using kit formulation,[46,47,68−70] while DOTA and NOTA derivatives are better suited for chelation of ^{64}Cu and ^{68}Ga.[7,67,68,71,72] Successful development of Al(NOTA) as a prosthetic group for ^{18}F-labeling of biomolecules represents a milestone for routine radiosynthesis of receptor-based target-specific ^{18}F radiotracers.[90−97] Another significant challenge that many academic researchers have to face is how to translate the results from bench discovery and preclinical evaluations in small animal models into actual clinical practice. Academic researchers often consider clinical translation to be the first use of a new radiotracer in humans.[232] From the industrial point of view, clinical translation means sustained sales and an impact of a new radiotracer on patient care.[232] The costs to develop a new radiotracer into a successful "diagnostic drug" routinely used in nuclear medicine clinics are much more than those to test a new radiotracer in the physician-sponsored clinical trials. Successful development of a new radiotracer requires teamwork from several different disciplines and strong commitment from radiopharmaceutical and pharmaceutical industry. Otherwise, clinical translation will remain "an elusive goal" for many, including academic researchers, industrial drug developer, clinicians, and cancer patients.

Potential Impact of Future SPECT Scanners. The success of a new SPECT radiotracer also depends on availability of high-quality SPECT scanners. It is well-accepted that conventional dual-head SPECT scanners currently available in nuclear medicine clinics have significant drawbacks in radioactivity quantification, speed of dynamic imaging, spatial resolution, and tissue attenuation. If the industry is willing to devote the resources for development of new SPECT cameras as much as those for PET cameras, most of these challenges can be overcome. The development of ultrafast SPECT scanners (e.g., D-SPECT from Spectrum Dynamics, IQ SPECT developed by Siemens Medical Solutions and CardiArc manufactured by CardiArc Inc.) represents an excellent example of future SPECT cameras with the capability for quantification of organ uptake and fast speed of dynamic imaging with good spatial resolution.[233−240] The larger radiation collection angles along with the use of many stationary solid state CZT (cadmium zinc telluride) detectors in a D-SPECT scanner provide 10× more efficient photon collection, leading to improved count statistics and higher quality images. Furthermore, development of the CZT-based whole-body SPECT/CT scanners and new computer software with the capability for attenuation and photon-scattering correction will help to achieve full clinical potentials of the $\alpha_v\beta_3$-targeted SPECT radiotracers.

■ CONCLUSIONS

Radiolabeled cyclic RGD peptides are called "$\alpha_v\beta_3$-targeted" radiotracers because $\alpha_v\beta_3$ is studied most extensively for its role in tumor angiogenesis and metastasis. The capability of radiolabeled cyclic RGD peptides to target multiple integrins will improve their tumor uptake due to the increased receptor population. Multimerization of cyclic RGD peptides increases the tumor uptake and retention times of their radiotracers. The two most important factors (bivalency and locally enhanced RGD concentration) contribute to the higher $\alpha_v\beta_3$ binding affinity of multimeric cyclic RGD peptides than their corresponding monomeric analogues. The concentration factor exists in all multimeric cyclic RGD peptides regardless of the linker length between two cyclic RGD motifs. The key to achieving bivalency is the distance between two cyclic RGD

DOI: 10.1021/acs.bioconjchem.5b00327
Bioconjugate Chem. 2015, 26, 1413−1438

motifs. Among the dimeric and tetrameric cyclic RGD peptides evaluated in our laboratories, 2P-RGD$_2$, 3P-RGD$_2$, 2G-RGD$_2$, 3G-RGD$_2$, and Galacto-RGD$_2$ show the most promising results with respect to T/B ratios of their radiotracers.[23,24,34−50] In the literature, a few ^{68}Ga-labeled trimeric RGD peptides were used as PET radiotracers.[11,14] It would be interesting to compare them with their dimeric and tetrameric analogues with respect to the tumor uptake and T/B ratios of ^{99m}Tc, ^{111}In, ^{64}Cu, and ^{68}Ga radiotracers in the same model, and determine the optimal multiplicity for development of $\alpha_v\beta_3$-targeted cyclic RGD peptides.

^{99m}Tc-3P-RGD$_2$, ^{18}F-Alfatide-I, and ^{18}F-Alfatide-II are currently evaluated as new radiotracers for early cancer detection in the clinic. Since ^{99m}Tc-3P-RGD$_2$ is prepared in >95% purity without purification, it offers significant advantages over the corresponding ^{18}F radiotracers, which often requires postlabeling chromatographic purification. It would be difficult for ^{18}F radiotracers to assume widespread clinical acceptance if they have poor clinical availability. Their high cost may also prove to be too much for a large population of cancer patients to afford the prescribed procedures. The beauty of new radiotracer development lies in science, but the success of a new radiotracer relies on its clinical availability at low cost and the ease of its routine radiosynthesis. The ultimate goal is to improve the quality of life for cancer patients with $\alpha_v\beta_3$-targeted radiotracers.

AUTHOR INFORMATION

Corresponding Author

*E-mail: liu100@purdue.edu. Phone: 765-494-0236. Fax 765-496-1377.

Notes

The authors declare no competing financial interest.

ACKNOWLEDGMENTS

The author would like to thank all his graduate students, postdoctoral fellows, and visiting scholars over past 10 years for their contributions to the development of dimeric and tetrameric cyclic RGD peptides, and their ^{18}F, ^{99m}Tc, ^{111}In, ^{64}Cu, and ^{68}Ga radiotracers. This work was supported by Purdue University and research grants: R01 CA115883 (S.L.) from the National Cancer Institute (NCI) and R21 EB017237-01 (S.L.) from the National Institute of Biomedical Imaging and Bioengineering (NIBIB).

ABBREVIATIONS

General Terms

BFC, bifunctional coupling agent; CT, X-ray computed tomography; DCE-MRI, dynamic contrast-enhanced magnetic resonance imaging; dasatinib, *N*-(2-chloro-6-methylphenyl)-2-[[6-[4-(2-hydroxyethyl)-1-piperazinyl]-2-methyl-4-pyrimidinyl]amino]-5-thiazolecarboxamide; ^{18}F-FDG, 2-deoxy-2-(^{18}F)fluoro-D-glucose; FITC, Fluorescein isothiocyanate isomer I; IHC, immunohistochemistry; MRI, magnetic resonance imaging; MW, molecular weight; PET, positron emission tomography; PDGFR, Platelet-derived growth factor receptors; RGD, arginine-glycine-aspartic (Arg-Gly-Asp); SPECT, single photon emission computed tomography; sunitinib, hydroxy-(2S)-compound with N-[2-(diethylamino)-ethyl]-5-[(Z)-(5-fluoro1,2-dihydro-2-oxo-3H-indol-3-ylidine)-methyl]-2,4-dimethyl-1H-pyrrole-3-carboxamide; VEGFR, vascular endothelial growth factor receptors

Chelators

DOTA, 1,4,7,10-tetraazacyclododecane-1,4,7,10-tetracetic acid; HYNIC, 6-hydazinonicotinic acid; NOTA, 1,4,7-tritazacyclononane-1,4,7-triacetic acid

Cyclic Peptides

P-RGD, PEG$_4$-c(RGDfK) = cyclo(Arg-Gly-Asp-D-Phe-Lys-(PEG$_4$)) (PEG$_4$ = 15-amino-4,7,10,13-tetraoxapentadecanoic acid); RGD$_2$, E[c(RGDfK)]$_2$ = Glu[cyclo(Arg-Gly-Asp-D-Phe-Lys)]$_2$; Galacto-RGD$_2$, Glu[cyclo[Arg-Gly-Asp-D-Phe-Lys-(SAA-PEG$_2$-(1,2,3-triazole)-1-yl-4-methylamide)]]$_2$ (SAA = 7-amino-L-glycero-L-galacto-2,6-anhydro-7-deoxyheptanamide, and PEG$_2$ = 3,6-dioxaoctanoic acid); P-RGD$_2$, PEG$_4$-E[c-(RGDfK)]$_2$ = PEG$_4$-Glu[cyclo(Arg-Gly-Asp-D-Phe-Lys)]$_2$; P2D-RGD$_2$, PEG$_4$-E[D$_3$-c(RGDfK)]$_2$ = PEG$_4$-Glu[cyclo[Arg-Gly-Asp-D-Phe-Lys(D$_3$)]]$_2$ (D$_3$ = Asp-Asp-Asp); P2G-RGD$_2$, PEG$_4$-E[G$_3$-c(RGDfK)]$_2$ = PEG$_4$-Glu[cyclo[Arg-Gly-Asp-D-Phe-Lys(G$_3$)]]$_2$ (G$_3$ = Gly-Gly-Gly); 2G-RGD$_2$, E[G$_3$-c-(RGDfK)]$_2$ = Glu[cyclo[Arg-Gly-Asp-D-Phe-Lys(G$_3$)]]$_2$; 2P-RGD$_2$, E[PEG$_4$-c(RGDfK)]$_2$ = Glu[cyclo[Arg-Gly-Asp-D-Phe-Lys(PEG$_4$)]]$_2$; 3G-RGD$_2$, G$_3$-E[G$_3$-c(RGDfK)]$_2$ = G$_3$-Glu-[cyclo[Arg-Gly-Asp-D-Phe-Lys(G$_3$)]]$_2$; 3P-RGD$_2$, PEG$_4$-E-[PEG$_4$-c(RGDfK)]$_2$ = PEG$_4$-Glu[cyclo[Arg-Gly-Asp-D-Phe-Lys(PEG$_4$)]]$_2$; 3P-RGK$_2$, PEG$_4$-E[PEG$_4$-c(RGKfD)]$_2$ = PEG$_4$-Glu[cyclo[Arg-Gly-Lys(PEG$_4$)-D-Phe-Asp]]$_2$); RGD$_4$, E-{E[c(RGDfK)]$_2$}$_2$ = Glu{Glu[cyclo(Arg-Gly-Asp-D-Phe-Lys)]$_2$}$_2$; 6G-RGD$_4$, E{G$_3$-E[G$_3$-c(RGDfK)]$_2$}$_2$ = Glu{G$_3$-Glu[cyclo(Lys(G$_3$)-Arg-Gly-Asp-D-Phe)]-cyclo(Lys(G$_3$)-Arg-Gly-Asp-D-Phe)}-{PEG$_4$-Glu[cyclo(Lys(G$_3$)-Arg-Gly-Asp-D-Phe)]-cyclo(Lys(G$_3$)-Arg-Gly-Asp-D-Phe)}; and; 6P-RGD$_4$, E-{PEG$_4$-E[PEG$_4$-c(RGDfK)]$_2$}$_2$ = Glu{PEG$_4$-Glu[cyclo(Lys-(PEG$_4$)-Arg-Gly-Asp-D-Phe)]-cyclo(Lys(PEG$_4$)-Arg-Gly-Asp-D-Phe)}-{PEG$_4$-Glu[cyclo(Lys(PEG$_4$)-Arg-Gly-Asp-D-Phe)]-cyclo(Lys(PEG$_4$)-Arg-Gly-Asp-D-Phe)}

Cyclic Peptide Bioconjugates

DOTA-RGD, DOTA-c(RGDfK); DOTA-P-RGD, DOTA-PEG$_4$-c(RGDfK); DOTA-RGD$_2$, DOTA-E[c(RGDfK)]$_2$; DOTA-P-RGD$_2$, DOTA-PEG$_4$-E[c(RGDfK)]$_2$; DOTA-2G-RGD$_2$, DOTA-E[G$_3$-c(RGDfK)]$_2$; DOTA-2P-RGD$_2$, DOTA-E[PEG$_4$-c(RGDfK)]$_2$; DOTA-3G-RGD$_2$, DOTA-G$_3$-E[G$_3$-c-(RGDfK)]$_2$; DOTA-3P-RGD$_2$, DOTA-PEG$_4$-E[PEG$_4$-c-(RGDfK)]$_2$; DOTA-3P-RGK$_2$, DOTA-PEG$_4$-E[PEG$_4$-c-(RGKfD)]$_2$; DOTA-Galacto-RGD$_2$, DOTA-Glu[c[RGDfK-(SAA-PEG$_2$-(1,2,3-triazole)-1-yl-4-methylamide)]]$_2$; DOTA-RGD$_4$, DOTA-E{E[c(RGDfK)]$_2$}$_2$; DOTA-6G-RGD$_4$:DOTA-E{G$_3$-E[G$_3$-c(RGDfK)]$_2$}$_2$;; DOTA-6P-RGD$_4$, E{PEG$_4$-E-[PEG$_4$-c(RGDfK)]$_2$}$_2$; FITC-3P-RGD$_2$, FITC-PEG$_4$-E[PEG$_4$-c(RGDfK)]$_2$; FITC-3P-RGK$_2$, FITC-PEG$_4$-E[PEG$_4$-c-(RGKfD)]$_2$; FITC-Galacto-RGD$_2$, FITC-Glu[c[RGDfK(SAA-PEG$_2$-(1,2,3-triazole)-1-yl-4-methylamide)]]$_2$; HYNIC-RGD$_2$, HYNIC-E[c(RGDfK)]$_2$; HYNIC-P-RGD$_2$, HYNIC-PEG$_4$-E[c-(RGDfK)]$_2$; HYNIC-P2D-RGD$_2$, HYNIC-PEG$_4$-E[D$_3$-c-(RGDfK)]$_2$; HYNIC-P2G-RGD$_2$, HYNIC-PEG$_4$-E[G$_3$-c-(RGDfK)]$_2$; HYNIC-2G-RGD$_2$, HYNIC-E[G$_3$-c(RGDfK)]$_2$; HYNIC-2P-RGD$_2$, HYNIC-E[PEG$_4$-c(RGDfK)]$_2$; HYNIC-3G-RGD$_2$, HYNIC-G$_3$-E[G$_3$-c(RGDfK)]$_2$; HYNIC-3P-RGD$_2$, HYNIC-PEG$_4$-E[PEG$_4$-c(RGDfK)]$_2$; HYNIC-K(NIC)-3P-RGD$_2$, HYNIC-K(NIC)-PEG$_4$-E[PEG$_4$-c(RGDfK)]$_2$ (NIC = nicotinyl); K(HYNIC)$_2$-3P-RGD$_2$, K(HYNIC)$_2$-PEG$_4$-E[PEG$_4$-c(RGDfK)]$_2$; HYNIC-Galacto-RGD$_2$, HYNIC-E[c[RGDfK-(SAA-PEG$_2$-(1,2,3-triazole)-1-yl-4-methylamide)]]$_2$; HYNIC-RGD$_4$, HYNIC-E{E[c(RGDfK)]$_2$}$_2$; NOTA-P-RGD$_2$, NOTA-PEG$_4$-E[c(RGDfK)]$_2$; NOTA-2G-RGD$_2$, NOTA-E[G$_3$-c-

DOI: 10.1021/acs.bioconjchem.5b00327
Bioconjugate Chem. 2015, 26, 1413−1438

$(RGDfK)]_2$; NOTA-2P-RGD_2, NOTA-E[PEG_4-c(RGDfK)]$_2$; NOTA-3G-RGD_2, NOTA-G_3-E[G_3-c(RGDfK)]$_2$; NOTA-3P-RGD_2, NOTA-PEG_4-E[PEG_4-c(RGDfK)]$_2$

Radiolabeled Cyclic RGD Peptides

^{18}F-Alfatide-I, [^{18}F]AlF(NOTA-P-RGD_2); ^{18}F-Alfatide-II, [^{18}F]-AlF(NOTA-2P-RGD_2); ^{18}F-Galacto-RGD, 2-[^{18}F]-fluoropropanamide c(RGDfK(SAA); ^{64}Cu−P-RGD_2, ^{64}Cu-(DOTA-P-RGD_2); ^{64}Cu-2G-RGD_2, ^{64}Cu(DOTA-2G-RGD_2); ^{64}Cu-2P-RGD_2, ^{64}Cu(DOTA-2P-RGD_2); ^{64}Cu-3G-RGD_2, ^{64}Cu(DOTA-3G-RGD_2); ^{64}Cu-3P-RGD_2, ^{64}Cu(DOTA-3P-RGD_2); ^{68}Ga-3G-RGD_2, ^{68}Ga(DOTA-3G-RGD_2); ^{68}Ga-3P-RGD_2, ^{68}Ga(DOTA-3P-RGD_2); ^{111}In-P-RGD, ^{111}In(DOTA-P-RGD); ^{111}In-P-RGD_2, ^{111}In(DOTA-P-RGD_2); ^{111}In-3G-RGD_2, ^{111}In(DOTA-3G-RGD_2); ^{111}In-3P-RGD_2, ^{111}In(DOTA-3P-RGD_2); ^{111}In-Galacto-RGD_2, ^{111}In(DOTA-Galacto-RGD_2); ^{111}In-6G-RGD_4, ^{111}In(DOTA-6G-RGD_4); ^{111}In-6P-RGD_4, ^{111}In(DOTA-6P-RGD_4); ^{99m}Tc-Galacto-RGD_2, [^{99m}Tc-(HYNIC-Galacto-RGD_2) (tricine) (TPPTS)]); ^{99m}Tc-RGD_2, [^{99m}Tc(HYNIC-RGD_2) (tricine) (TPPTS)]); ^{99m}Tc-P-RGD_2, [^{99m}Tc(HYNIC-P-RGD_2) (tricine) (TPPTS)]; ^{99m}Tc-P2D-RGD_2, [^{99m}Tc(HYNIC-P2D-RGD_2) (tricine) (TPPTS)]; ^{99m}Tc-P2G-RGD_2, [^{99m}Tc(HYNIC-P2G-RGD_2) (tricine) (TPPTS)]; ^{99m}Tc-2G-RGD_2, [^{99m}Tc(HYNIC-2G-RGD_2) (tricine) (TPPTS)]; ^{99m}Tc-2P-RGD_2, [^{99m}Tc(HYNIC-2P-RGD_2) (tricine) (TPPTS)]; ^{99m}Tc-3G-RGD_2, [^{99m}Tc(HYNIC-3G-RGD_2) (tricine) (TPPTS)]; ^{99m}Tc-3P-RGD_2, [^{99m}Tc(HYNIC-3P-RGD_2) (tricine) (TPPTS)]; ^{99m}Tc-3P-RGD_2-A, [^{99m}Tc-(HYNIC-K(NIC)-3P-RGD_2) (tricine)]; ^{99m}Tc-3P-RGD_2-B, [^{99m}Tc(K(HYNIC)$_2$-3P-RGD_2) (tricine)]; ^{99m}Tc-RGD_4, [^{99m}Tc(HYNIC-RGD_4) (tricine) (TPPTS)])

REFERENCES

(1) Siegel, R., Ma, J., Zou, Z., and Jemal, A. (2014) Cancer statistics, 2014. *Ca-Cancer J. Clin. 64*, 9−29.

(2) Mankoff, D. A., Link, J. M., Linden, H. M., Sundararajan, L., and Krohn, K. A. (2008) Tumor receptor imaging. *J. Nucl. Med. 49*, 149S−163S.

(3) Tweedle, M. F. (2009) Peptide-targeted diagnostics and radiotherapeutics. *Acc. Chem. Res. 42*, 958−968.

(4) Fani, M., and Maecke, H. R. (2012) Radiopharmaceutical development of radiolabelled peptides. *Eur. J. Nucl. Med. Mol. Imaging 39* (Suppl 1), S11−S30.

(5) Fani, M., Maecke, H. R., and Okarvi, S. M. (2012) Radiolabeled peptides: valuable tools for the detection and treatment of cancer. *Theranostics 2*, 481−501.

(6) Gaertner, F. C., Kessler, H., Wester, H. J., Schwaiger, M., and Beer, A. J. (2012) Radiolabelled RGD peptides for imaging and therapy. *Eur. J. Nucl. Med. Mol. Imaging 39* (Suppl 1), S126−138.

(7) Laverman, P., Sosabowski, J. K., Boerman, O. C., and Oyen, W. J. G. (2012) Radiolabelled peptides for oncological diagnosis. *Eur. J. Nucl. Med. Mol. Imaging 39* (Suppl 1), S78−S92.

(8) Jamous, M., Haberkorn, U., and Mier, W. (2013) Synthesis of peptide radiopharmaceuticals for the therapy and diagnosis of tumor diseases. *Molecules 18*, 3379−3409.

(9) Shokeen, M., and Anderson, C. J. (2009) Molecular imaging of cancer with copper-64 radiopharmaceuticals and positron emission tomography (PET). *Acc. Chem. Res. 42*, 832−841.

(10) Correia, J. D. G., Paulo, A., Raposinho, P. D., and Santos, I. (2011) Radiometallated peptides for molecular imaging and targeted therapy. *Dalton Trans. 40*, 6144−6167.

(11) Kubas, H., Schäfer, M., Bauder-Wüst, U., Eder, M., Oltmanns, D., Haberkorn, U., Mier, W., and Eisenhut, M. (2010) Multivalent cyclic RGD ligands: influence of linker lengths on receptor binding. *Nucl. Med. Biol. 37*, 885−891.

(12) Šimečcek, J., Hermann, P., Havíčková, J., Herdtweck, E., Kapp, T. G., Engelbogen, N., Kessler, H., Wester, H. J., and Notni, J. (2013) Cyclen-based tetraphosphinate chelator for the preparation of radiolabeled tetrameric bioconjugates. *Chem. - Eur. J. 19*, 7748−7757.

(13) Dumont, R. A., Deininger, F., Haubner, R., Maecke, H. R., Weber, W. A., and Fani, M. (2011) Novel ^{64}Cu- and ^{68}Ga-labeled RGD conjugates show improved PET imaging of $\alpha_v\beta_3$ integrin expression and facile radiosynthesis. *J. Nucl. Med. 52*, 1276−1284.

(14) Knetsch, P. A., Zhai, C., Rangger, C., Blatzer, M., Haas, H., Kaeopookum, P., Haubner, R., and Decristoforo, C. (2015) [^{68}Ga]-FSC-$(RGD)_3$ a trimeric RGD peptide for imaging $\alpha_v\beta_3$ integrin expression based on a novel siderophore derived chelating scaffold-synthesis and evaluation. *Nucl. Med. Biol. 42*, 115−122.

(15) Pohle, K., Notni, J., Bussemer, J., Kessler, H., Schwaiger, M., and Beer, A. J. (2012) ^{68}Ga-NODAGA-RGD is a suitable substitute for ^{18}F-Galacto-RGD and can be produced with high specific activity in a cGMP/GRP compliant automated process. *Nucl. Med. Biol. 39*, 777−784.

(16) Li, Y., Guo, J., Tang, S., Lang, L., Chen, X., and Perrin, D. M. (2013) One-step and one-pot-two-step radiosynthesis of cyclo-RGD-^{18}F-aryltrifluoroborate conjugates for functional imaging. *Am. J. Nucl. Med. Mol. Imaging 3*, 44−56.

(17) Tsiapa, I., Loudos, G., Varvarigou, A., Fragogeorgi, E., Psimadas, D., Tsotakos, T., Xanthopoulos, S., Mihailidis, D., Bouziotis, P., Nikiforidis, G. C., et al. (2013) Biological evaluation of an ornithine-modified ^{99m}Tc-labeled RGD peptide as an angiogenesis imaging agent. *Nucl. Med. Biol. 40*, 262−272.

(18) Maschauer, S., Haubner, R., Kuwert, T., and Prante, O. (2014) ^{18}F-Glyco-RGD peptides for PET imaging of integrin expression: efficient radiosynthesis by click chemistry and modulation of biodistribution by glycosylation. *Mol. Pharmaceutics 11*, 505−515.

(19) Wu, Y., Zhang, X., Xiong, Z., Cheng, Z., Fisher, D. R., Liu, S., Gambhir, S. S., and Chen, X. (2005) MicroPET imaging of glioma integrin $\alpha_v\beta_3$ expression using ^{64}Cu-labeled tetrameric RGD peptide. *J. Nucl. Med. 46*, 1707−1718.

(20) Zhang, X., Xiong, Z., Wu, Y., Cai, W., Tseng, J. R., Gambhir, S. S., and Chen, X. (2005) Quantitative PET imaging of tumor integrin $\alpha_v\beta_3$ expression with ^{18}F-FRGD2. *J. Nucl. Med. 47*, 113−121.

(21) Wu, Z., Li, Z., Chen, K., Cai, W., He, L., Chin, F. T., Li, F., and Chen, X. (2007) (2005) MicroPET of tumor integrin $\alpha_v\beta_3$ expression using ^{18}F-labeled PEGylated tetrameric RGD peptide (^{18}F-FPRGD4). *J. Nucl. Med. 48*, 1536−1544.

(22) Li, Z. B., Chen, K., and Chen, X. (2008) ^{68}Ga-labeled multimeric RGD peptides for microPET imaging of integrin $\alpha_v\beta_3$ expression. *Eur. J. Nucl. Med. Mol. Imaging 35*, 1100−1108.

(23) Liu, Z., Niu, G., Shi, J., Liu, S., Wang, F., and Chen, X. (2009) ^{68}Ga-labeled cyclic RGD dimers with Gly_3 and PEG_4 linkers: promising agents for tumor integrin $\alpha_v\beta_3$ PET imaging. *Eur. J. Nucl. Med. Mol. Imaging 36*, 947−957.

(24) Liu, Z., Liu, S., Wang, F., and Chen, X. (2009) Noninvasive imaging of tumor integrin expression using ^{18}F-labeled RGD dimer peptide with PEG_4 linkers. *Eur. J. Nucl. Med. Mol. Imaging 36*, 1296−1307.

(25) Dijkgraaf, I., Liu, S., Kruijtzer, J. A., Soede, A. C., Oyen, W. J. G., Liskamp, R. M., Corstens, F. H., and Boerman, O. C. (2007) Effect of linker variation on the in vitro and in vivo characteristics of an ^{111}In-labeled RGD Peptide. *Nucl. Med. Biol. 34*, 29−35.

(26) Dijkgraaf, I., Kruijtzer, J. A., Liu, S., Soede, A. C., Oyen, W. J. G., Corstens, F. H., Liskamp, R. M., and Boerman, O. C. (2007) Improved targeting of the $\alpha_v\beta_3$ integrin by multimerization of RGD peptides. *Eur. J. Nucl. Med. Mol. Imaging 34*, 267−273.

(27) Liu, S., Hsieh, W. Y., Kim, Y. S., and Mohammed, S. I. (2005) Effect of coligands on biodistribution characteristics of ternary ligand ^{99m}Tc complexes of a HYNIC-conjugated cyclic RGDfK dimer. *Bioconjugate Chem. 16*, 1580−1588.

(28) Jia, B., Shi, J., Yang, Z., Xu, B., Liu, Z., Zhao, H., Liu, S., and Wang, F. (2006) ^{99m}Tc-labeled cyclic RGDfK dimer: initial evaluation for SPECT imaging of glioma integrin $\alpha_v\beta_3$ expression. *Bioconjugate Chem. 17*, 1069−1076.

DOI: 10.1021/acs.bioconjchem.5b00327
Bioconjugate Chem. 2015, 26, 1413−1438

(29) Liu, S., He, Z. J., Hsieh, W. Y., Kim, Y. S., and Jiang, Y. (2006) Impact of PKM linkers on biodistribution characteristics of the ^{99m}Tc-labeled cyclic RGDfK dimer. *Bioconjugate Chem. 17*, 1499−1507.
(30) Liu, S., Hsieh, W. Y., Jiang, Y., Kim, Y. S., Sreerama, S. G., Chen, X., Jia, B., and Wang, F. (2007) Evaluation of a ^{99m}Tc-labeled cyclic RGD tetramer for noninvasive imaging integrin $\alpha_v\beta_3$-positive breast cancer. *Bioconjugate Chem. 18*, 438−446.
(31) Liu, S., Kim, Y. S., Hsieh, W. Y., and Sreerama, S. G. (2008) Coligand effects on solution stability, biodistribution and metabolism of ^{99m}Tc-labeled cyclic RGDfK tetramer. *Nucl. Med. Biol. 35*, 111−121.
(32) Jia, B., Liu, Z., Shi, J., Yu, Z. L., Yang, Z., Zhao, H. Y., He, Z. J., Liu, S., and Wang, F. (2008) Linker effects on biological properties of ^{111}In-labeled DTPA conjugates of a cyclic RGDfK dimer. *Bioconjugate Chem. 19*, 201−210.
(33) Wang, J. J., Kim, Y. S., He, Z. J., and Liu, S. (2008) ^{99m}Tc-labeling of HYNIC-conjugated cyclic RGDfK dimer and tetramer using EDDA as coligand. *Bioconjugate Chem. 19*, 634−642.
(34) Shi, J., Wang, L., Kim, Y. S., Zhai, S., Liu, Z., Chen, X., and Liu, S. (2008) Improving tumor uptake and excretion kinetics of ^{99m}Tc-labeled cyclic Arginine-Glycine-Aspartic (RGD) dimers with triglycine linkers. *J. Med. Chem. 51*, 7980−7990.
(35) Wang, L., Shi, J., Kim, Y. S., Zhai, S., Jia, B., Zhao, H., Liu, Z., Wang, F., Chen, X., and Liu, S. (2009) Improving tumor targeting capability and pharmacokinetics of ^{99m}Tc-labeled cyclic RGD dimers with PEG_4 linkers. *Mol. Pharmaceutics 6*, 231−245.
(36) Shi, J., Wang, L., Kim, Y. S., Zhai, S., Jia, B., Wang, F., and Liu, S. (2009) ^{99m}TcO(MAG_2-$3G_3$-dimer): A new integrin $\alpha_v\beta_3$-targeted radiotracer with high tumor uptake and favorable pharmacokinetics. *Eur. J. Nucl. Med. Mol. Imaging 36*, 1874−1884.
(37) Shi, J., Kim, Y. S., Zhai, S., Liu, Z., Chen, X., and Liu, S. (2009) Improving tumor uptake and pharmacokinetics of ^{64}Cu-labeled cyclic RGD dimers with triglycine and PEG_4 linkers. *Bioconjugate Chem. 20*, 750−759.
(38) Shi, J., Kim, Y. S., Chakraborty, S., Jia, B., Wang, F., and Liu, S. (2009) 2-Mercaptoacetylglycylglycyl (MAG_2) as a bifunctional chelator for ^{99m}Tc-labeling of cyclic RGD dimers: effects of technetium chelate on tumor uptake and pharmacokinetics. *Bioconjugate Chem. 20*, 1559−1568.
(39) Chakraborty, S., Liu, S., Kim, Y. S., Shi, J., Zhou, Y., and Wang, F. (2010) Evaluation of ^{111}In-labeled cyclic RGD peptides: tetrameric not tetravalent. *Bioconjugate Chem. 21*, 969−978.
(40) Zhou, Y., Kim, Y. S., Chakraborty, S., Shi, J., Gao, H., and Liu, S. (2011) ^{99m}Tc-Labeled cyclic RGD peptides for noninvasive monitoring of tumor integrin $\alpha_v\beta_3$ expression. *Mol. Imaging 10*, 386−97.
(41) Shi, J., Zhou, Y., Chakraborty, S., Kim, Y. S., Jia, B., Wang, F., and Liu, S. (2011) Evaluation of ^{111}In-labeled cyclic RGD peptides: effects of peptide and PEG_4 multiplicity on their tumor uptake, excretion kinetics and metabolic stability. *Theranostics 1*, 322−340.
(42) Shi, J., Jia, B., Kim, Y. S., Chakraborty, S., Zhou, Y., Wang, F., and Liu, S. (2011) Impact of bifunctional chelators on biological properties of ^{111}In-labeled cyclic peptide RGD dimers. *Amino Acids 41*, 1059−1070.
(43) Jia, B., Liu, Z., Zhu, Z., Shi, J., Jin, X., Zhao, H., Li, F., Liu, S., and Wang, F. (2011) Blood clearance kinetics, biodistribution and radiation dosimetry of a kit-formulated integrin $\alpha_v\beta_3$-selective radiotracer ^{99m}Tc-$3PRGD_2$ in non-human primates. *Mol. Imaging Biol. 13*, 730−736.
(44) Zhou, Y., Kim, Y. S., Chakraborty, S., Shi, J., Gao, H., and Liu, S. (2011) ^{99m}Tc-labeled cyclic RGD peptides for noninvasive monitoring of tumor integrin $\alpha_v\beta_3$ expression. *Mol. Imaging 10*, 386−397.
(45) Jacobson, O., Zhu, L., Niu, G., Szajek, L., Ma, Y., Sun, X., Yan, Y., Kiesewetter, D. O., Liu, S., and Chen, X. (2011) MicroPET imaging of integrin $\alpha_v\beta_3$ expressing tumors using ^{89}Zr-RGD peptides. *Mol. Imaging Biol. 13*, 1224−1233.
(46) Zhou, Y., Kim, Y. S., Lu, X., and Liu, S. (2012) Evaluation of ^{99m}Tc-labeled cyclic RGD dimers: impact of cyclic RGD peptides and ^{99m}Tc chelates on biological properties. *Bioconjugate Chem. 23*, 586−595.
(47) Ji, S., Zhou, Y., Shao, G., and Liu, S. (2013) $(HYNIC)_2$K: A bifunctional chelator useful for ^{99m}Tc-labeling of small biomolecules. *Bioconjugate Chem. 24*, 701−711.
(48) Ji, S., Czerwinski, A., Zhou, Y., Shao, G., Valenzuela, F., Sowiński, P., Chauhan, S., Pennington, M., and Liu, S. (2013) ^{99m}Tc-Galacto-RGD_2: a ^{99m}Tc-labeled cyclic RGD peptide dimer useful for tumor imaging. *Mol. Pharmaceutics 10*, 3304−3314.
(49) Yang, Y., Ji, S., and Liu, S. (2014) Impact of multiple negative charges on blood clearance and biodistribution characteristics of ^{99m}Tc-labeled dimeric cyclic RGD peptides. *Bioconjugate Chem. 25*, 1720−1729.
(50) Zheng, Y., Ji, S., Yang, Y., Tomaselli, E., and Liu, S. (2015) ^{111}In-Labeled cyclic RGD peptides useful as integrin $\alpha_v\beta_3$-targeted radiotracers for breast tumor imaging. *Nucl. Med. Biol. 42*, 137−145.
(51) Meyer, A., Auernheimer, J., Modlinger, A., and Kessler, H. (2006) Targeting RGD recognizing integrins: drug development, biomaterial research, tumor imaging and targeting. *Curr. Pharm. Des. 12*, 2723−2747.
(52) Liu, S. (2006) Radiolabeled multimeric cyclic RGD peptides as integrin $\alpha_v\beta_3$-targeted radiotracers for tumor imaging. *Mol. Pharmaceutics 3*, 472−487.
(53) Beer, A. J., and Schwaiger, M. (2008) Imaging of integrin $\alpha_v\beta_3$ expression. *Cancer Metastasis Rev. 27*, 631−644.
(54) Liu, Z., Wang, F., and Chen, X. (2008) Integrin $\alpha_v\beta_3$-targeted cancer therapy. *Drug Dev. Res. 69*, 329−339.
(55) Liu, S. (2009) Radiolabeled RGD peptides as integrin $\alpha_v\beta_3$-targeted radiotracers: maximizing binding affinity via bivalency. *Bioconjugate Chem. 20*, 2199−2213.
(56) Stollman, T. H., Ruers, T. J. M., Oyen, W. J. G., and Boerman, O. C. (2009) New targeted probes for radioimaging of angiogenesis. *Methods 48*, 188−192.
(57) Haubner, R., Beer, A. J., Wang, H., and Chen, X. (2010) Positron emission tomography tracers for imaging angiogenesis. *Eur. J. Nucl. Med. Mol. Imaging 37* (Suppl 1), S86−103.
(58) Beer, A. J., and Chen, X. (2010) Imaging of angiogenesis: from morphology to molecules and from bench to bedside. *Eur. J. Nucl. Med. Mol. Imaging 37* (Suppl 1), S1−3.
(59) Dijkgraaf, I., and Boerman, O. C. (2010) Molecular imaging of angiogenesis with SPECT. *Eur. J. Nucl. Med. Mol. Imaging 37* (Suppl 1), S104−S113.
(60) Chakraborty, S., and Liu, S. (2010) ^{99m}Tc and ^{111}In-labeling of small biomolecules: bifunctional chelators and related coordination chemistry. *Curr. Top. Med. Chem. 10*, 1113−1134.
(61) Zhou, Y., Chakraborty, S., and Liu, S. (2011) Radiolabeled cyclic RGD peptides as radiotracers for imaging tumors and thrombosis by SPECT. *Theranostics 1*, 58−82.
(62) Michalski, M. H., and Chen, X. (2011) Molecular imaging in cancer treatment. *Eur. J. Nucl. Med. Mol. Imaging 38*, 358−377.
(63) Beer, A. J., Kessler, H., Wester, H. J., and Schwaiger, M. (2011) PET Imaging of integrin $\alpha_V\beta_3$ expression. *Theranostics 1*, 48−57.
(64) Danhier, F., Le Breton, A., and Préat, V. (2012) RGD-based strategies to target alpha(v) beta(3) integrin in cancer therapy and diagnosis. *Mol. Pharmaceutics 9*, 2961−2973.
(65) Tateishi, U., Oka, T., and Inoue, T. (2012) Radiolabeled RGD Peptides as integrin $\alpha_v\beta_3$−targeted PET tracers. *Curr. Med. Chem. 19*, 3301−3309.
(66) Daghestani, H. N., and Day, B. W. (2010) (2010) Theory and applications of surface plasmon resonance, resonant Mirror, resonant waveguide grating, and dual polarization interferometry biosensors. *Sensors 10*, 9630−9646.
(67) Wienken, C. J., Baaske, P., Rothbauer, U., Braun, D., and Duhr, S. (2010) Protein-binding assays in biological liquid using microscale thermoresis. *Nat. Commun. 1*, 100.
(68) Liu, S. (2008) Bifunctional coupling agents for radiolabeling of biomolecules and target-specific delivery of metallic radionuclides. *Adv. Drug Delivery Rev. 60*, 1347−70.
(69) Liu, S., and Chakraborty, S. (2011) ^{99m}Tc-centered one-pot synthesis for preparation of ^{99m}Tc radiotracers. *Dalton Trans. 40*, 6077−6086.

DOI: 10.1021/acs.bioconjchem.5b00327
Bioconjugate Chem. 2015, 26, 1413−1438

(70) Liu, S. (2005) 6-Hydrazinonicotinamide derivatives as bifunctional coupling agents for ^{99m}Tc-labeling of small biomolecules. *Top. Curr. Chem. 252*, 193−216.
(71) Anderson, C. J., Green, M. A., and Yashi, Y. F. (2003) Chemistry of copper radionuclides and radiopharmaceutical products. In *Handbook of Radiopharmaceuticals: Radiochemistry and Applications* (Welch, M. J., and Redvanly, C. S., Eds.) pp 402−422, John Wiley & Sons, New York.
(72) Maecke, H., Hofmann, M., and Haberkorn, U. (2005) ^{68}Ga-labeled peptides in tumor imaging. *J. Nucl. Med. 46*, 172S−178S.
(73) Koukouraki, S., Strauss, L. G., Georgoulias, V., Schuhmacher, J., Haberkorn, U., Karkavitsas, N., and Dimitrakopoulou-Strauss, A. (2006) Evaluation of the pharmacokinetics of ^{68}Ga-DOTATOC in patients with metastatic neuroendocrine tumours scheduled for ^{90}Y-DOTATOC therapy. *Eur. J. Nucl. Med. Mol. Imaging 33*, 460−466.
(74) Henze, M., Dimitrakopoulou-Strauss, A., Milker-Zabel, S., Schuhmacher, J., Strauss, L. G., Doll, J., Mäcke, H. R., Eisenhut, M., Debus, J., and Haberkorn, U. (2005) Characterization of (^{68}Ga)-DOTA-D-Phe1-Tyr^3-octreotide (DOTATOC) kinetics in patients with meningiomas. *J. Nucl. Med. 46*, 763−769.
(75) Koukouraki, S., Strauss, L. G., Georgoulias, V., Eisenhut, M., Haberkorn, U., and Dimitrakopoulou-Strauss, A. (2006) Comparison of the pharmacokinetics of ^{68}Ga-DOTATOC and [^{18}F]FDG in patients with metastatic neuroendocrine tumours scheduled for ^{90}Y-DOTATOC therapy. *Eur. J. Nucl. Med. Mol. Imaging 33*, 1115−1122.
(76) Vaidyanathan, G., White, B. J., and Zalutsky, M. R. (2009) Propargyl 4-[^{18}F]fluorobenzoate: a putatively more stable prosthetic group for the fluorine-18 labeling of biomolecules *via* click chemistry. *Curr. Radiopharm. 2*, 63−74.
(77) Liu, S., Liu, Z., Chen, K., Yan, Y., Watzlowik, P., Wester, H. J., Chin, F. T., and Chen, X. (2010) ^{18}F-labeled galacto and PEGylated RGD dimers for PET imaging of $\alpha_v\beta_3$ integrin expression. *Mol. Imaging Biol. 12*, 530−538.
(78) Jacobson, O., Zhu, L., Ma, Y., Weiss, I. D., Sun, X., Niu, G., Kiesewetter, D. O., and Chen, X. (2011) Rapid and simple one-step F-18 labeling of peptides. *Bioconjugate Chem. 22*, 422−428.
(79) Glaser, M., Morrison, M., Solbakken, M., Arukwe, J., Karlsen, H., Wiggen, U., Champion, S., Kindberg, G. M., and Cuthbertson, A. (2008) Radiosynthesis and biodistribution of cyclic RGD peptides conjugated with novel [^{18}F]fluorinated aldehydecontaining prosthetic groups. *Bioconjugate Chem. 19*, 951−957.
(80) Li, Z. B., Wu, Z., Chen, K., Chin, F. T., and Chen, X. (2007) Click chemistry for ^{18}F-labeling of RGD peptides and microPET imaging of tumor integrin $\alpha_v\beta_3$ expression. *Bioconjugate Chem. 18*, 1987−1994.
(81) Hausner, S. H., Marik, J., Gagnon, M. K., and Sutcliffe, J. L. (2008) In vivo positron emission tomography (PET) imaging with an $\alpha_v\beta_6$ specific peptide radiolabeled using ^{18}F-"click" chemistry: evaluation and comparison with the corresponding 4-[^{18}F]-fluorobenzoyl- and 2-[^{18}F]fluoropropionyl-peptides. *J. Med. Chem. 51*, 5901−5904.
(82) Li, X., Link, J. M., Stekhova, S., Yagle, K. J., Smith, C., Krohn, K. A., and Tait, J. F. (2008) Site-specific labeling of annexin V with F-18 for apoptosis imaging. *Bioconjugate Chem. 19*, 1684−1688.
(83) Becaud, J., Mu, L., Karramkam, M., Schubiger, P. A., Ametamey, S. M., Graham, K., Stellfeld, T., Lehmann, L., Borkowski, S., Berndorff, D., et al. (2009) Direct one-step ^{18}F-labeling of peptides via nucleophilic aromatic substitution. *Bioconjugate Chem. 20*, 2254−2261.
(84) Hohne, A., Mu, L., Honer, M., Schubiger, P. A., Ametamey, S. M., Graham, K., Stellfeld, T., Borkowski, S., Berndorff, D., Klar, U., et al. (2008) Synthesis, ^{18}F-labeling, and in vitro and in vivo studies of bombesin peptides modified with silicon-based building blocks. *Bioconjugate Chem. 19*, 1871−1879.
(85) Mu, L., Hohne, A., Schubiger, P. A., Ametamey, S. M., Graham, K., Cyr, J. E., Dinkelborg, L., Stellfeld, T., Srinivasan, A., Voigtmann, U., et al. (2008) Silicon-based building blocks for one-step ^{18}F-radiolabeling of peptides for PET imaging. *Angew. Chem., Int. Ed. 47*, 4922−4925.
(86) Namavari, M., Cheng, Z., Zhang, R., De, A., Levi, J., Hoerner, J. K., Yaghoubi, S. S., Syud, F. A., and Gambhir, S. S. (2009) A novel method for direct site-specific radiolabeling of peptides using [^{18}F]FDG. *Bioconjugate Chem. 20*, 432−436.
(87) Wangler, C., Schirrmacher, R., Bartenstein, P., and Wangler, B. (2010) Click-chemistry reactions in radiopharmaceutical chemistry: fast and easy introduction of radiolabels into biomolecules for in vivo imaging. *Curr. Med. Chem. 17*, 1092−1116.
(88) Schirrmacher, R., Wängler, C., and Schirrmacher, E. (2007) Recent developments and trends in ^{18}F-radiochemistry: syntheses and applications. *Mini-Rev. Org. Chem. 4*, 317−329.
(89) Jacobson, O., and Chen, X. (2010) PET designated flouride-18 production and chemistry. *Curr. Top. Med. Chem. 10*, 1048−1059.
(90) McBride, W. J., Sharkey, R. M., Karacay, H., D'Souza, C. A., Rossi, E. A., Laverman, P., Chang, C. H., Boerman, O. C., and Goldenberg, D. M. (2009) A novel method of ^{18}F radiolabeling for PET. *J. Nucl. Med. 50*, 991−998.
(91) McBride, W. J., D'Souza, C. A., Sharkey, R. M., Karacay, H., Rossi, E. A., Chang, C. H., and Goldenberg, D. M. (2010) Improved ^{18}F labeling of peptides with a fluoride-aluminum-chelate complex. *Bioconjugate Chem. 21*, 1331−1340.
(92) Laverman, P., McBride, W. J., Sharkey, R. M., Eek, A., Joosten, L., Oyen, W. J. G., Goldenberg, D. M., and Boerman, O. C. (2010) A novel facile method of labeling octreotide with ^{18}F-fluorine. *J. Nucl. Med. 51*, 454−461.
(93) Liu, S., Liu, H., Jiang, H., Xu, Y., Zhang, H., and Cheng, Z. (2011) One-step radiosynthesis of ^{18}F-AlF-NOTA-RGD$_2$ for tumor angiogenesis PET imaging. *Eur. J. Nucl. Med. Mol. Imaging 38*, 1732−1741.
(94) D'Souza, C. A., McBride, W. J., Sharkey, R. M., Todaro, L. J., and Goldenberg, D. M. (2011) High-yielding aqueous ^{18}F-labeling of peptides via Al^{18}F chelation. *Bioconjugate Chem. 22*, 1793−1803.
(95) Lang, L., Li, W., Guo, N., Ma, Y., Zhu, L., Kiesewetter, D. O., Shen, B., Niu, G., and Chen, X. (2011) Comparison study of [^{18}F]FAl-NOTA-PRGD$_2$, [^{18}F]FPPRGD$_2$, and [^{68}Ga]Ga-NOTA-PRGD$_2$ for PET imaging of U87MG tumors in mice. *Bioconjugate Chem. 22*, 2415−2422.
(96) McBride, W. J., D'Souza, C. A., Karacay, H., Sharkey, R. M., and Goldenberg, D. M. (2012) New lyophilized kit for rapid radiofluorination of peptides. *Bioconjugate Chem. 23*, 538−547.
(97) Laverman, P., D'Souza, C. A., Eek, A., McBride, W. J., Sharkey, R. M., Oyen, W. J. G., Goldenberg, D. M., and Boerman, O. C. (2012) Optimized labeling of NOTA-conjugated octreotide with F-18. *Tumor Biol. 33*, 427−434.
(98) Sheldrake, H. M., and Patterson, L. P. (2014) Strategies to inhibit tumor associated integrin receptors: rationale for dual and multi-antagonists. *J. Med. Chem. 57*, 6301−6315.
(99) Barczyk, M., Carracedo, S., and Gullberg, D. (2010) Integrins. *Cell Tissue Res. 339*, 269−280.
(100) Hodivala-Dilke, K. (2008) $\alpha_v\beta_3$ integrin and angiogenesis: a moody integrin in a changing Environment. *Curr. Opin. Cell Biol. 20*, 514−519.
(101) Desgrosellier, J. S., and Cheresh, D. A. (2010) Integrins in cancer: biological implications and therapeutic opportunities. *Nat. Rev. Cancer 10*, 9−22.
(102) Chao, J. T., Meininger, G. A., Patterson, J. L., Jones, S. A., Partridge, C. R., Neiger, J. D., Williams, E. S., Kaufman, S. J., Ramos, K. S., and Wilson, E. (2004) Regulation of α7-integrin expression in vascular smooth muscle by injury-induced atherosclerosis. *Am. J. Physiol. Heart Circ. Physiol. 287*, H381−389.
(103) Antonov, A. S., Kolodgie, F. D., Munn, D. H., and Gerrity, R. G. (2004) Regulation of macrophage foam cell formation by $\alpha_v\beta_3$ integrin: potential role in human atherosclerosis. *Am. J. Pathol. 165*, 247−58.
(104) Zecchinon, L., Fett, T., Baise, E., and Desmecht, D. (2004) Characterization of the caprine (Capra hircus) beta-2 integrin CD18-encoding cDNA and identification of mutations potentially responsible for the ruminantspecific virulence of Mannheimia haemolytica. *Mol. Membr. Biol. 21*, 289−95.

DOI: 10.1021/acs.bioconjchem.5b00327
Bioconjugate Chem. 2015, 26, 1413−1438

(105) Isberg, R. R., and Van Nhieu, G. T. (1995) The mechanism of phagocytic uptake promoted by invasin-integrin interaction. *Trends Cell Biol. 5*, 120−4.
(106) Morris, M. A., and Ley, K. (2004) Trafficking of natural killer cells. *Curr. Mol. Med. 4*, 431−438.
(107) Sloan, E. K., Pouliot, N., Stanley, K. L., Chia, J., Moseley, J. M., Hards, D. K., and Anderson, R. L. (2006) Tumor-specific expression of $\alpha_v\beta_3$ integrin promotes spontaneous metastasis of breast cancer to bone. *Breast Cancer Res. 8*, R20.
(108) Zhao, Y., Bachelier, R., Treilleux, I., Pujuguet, P., Peyruchaud, O., Baron, R., Clément-Lacroix, P., and Clézardin, P. (2007) Tumor $\alpha_v\beta_3$ integrin is a therapeutic target for breast cancer bone metastases. *Cancer Res. 67*, 5821−5830.
(109) Trikha, M., Timar, J., Zacharek, A., Nemeth, J. A., Cai, Y., Dome, B., Somlai, B., Raso, E., Ladanyi, A., and Honn, K. V. (2002) Role for β_3 integrins in human melanoma growth and survival. *Int. J. Cancer 101*, 156−167.
(110) Bello, L., Francolini, M., Marthyn, P., Zhang, J., Carroll, R. S., Nikas, D. C., Strasser, J. F., Villani, R., Cheresh, D. A., and Black, P. M. (2001) $\alpha_v\beta_3$ and $\alpha_v\beta_5$ integrin expression in glioma periphery. *Neurosurgery 49*, 380−390.
(111) Gasparini, G., Brooks, P. C., Biganzoli, E., Vermeulen, P. B., Bonoldi, E., Dirix, L. Y., Ranieri, G., Miceli, R., and Cheresh, D. A. (1998) Vascular integrin $\alpha_v\beta_3$: a new prognostic indicator in breast cancer. *Clin. Cancer Res. 4*, 2625−2634.
(112) Albelda, S. M., Mette, S. A., Elder, D. E., Stewart, R., Damjanovich, L., Herlyn, M., and Buck, C. A. (1990) Integrin distribution in malignant melanoma: association of the β_3 subunit with tumor progression. *Cancer Res. 50*, 6757−6764.
(113) Falcioni, R., Cimino, L., Gentileschi, M. P., D'Agnano, I., Zupi, G., Kennel, S. J., and Sacchi, A. (1994) Expression of β_1, β_3, β_4, and β_5 integrins by human lung carcinoma cells of different histotypes. *Exp. Cell Res. 210*, 113−122.
(114) Sengupta, S., Chattopadhyay, N., Mitra, A., Ray, S., Dasgupta, S., and Chatterjee, A. (2001) Role of $\alpha_v\beta_3$ integrin receptors in breast tumor. *J. Exp. Clin. Cancer Res. 20*, 585−590.
(115) Zitzmann, S., Ehemann, V., and Schwab, M. (2002) Arginine-Glycine-Aspartic acid (RGD)-peptide binds to both tumor and tumor-endothelial cells in vivo. *Cancer Res. 62*, 5139−43.
(116) Taherian, A., Li, X., Liu, Y., and Haas, T. A. (2011) Differences in integrin expression and signalling within human breast cancer cells. *BMC Cancer 11*, 293.
(117) Gupta, A., Cao, W., and Chellaiah, M. A. (2012) Integrin $\alpha_v\beta_3$ and CD44 pathways in metastatic prostate cancer cells support osteoclastogenesis via a Runx2/Smad 5/receptor activator of NF-κB ligand signaling axis. *Mol. Cancer 11*, 66.
(118) Cooper, C. R., Chay, C. H., and Pienta, K. J. (2002) The role of $\alpha_v\beta_3$ in prostate cancer progression. *Neoplasia 4*, 191−194.
(119) Pilch, J., Habermann, R., and Felding-Habermann, B. (2002) Unique ability of integrin $\alpha_v\beta_3$ to support tumor cell arrest under dynamic flow conditions. *J. Biol. Chem. 277*, 21930−21938.
(120) Dittmar, T., Heyder, C., Gloria-Maercker, E., Hatzmann, W., and Zänker, K. S. (2008) Adhesion molecules and chemokines: the navigation system for circulating tumor (stem) cells to metastasize in an organ-specific manner. *Clin. Exp. Metastasis 25*, 11−32.
(121) Omar, O., Lennerås, M., Svensson, S., Suska, F., Emanuelsson, L., Hall, J., Nannmark, U., and Thomsen, P. (2010) Integrin and chemokine receptor gene expression in implant-adherent cells during early osseointegration. *J. Mater. Sci.: Mater. Med. 21*, 969−980.
(122) Minn, A. J., Kang, Y., Serganova, I., Gupta, G. P., Giri, D. D., Doubrovin, M., Ponomarev, V., Gerald, W. L., Blasberg, R., and Massagué, J. (2005) Distinct organ-specific metastatic potential of individual breast cancer cells and primary tumors. *J. Clin. Invest. 115*, 44−55.
(123) Lorger, M., Krueger, J. S., O'Neal, M., Staflin, K., and Felding-Habermann, B. (2009) Activation of tumor cell integrin $\alpha_v\beta_3$ controls angiogenesis and metastatic growth in the brain. *Proc. Natl. Acad. Sci. U. S. A. 106*, 10666−10671.
(124) Sloan, E. K., Pouliot, N., Stanley, K. L., Chia, J., Moseley, J. M., Hards, D. K., and Anderson, R. L. (2006) Tumor-specific expression of $\alpha_v\beta_3$ integrin promotes spontaneous metastasis of breast cancer to bone. *Breast Cancer Res. 8*, R20.
(125) Gottschalk, K. E., and Kessler, H. (2002) The structures of integrins and integrin-ligand complexes: Implications for drug design and signal transduction. *Angew. Chem., Int. Ed. 41*, 3767−3774.
(126) Kumar, C. C. (2003) Integrin $\alpha_v\beta_3$ as a therapeutic target for blocking tumor-induced angiogenesis. *Curr. Drug Targets 4*, 123−131.
(127) D'Andrea, L. D., Del Gatto, A., Pedone, C., and Benedetti, E. (2006) Peptide-based molecules in angiogenesis. *Chem. Biol. Drug Des. 67*, 115−26.
(128) Gottschalk, K. E., and Kessler, H. (2002) The structures of integrins and integrin-ligand complexes: Implications for drug design and signal transduction. *Angew. Chem., Int. Ed. 41*, 3767−3774.
(129) Pfaff, M., Tangemann, K., Müller, B., Gurrath, M., Muller, G., Kessler, H., Timpl, R., and Engel, J. (1994) Selective recognition of cyclic RGD peptides of NMR defined conformation by $\alpha_{IIb}\beta_3$, $\alpha_v\beta_3$, and $\alpha_5\beta_1$ integrins. *J. Biol. Chem. 269*, 20233−20238.
(130) Gurrath, M., Müller, G., Kessler, H., Aumailley, M., and Timpl, R. (1992) Conformation/activity studies of rationally designed potent anti-adhesive RGD peptides. *Eur. J. Biochem. 210*, 911−921.
(131) Muller, G., Gurrath, M., Kessler, H., and Timpl, R. (1992) Dynamic forcing, a method for evaluating activity and selectivity profiles of RGD (Arg-Gly-Asp) peptides. *Angew. Chem., Int. Ed. Engl. 31*, 326−8.
(132) Haübner, R., Gratias, R., Diefenbach, B., Goodman, S. L., Jonczyk, A., and Kessler, H. (1996) Structural and functional aspect of RGD-containing cyclic pentapeptides as highly potent and selective integrin $\alpha_v\beta_3$ antagonist. *J. Am. Chem. Soc. 118*, 7461−7472.
(133) Giannis, A., and Rubsam, F. (1997) Integrin antagonists and other low molecular weight compounds as inhibitors of angiogenesis: new drugs in cancer therapy. *Angew. Chem., Int. Ed. Engl. 36*, 588−590.
(134) Haubner, R., Finsinger, D., and Kessler, H. (1997) Stereoisomeric peptide libraries and peptidomimetics for designing selective inhibitors of the $\alpha_v\beta_3$ integrin for a new cancer therapy. *Angew. Chem., Int. Ed. Engl. 36*, 1374−1389.
(135) Alghisi, G. C., Ponsonnet, L., and Rüegg, C. (2009) The integrin antagonist cilengitide activates $\alpha_v\beta_3$, disrupts VE-cadherin localization at cell junctions and enhances permeability in endothelial cells. *PLoS One 4*, e4449.
(136) Yamada, S., Bu, X. Y., Khankaldyyan, V., Gonzales-Gomez, I., McComb, J. G., and Laug, W. E. (2006) Effect of the angiogenesis inhibitor Cilengitide (EMD 121974) on glioblastoma growth in nude mice. *Neurosurgery 59*, 1304−1312.
(137) Bello, L., Lucini, V., Giussani, C., Carrabba, G., Pluderi, M., Scaglione, F., Tomei, G., Villani, R., Black, P. M., Bikfalvi, A., et al. (2003) IS20I, a specific $\alpha_v\beta_3$ integrin inhibitor, reduces glioma growth in vivo. *Neurosurgery 52*, 177−185.
(138) Burke, P. A., DeNardo, S. J., Miers, L. A., Lamborn, K. R., Matzku, S., and DeNardo, G. L. (2002) Cilengitide targeting of $\alpha_v\beta_3$ integrin receptor synergizes with radioimmunotherapy to increase efficacy and apoptosis in breast cancer xenografts. *Cancer Res. 62*, 4263−4272.
(139) Nabors, L. B., Mikkelsen, T., Rosenfeld, S. S., Hochberg, F., Akella, N. S., Fisher, J. D., Cloud, G. A., Zhang, Y., Carson, K., Wittemer, S. M., et al. (2007) Phase I and correlative biology study of Cilengitide in patients with recurrent malignant glioma. *J. Clin. Oncol. 25*, 1651−1657.
(140) Reardon, D. A., Fink, K. L., Mikkelsen, T., Cloughesy, T. F., O'Neill, A., Plotkin, S., Glantz, M., Ravin, P., Raizer, J. J., Rich, K. M., et al. (2008) Randomized phase II study of cilengitide, an integrin-targeting arginine-glycine-aspartic acid peptide, in recurrent glioblastoma multiforme. *J. Clin. Oncol. 26*, 5610−5617.
(141) Friess, H., Langrehr, J. M., Oettle, H., Raedle, J., Niedergethmann, M., Dittrich, C., Hossfeld, D. K., Stöger, H., Neyns, B., Herzog, P., et al. (2006) A randomized multicenter phase II trial of the angiogenesis inhibitor Cilengitide (EMD 121974) and

DOI: 10.1021/acs.bioconjchem.5b00327
Bioconjugate Chem. 2015, 26, 1413−1438

gemcitabine compared with gemcitabine alone in advanced unresectable pancreatic cancer. *BMC Cancer 6*, 285.
(142) Reardon, D. A., Nabors, L. B., Stupp, R., and Mikkelsen, T. (2008) Cilengitide: an integrin-targeting arginine-glycine-aspartic acid peptide with promising activity for glioblastoma multiforme. *Expert Opin. Invest. Drugs 17*, 1225−1235.
(143) Bach, A. C., Espina, J. R., Jackson, S. A., Stouten, P. F. W., Duke, J. L., Mousa, S. A., and DeGrado, W. F. (1996) Type II′ to type Iβ-turn swap changes specificity for integrins. *J. Am. Chem. Soc. 118*, 293−294.
(144) Harlow, R. L. (1993) The structure of water as organized in an RGD peptide crystal at −80 °C. *J. Am. Chem. Soc. 115*, 9838−9839.
(145) Saitoh, H., and Aungst, B. J. (1997) Prodrug and analog approaches to improving the intestinal absorption of a cyclic peptide, GPIIb/IIIa receptor antagonist. *Pharm. Res. 14*, 1026−9.
(146) Edwards, D. S., Liu, S., Barrett, J. A., Harris, A. R., Looby, R. J., Ziegler, M. C., Heminway, S. J., and Carroll, T. R. (1997) New and versatile ternary ligand system for technetium radiopharmaceuticals: water soluble phosphines and tricine as coligands in labeling a hydrazinonicotinamide-modified cyclic glycoprotein IIb/IIIa receptor antagonist with ^{99m}Tc. *Bioconjugate Chem. 8*, 146−154.
(147) Oyen, W. J. G., Boerman, O. C., Brouwers, F. M., Barrett, J. A., Verheugt, F. W., Ruiter, D. J., Corstens, F. H., and van der Meer, J. W. (2000) Scintigraphic detection of acute experimental endocarditis with the technetium-99m labelled glycoprotein IIb/IIIa receptor antagonist DMP444. *Eur. J. Nucl. Med. Mol. Imaging 27*, 392−399.
(148) Mitchel, J., Waters, D., Lai, T., White, M., Alberghini, T., Salloum, A., Knibbs, D., Li, D., and Heller, G. V. (2000) Identification of coronary thrombus with a IIb/IIIa platelet inhibitor radiopharmaceutical, technetium-99m DMP-444: a canine model. *Circulation 101*, 1643−1646.
(149) Scharn, D. M., Oyen, W. J. G., Klemm, P. L., Wijnen, M. H., and vanderVliet, J. A. (2002) Assessment of prosthetic vascular graft thrombogenicity using the technetium-99m labeled glycoprotein IIb/IIIa receptor antagonist DMP444 in a dog model. *Cardiovasc. Surg. 10*, 566−569.
(150) Sakuma, T., Sari, I., Goodman, C. N., Lindner, J. R., Klibanov, A. L., and Kaul, S. (2005) Simultaneous integrin $\alpha_v\beta_3$ and glycoprotein IIb/IIIa inhibition causes reduction in infarct size in a model of acute coronary thrombosis and primary angioplasty. *Cardiovasc. Res. 66*, 552−561.
(151) Sakuma, T., Sklenar, J., Leong-Poi, H., Goodman, N. C., Glover, D. K., and Kaul, S. (2004) Molecular imaging identifies regions with microthromboemboli during primary angioplasty in acute coronary thrombosis. *J. Nucl. Med. 45*, 1194−1200.
(152) Klem, J. A., Schaffer, J. V., Crane, P. D., Barrett, J. A., Henry, G. A., Canestri, L., and Ezekowitz, M. D. (2000) Detection of deep venous thrombosis by DMP 444, a platelet IIb/IIIa antagonist: a preliminary report. *J. Nucl. Cardiol. 7*, 359−364.
(153) Brouwers, F. M., Oyen, W. J. J., Boerman, O. C., Barrett, J. A., Verheugt, F. W., Corstens, F. H., and Van der Meer, J. W. (2003) Evaluation of Tc-99m-labeled glycoprotein IIb/IIIa receptor antagonist DMP444 SPECT in patients with infective endocarditis. *Clin. Nucl. Med. 28*, 480−484.
(154) Fang, W., He, J., Kim, Y. S., Zhou, Y., and Liu, S. (2011) Evaluation of ^{99m}Tc-labeled cyclic RGD peptide with a PEG_4 linker for thrombosis imaging: comparison with DMP444. *Bioconjugate Chem. 22*, 1715−1722.
(155) Beer, A. J., Haubner, R., Goebel, M., Luderschmidt, S., Spilker, M. E., Wester, H. J., Weber, W. A., and Schwaiger, M. (2005) Biodistribution and pharmacokinetics of the $\alpha_v\beta_3$-selective tracer ^{18}F-Galacto-RGD in cancer patients. *J. Nucl. Med. 46*, 1333−1341.
(156) Haubner, R., Weber, W. A., Beer, A. J., Vabulience, E., Reim, D., Sarbia, M., Becker, K. F., Goebel, M., Hein, R., Wester, H. J., et al. (2005) Noninvasive visualization of the activated $\alpha_v\beta_3$ integrin in cancer patients by positron emission tomography and [^{18}F]Galacto-RGD. *PLoS Med. 2* (e70), 244−252.
(157) Beer, A. J., Grosu, A. L., Carlsen, J., Kolk, A., Sarbia, M., Stangier, I., Watzlowik, P., Wester, H. J., Haubner, R., and Schwaiger, M. (2007) [^{18}F]Galacto-RGD positron emission tomography for imaging of $\alpha_v\beta_3$ expression on the neovasculature in patients with squamous cell carcinoma of the head and neck. *Clin. Cancer Res. 13*, 6610−6616.
(158) Beer, A. J., Niemeyer, M., Carlsen, J., Sarbia, M., Nahrig, J., Watzlowik, P., Wester, H. J., Harbeck, N., and Schwaiger, M. (2008) Patterns of $\alpha_v\beta_3$ expression in primary and metastatic human breast cancer as shown by ^{18}F-Galacto-RGD PET. *J. Nucl. Med. 49*, 255−259.
(159) Kenny, L. M., Coombes, R. C., Oulie, I., Contractor, K. B., Miller, M., Spinks, T. J., McParland, B., Cohen, P. S., Hui, A., Palmieri, C., et al. (2008) Phase I trial of the positron-emitting Arg-Gly-Asp (RGD) peptide radioligand ^{18}F-AH111585 in breast cancer patients. *J. Nucl. Med. 49*, 879−886.
(160) Felding-Habermann, B., Habermann, R., Saldivar, E., and Ruggeri, Z. M. (1996) Role of β_3 integrins in melanoma cell adhesion to activated platelets under flow. *J. Biol. Chem. 271*, 5892−900.
(161) Bakewell, S. J., Nestor, P., Prasad, S., Tomasson, M. H., Dowland, N., Mehrotra, M., Scarborough, R., Kanter, J., Abe, K., Phillips, D., et al. (2003) Platelet and osteoclast β_3 integrins are critical for bone metastasis. *Proc. Natl. Acad. Sci. U. S. A. 100*, 14205−14210.
(162) Goodman, S. L., Grote, H. J., and Wilm, C. (2012) Matched rabbit monoclonal antibodies against αv-series integrins reveal a novel $\alpha_v\beta_3$-LIBS epitope, and permit routine staining of archival paraffin samples of human tumors. *Biol. Open 1*, 329−340.
(163) Böger, C., Kalthoff, H., Goodman, S. L., Behrens, H. M., and Röcken, C. (2014) Integrins and their ligands are expressed in non-small cell lung cancer but not correlated with parameters of disease progression. *Virchows Arch. 464*, 69−78.
(164) Roth, P., Silginer, M., Goodman, S. L., Hasenbach, K., Thies, S., Maurer, G., Schraml, P., Tabatabai, G., Moch, H., Tritschler, I., et al. (2013) Integrin control of the transforming growth factor-β pathway in glioblastoma. *Brain 136*, 564−576.
(165) Vogetseder, A., Thies, S., Ingold, B., Roth, P., Weller, M., Schraml, P., Goodman, S. L., and Moch, H. (2013) av-Integrin isoform expression in primary human tumors and brain metastases. *Int. J. Cancer 133*, 2362−2371.
(166) Monferran, S., Skuli, N., Delmas, C., Favre, G., Bonnet, J., Cohen-Jonathan-Moyal, E., and Toulas, C. (2008) $\alpha_v\beta_3$ and $\alpha_v\beta_5$ Integrins control glioma cell response to ionizing radiation through ILK and RhoB. *Int. J. Cancer 123*, 357−364.
(167) Bianchi-Smiraglia, A., Paesante, S., and Bakin, A. V. (2013) Integrin β_5 contributes to the tumorigenic potential of breast cancer cells through the Src-FAK and MEK-ERK signaling pathways. *Oncogene 32*, 3049−3058.
(168) Sung, V., Stubbs, J. T. I., Fisher, L., Aaron, A. D., and Thompson, E. W. (1998) Bone sialoprotein supports breast cancer cell adhesion proliferation and migration through differential usage of the $\alpha_v\beta_3$ and $\alpha_v\beta_5$ integrins. *J. Cell. Physiol. 176*, 482−494.
(169) Humphries, J. D., Byron, A., and Humphries, M. J. (2006) Integrin ligands at a glance. *J. Cell Sci. 119*, 3901−3903.
(170) De Corte, B. L., Kinney, W. A., Liu, L., Ghosh, S., Brunner, L., Hoekstra, W. J., Santulli, R. J., Tuman, R. W., Baker, J., Burns, C., et al. (2004) Piperidine-containing β- arylpropionic acids as potent antagonists of $\alpha_v\beta_3/\alpha_v\beta_5$ integrins. *Bioorg. Med. Chem. Lett. 14*, 5227−5232.
(171) Letourneau, J. J., Liu, J., Ohlmeyer, M. H. J., Riviello, C., Rong, Y., Li, H., Appell, K. C., Bansal, S., Jacob, B., Wong, A., et al. (2009) Synthesis and initial evaluation of novel, non-peptidic antagonists of the αv-integrins $\alpha_v\beta_3$ and $\alpha_v\beta_5$. *Bioorg. Med. Chem. Lett. 19*, 352−355.
(172) Mammen, M., Choi, S. K., and Whitesides, G. M. (1998) Polyvalent interactions in biological systems: implications for design and use of multivalent ligands and inhibitors. *Angew. Chem., Int. Ed. 37*, 2754−2794.
(173) Goel, A., Baranowska-Kortylewicz, J., Hinrichs, S. H., Wisecarver, J., Pavlinkova, G., Augustine, S., Colcher, D., Booth, B. J. M., and Batra, S. K. (2001) ^{99m}Tc-labeled divalent and tetravalent CC49 single-chain Fv's: novel imaging agents for rapid *in vivo* localization of human colon carcinoma. *J. Nucl. Med. 42*, 1519−1527.

DOI: 10.1021/acs.bioconjchem.5b00327
Bioconjugate Chem. 2015, 26, 1413−1438

(174) Viti, F., Tarli, L., Giovannoni, L., Zardi, L., and Neri, D. (1999) Increased binding affinity and valence of recombinant antibody fragments lead to improved targeting of tumoral angiogenesis. *Cancer Res. 59*, 347−352.
(175) Liu, S., Edwards, D. S., Ziegler, M. C., Harris, A. R., Hemingway, S. J., and Barrett, J. A. (2001) ^{99m}Tc-Labeling of a hydrazinonictotinamide-conjugated vitronectin receptor antagonist. *Bioconjugate Chem. 12*, 624−629.
(176) Liu, S., Cheung, E., Rajopadhye, M., Ziegler, M. C., and Edwards, D. S. (2001) ^{90}Y- and ^{177}Lu-labeling of a DOTA-conjugated vitronectin receptor antagonist for tumor therapy. *Bioconjugate Chem. 12*, 559−568.
(177) Janssen, M., Oyen, W. J. G., Massuger, L. F. A. G., Frielink, C., Dijkgraaf, I., Edwards, D. S., Rajopadhye, M., Corsten, F. H. M., and Boerman, O. C. (2002) Comparison of a monomeric and dimeric radiolabeled RGD-peptide for tumor targeting. *Cancer Biother.Radiopharm. 17*, 641−646.
(178) Janssen, M., Oyen, W. J. G., Dijkgraaf, I., Massuger, L. F. A. G., Frielink, C., Edwards, D. S., Radjopadhye, M., Boonstra, H., Corstens, F. H. M., and Boerman, O. C. (2002) Tumor targeting with radiolabeled $\alpha_v\beta_3$ integrin binding peptides in a nude mice model. *Cancer Res. 62*, 6146−6151.
(179) Chen, X., Liu, S., Hou, Y., Tohme, M., Park, R., Bading, J. R., and Conti, P. S. (2004) MicroPET imaging of breast cancer α_v-integrin expression with ^{64}Cu-labeled dimeric RGD peptides. *Mol. Imag. Biol. 6*, 350−359.
(180) Li, Z., Wu, Z., Chen, K., Ryu, E. K., and Chen, X. (2008) ^{18}F-Labeled BBN-RGD heterodimer for prostate cancer imaging. *J. Nucl. Med. 49*, 453−461.
(181) Liu, Z., Yan, Y., Liu, S., Wang, F., and Chen, X. (2009) ^{18}F, ^{64}Cu, and ^{68}Ga labeled RGD-bombesin heterodimeric peptides for PET imaging of breast cancer. *Bioconjugate Chem. 20*, 1016−1025.
(182) Liu, Z., Yan, Y., Chin, F. T., Wang, F., and Chen, X. (2009) Dual integrin and gastrin-releasing peptide receptor targeted tumor imaging using ^{18}F-labeled PEGylated RGD-bombesin heterodimer ^{18}F-FB-PEG3-Glu-RGD-BBN. *J. Med. Chem. 52*, 425−432.
(183) Zheng, Y., Ji, S., Czerwinski, A., Valenzuela, F., Pennington, M., and Liu, S. (2014) FITC-conjugated dimeric cyclic RGD peptides as fluorescent probes for in vitro assays of integrin $\alpha_v\beta_3$. *Bioconjugate Chem. 25*, 1925−1941.
(184) O'Connor, J. P., Jackson, A., Parker, G. J., and Jayson, G. C. (2007) DCE-MRI biomarkers in the clinical evaluation of antiangiogenic and vascular disrupting agents. *Br. J. Cancer 96*, 189−195.
(185) de Groot, J. F., Fuller, G., Kumar, A. J., Piao, Y., Eterovic, K., Ji, Y., and Conrad, C. A. (2010) Tumor invasion after treatment of glioblastoma with bevacizumab: radiographic and pathologic correlation in humans and mice. *Neuro-oncology 12*, 233−242.
(186) Foote, R. L., Weidner, N., Harris, J., Hammond, E., Lewis, J. E., Vuong, T., Ang, K. K., and Fu, K. K. (2005) Evaluation of tumor angiogenesis measured with microvessel density (MVD) as a prognostic indicator in nasopharyngeal carcinoma: results of RTOG 9505. *Int. J. Radiat. Oncol., Biol., Phys. 61*, 745−753.
(187) Bauerle, T., Komljenovic, D., Merz, M., Berger, M. R., Goodman, S. L., and Semmler, W. (2011) Cilengitide inhibits progression of experimental breast cancer bone metastases as imaged noninvasively using VCT, MRI and DCE-MRI in a longitudinal in vivo study. *Int. J. Cancer 128*, 2453−2462.
(188) Zhang, Y., Cole, T., Tapang, P., Luo, F., Hradil, V., Jiang, F., Luo, Y., Albert, D., and Fox, G. B. (2010) Total lesion glycolysis and FDG SUV as early readouts of tumor response to Linifanib (ABT-869) in SCID mice with HT1080 xenografts. *J. Nucl. Med. 51*, 111−111.
(189) Heldin, C. H., Ostman, A., and Ronnstrand, L. (1998) Signal transduction via platelet-derived growth factor receptors. *Biochim. Biophys. Acta, Rev. Cancer 1378*, F79−113.
(190) Woodard, A. S., Garcia-Cardena, G., Leong, M., Madri, J. A., Sessa, W. C., and Languino, L. R. (1998) The synergistic activity of $\alpha_v\beta_3$ integrin and PDGF receptor increases cell migration. *J. Cell Sci. 111*, 469−478.
(191) Soldi, R., Mitola, S., Strasly, M., Defilippi, P., Tarone, G., and Bussolino, F. (1999) Role of $\alpha_v\beta_3$ integrin in the activation of vascular endothelial growth factor receptor-2. *EMBO J. 18*, 882−892.
(192) Borges, E., Jan, Y., and Ruoslahti, E. (2000) Platelet-derived growth factor receptor beta and vascular endothelial growth factor receptor 2 bind to the beta 3 integrin through its extracellular domain. *J. Biol. Chem. 275*, 39867−39873.
(193) Mahabeleshwar, G. H., Feng, W., Reddy, K., Plow, E. F., and Byzova, T. V. (2007) Mechanisms of integrin-vascular endothelial growth factor receptor cross-activation in angiogenesis. *Circ. Res. 101*, 570−580.
(194) Somanath, P. R., Ciocea, A., and Byzova, T. V. (2009) Integrin and growth factor receptor alliance in angiogenesis. *Cell Biochem. Biophys. 53*, 53−64.
(195) Beer, A. J., and Schwaiger, M. (2011) PET of $\alpha_v\beta_3$-integrin and $\alpha_v\beta_5$-integrin expression with ^{18}F-fluciclatide for assessment of response to targeted therapy: ready for prime time? *J. Nucl. Med. 52*, 335−337.
(196) Morrison, M. S., Ricketts, S. A., Barnett, J., Cuthbertson, A., Tessier, J., and Wedge, S. R. (2008) Use of a novel Arg-Gly-Asp radioligand, ^{18}F-AH111585, to determine changes in tumor vascularity after antitumor therapy. *J. Nucl. Med. 50*, 116−122.
(197) Battle, M. R., Goggi, J. L., Allen, L., Barnett, J., and Morrison, M. S. (2011) Monitoring tumor response to antiangiogenic sunitinib therapy with ^{18}F-fluciclatide, an ^{18}F-labeled $\alpha_v\beta_3$-integrin and $\alpha_v\beta_5$-integrin imaging agent. *J. Nucl. Med. 52*, 424−430.
(198) Dumont, R. A., Hildebrandt, I., Su, H., Haubner, R., Reischl, G., Czernin, J. G., Mischel, P. S., and Weber, W. A. (2009) Noninvasive imaging of $\alpha_v\beta_3$ function as a predictor of the antimigratory and antiproliferative effects of dasatinib. *Cancer Res. 69*, 3173−3179.
(199) Ji, S., Zhou, Y., Shao, G., Liu, S., Voorbach, M. J., Luo, Y., Cole, T., Zhang, Y., Albert, D. H., and Mudd, S. R. (2013) Monitoring tumor response to linifanib therapy with SPECT/CT using the $\alpha_v\beta_3$-targeted radiotracer ^{99m}Tc-3P-RGD$_2$. *J. Pharmacol. Exp. Ther. 346*, 251−258.
(200) Ji, S., Zheng, Y., Shao, G., Zhou, Y., and Liu, S. (2013) Integrin $\alpha_v\beta_3$−targeted radiotracer ^{99m}Tc-3P-RGD$_2$ useful for noninvasive monitoring of breast tumor response to antiangiogenic linifanib therapy but not anti-integrin $\alpha_v\beta_3$ RGD$_2$ therapy. *Theranostics 3*, 816−830.
(201) Zhou, J., Goh, B. C., Albert, D. H., and Chen, C. S. (2009) ABT-869, a promising multi-targeted tyrosine kinase inhibitor: from bench to bedside. *J. Hematol. Oncol. 2*, 33−46.
(202) Jiang, F., Albert, D. H., Luo, Y., Tapang, P., Zhang, K., Davidsen, S. K., Fox, G. B., Lesniewski, R., and McKeegan, E. M. (2011) ABT-869, a multitargeted receptor tyrosine kinase inhibitor, reduces tumor microvascularity and improves vascular wall integrity in preclinical tumor models. *J. Pharmacol. Exp. Ther. 338*, 134−142.
(203) Hernandez-Davies, J. E., Zape, J. P., Landaw, E. M., Tan, X., Presnell, A., Griffith, D., Heinrich, M. C., Glaser, K. B., and Sakamoto, K. M. (2011) The multitargeted receptor tyrosine kinase inhibitor linifanib (ABT-869) induces apoptosis through an Akt and glycogen synthase kinase 3beta-dependent pathway. *Mol. Cancer Ther. 10*, 949−959.
(204) Luo, Y., Jiang, F., Cole, T. B., Hradil, V. P., Reuter, D., Chakravartty, A., Albert, D. H., Davidsen, S. K., Cox, B. F., McKeegan, E. M., et al. (2012) A novel multi-targeted tyrosine kinase inhibitor, linifanib (ABT-869), produces functional and structural changes in tumor vasculature in an orthotopic rat glioma model. *Cancer Chemother. Pharmacol. 69*, 911−921.
(205) Wong, C. I., Koh, T. S., Soo, R., Hartono, S., Thng, C. H., McKeegan, E., Yong, W. P., Chen, C. S., Lee, S. C., Wong, J., et al. (2009) Phase I and biomarker study of ABT-869, a multiple receptor tyrosine kinase inhibitor, in patients with refractory solid malignancies. *J. Clin. Oncol. 27*, 4718−4726.
(206) Tannir, N. M., Wong, Y. N., Kollmannsberger, C. K., Ernstoff, M. S., Perry, D. J., Appleman, L. J., Posadas, E. M., Cho, D., Choueiri, T. K., Coates, A., et al. (2011) Phase 2 trial of linifanib (ABT-869) in

DOI: 10.1021/acs.bioconjchem.5b00327
Bioconjugate Chem. 2015, 26, 1413−1438

patients with advanced renal cell cancer after sunitinib failure. *Eur. J. Cancer 47*, 2706−2714.
(207) Shao, G., Zhou, Y., and Liu, S. (2013) Monitoring glioma growth and tumor necrosis with u-SPECT-II/CT for by targeting integrin $\alpha_v\beta_3$. *Mol. Imaging 12*, 39−48.
(208) Zhou, Y., Shao, G., Wang, F., and Liu, S. (2012) Imaging breast cancer lung metastasis by u-SPECT-II/CT with an integrin $\alpha_v\beta_3$-targeted radiotracer ^{99m}Tc-3P-RGD$_2$. *Theranostics 2*, 577−587.
(209) Ma, Q., Ji, B., Jia, B., Gao, S., Ji, T., Wang, X., Han, Z., and Zhao, G. (2011) Differential diagnosis of solitary pulmonary nodules using ^{99m}Tc-3P-RGD scintigraphy. *Eur. J. Nucl. Med. Mol. Imaging 38*, 2145−52.
(210) Zhu, Z., Miao, W., Li, Q., Dai, H., Ma, Q., Wang, F., Yang, A., Jia, B., Jing, X., Liu, S., et al. (2012) ^{99m}Tc-3PRGD2 for integrin receptor imaging of lung cancer: a multicenter study. *J. Nucl. Med. 53*, 716−722.
(211) Zhao, D., Jin, X., Li, F., Liang, J., and Lin, Y. (2012) Integrin $\alpha_v\beta_3$ imaging of radioactive iodine−refractory thyroid cancer using ^{99m}Tc-3PRGD2. *J. Nucl. Med. 53*, 1872−1877.
(212) Ma, Q., Chen, B., Gao, S., Ji, T., Wen, Q., Song, Y., Zhu, L., Xu, Z., and Liu, L. (2014) ^{99m}Tc-3P4-RGD2 Scintimammography in the assessment of breast lesions: comparative study with ^{99m}Tc-MIBI. *PLoS One 9*, e108349.
(213) Liu, L., Song, Y., Gao, S., Ji, T., Zhang, H., Ji, B., Chen, B., Jia, B., Wang, F., Xu, Z., and Ma, Q. (2014) ^{99m}Tc-3PRGD2 scintimammography in palpable and nonpalpable breast lesions. *Mol. Imaging 13*, 1−7.
(214) Wan, W., Guo, N., Pan, D., Yu, C., Weng, Y., Luo, S., Ding, H., Xu, Y., Wang, L., Lang, L., et al. (2013) First experience of ^{18}F-Alfatide in lung cancer patients using a new lyophilized kit for rapid radiofluorination. *J. Nucl. Med. 54*, 691−698.
(215) Cheng, W., Wu, Z., Liang, S., Fu, H., Wu, S., Tang, Y., Ye, Z., and Wang, H. (2014) Comparison of ^{18}F-AIF-NOTA-PRGD$_2$ and ^{18}F-FDG uptake in lymph node metastasis of differentiated thyroid cancer. *PLoS One 9*, e100521.
(216) Guo, J., Guo, N., Lang, L., Kiesewetter, D. O., Xie, Q., Li, Q., Eden, H. S., Niu, G., and Chen, X. (2014) ^{18}F-Alfatide II and ^{18}F-FDG dual-tracer dynamic PET for parametric, early prediction of tumor response to therapy. *J. Nucl. Med. 55*, 154−160.
(217) Yu, C., Pan, D., Mi, B., Xu, Y., Lang, L., Niu, G., Yang, M., Wan, W., and Chen, X. (2015) ^{18}F-Alfatide II PET/CT in healthy human volunteers and patients with brain metastases. *Eur. J. Nucl. Med. Mol. Imaging*, DOI: 10.1007/s00259-015-3118-2.
(218) Hoshiga, M., Alpers, C. E., Smith, L. L., Giachelli, C. M., and Schwartz, S. M. (1995) $\alpha_v\beta_3$ integrin expression in normal and atherosclerotic artery. *Circ. Res. 77*, 1129−1135.
(219) Antonov, A. S., Antonova, G. N., Munn, D. H., Mivechi, N., Lucas, R., Catravas, J. D., and Verin, A. D. (2011) $\alpha_v\beta_3$ integrin regulates macrophage inflammatory responses via PI3 kinase/akt-dependent NF-κB activation. *J. Cell. Physiol. 226*, 469−476.
(220) Antonov, A. S., Kolodgie, K. D., Munn, D. H., and Gerrity, R. G. (2004) Regulation of macrophage foam cell formation by $\alpha_v\beta_3$ integrin: potential role in human atherosclerosis. *Am. J. Pathol. 165*, 247−258.
(221) Saraste, A., Nekolla, S. G., and Schwaiger, M. (2009) Cardiovascular molecular imaging: an overview. *Cardiovasc. Res. 83*, 643−652.
(222) Meoli, D. F., Sadeghi, M. M., Krassilnikova, S., Bourke, B. N., Giordano, F. J., Dione, D. P., Su, H. L., Edwards, D. S., Liu, S., Harris, T. D., et al. (2004) Noninvasive imaging of myocardial angiogenesis following experimental myocardial infarction. *J. Clin. Invest. 113*, 1684−1691.
(223) Choi, H., Phi, J. H., Paeng, J. C., Kim, S. K., Lee, Y. S., Jeong, J. M., Chung, J. K., Lee, D. S., and Wang, K.-C. (2013) Imaging of integrin $\alpha_v\beta_3$ expression using ^{68}Ga-RGD positron emission tomography in pediatric cerebral infarct. *Mol. Imaging 12*, 213−217.
(224) Razavian, M., Marfatia, R., Mongue-Din, H., Tavakoli, S., Sinusas, A. J., Zhang, J., Nie, L., and Sadeghi, M. M. (2011) Integrin-targeted imaging of inflammation in vascular remodeling. *Arterioscler., Thromb., Vasc. Biol. 31*, 2820−2826.
(225) Hua, J., Dobrucki, L. W., Sadeghi, M. M., Zhang, J., Bourke, B. N., Cavaliere, P., Song, J., Chow, C., Jahanshad, N., van Royen, N., et al. (2005) Noninvasive imaging of angiogenesis with a ^{99m}Tc labeled peptide targeted at $\alpha_v\beta_3$ integrin after murine hindlimb ischemia. *Circulation 111*, 3255−3260.
(226) Waldeck, J., Häger, F., Höltke, C., Lanckohr, C., von Wallbrunn, A., Torsello, G., Heindel, W., Theilmeier, G., Schäfers, M., and Bremer, C. (2008) Fluorescent reflectance imaging of macrophage-rich atherosclerostic plaques using $\alpha_v\beta_3$ integrin-targeted fluorochrome. *J. Nucl. Med. 49*, 1845−1851.
(227) Su, H., Gorodny, N., Gomez, L. F., Gangadharmath, U. B., Mu, F., Chen, G., Walsh, J. C., Szardenings, K., Berman, D. S., Kolb, H. C., et al. (2014) Atherosclerotic plaque uptake of a novel integrin tracer ^{18}F-Flotegatide in a mouse model of atherosclerosis. *J. Nucl. Cardiol. 21*, 553−62.
(228) Pichler, B. J., Kneilling, M., Haubner, R., Braumüller, H., Schwaiger, M., Röcken, M., and Weber, W. A. (2005) Imaging of delayed-type hypersensitivity reaction by PET and ^{18}F-Galacto-RGD. *J. Nucl. Med. 46*, 184−189.
(229) Beer, A. J., Pelisek, J., Heider, P., Saraste, A., Reeps, C., Metz, S., Seidl, S., Kessler, H., Wester, H. J., Eckstein, H. H., et al. (2014) PET/CT imaging of integrin $\alpha_v\beta_3$ expression in human carotid atherosclerosis. *J. Am. Coll. Cardiol. Img. 7*, 178−187.
(230) Beer, A. J., Kessler, H., Wester, H. J., and Schwaiger, M. (2011) PET imaging of integrin $\alpha_v\beta_3$ expression. *Theranostics 1*, 48−57.
(231) Beer, A. J., Lorenzen, S., Metz, S., Herrmann, K., Watzlowik, P., Wester, H. J., Peschel, C., Lordick, F., and Schwaiger, M. (2007) Comparison of integrin $\alpha_v\beta_3$ expression and glucose metabolism in primary and metastatic lesions in cancer patients: a PET study using ^{18}F-Galacto-RGD and ^{18}F-FDG. *J. Nucl. Med. 49*, 22−29.
(232) Josephson, L., and Rudin, M. (2013) Barriers to clinical translation with diagnostic drugs. *J. Nucl. Med. 54*, 329−332.
(233) Esteves, F. P., Raggi, P., Folks, R. D., Keidar, Z., Askew, J. W., Rispler, S., O'Connor, M. K., Verdes, L., and Garcia, E. V. (2009) Novel solid-state-detector dedicated cardiac camera for fast myocardial perfusion imaging: multicenter comparison with standard dual detector cameras. *J. Nucl. Cardiol. 16*, 927−934.
(234) Duvall, W. L., Croft, L. B., Godiwala, T., Ginsberg, E., George, T., and Henzlova, M. J. (2010) Reduced isotope dose with rapid SPECT MPI imaging: initial experience with a CZT SPECT camera. *J. Nucl. Cardiol. 17*, 1009−1014.
(235) Pazhenkottil, A. P., Buechel, R. R., Herzog, B. A., Nkoulou, R. N., Valenta, I., Fehlmann, U., Ghadri, J. R., Wolfrum, M., Husmann, L., and Kaufmann, P. A. (2010) Ultrafast assessment of left ventricular dyssynchrony from nuclear myocardial perfusion imaging on a new high-speed gamma camera. *Eur. J. Nucl. Med. Mol. Imaging 37*, 2086−2092.
(236) Schillaci, O., and Danieli, R. (2010) Dedicated cardiac cameras: a new option for nuclear myocardial perfusion imaging. *Eur. J. Nucl. Med. Mol. Imaging 37*, 1706−1709.
(237) Fiechter, M., Ghadri, J. R., Kuest, S. M., Pazhenkottil, A. P., Wolfrum, M., Nkoulou, R. N., Goetti, R., Gaemperli, O., and Kaufmann, P. A. (2011) Nuclear myocardial perfusion imaging with a novel cadmium-zinc-telluride detector SPECT/CT device: first validation versus invasive coronary angiography. *Eur. J. Nucl. Med. Mol. Imaging 38*, 2025−2030.
(238) Gaemperli, O., and Kaufmann, P. A. (2011) Lower dose and shorter acquisition: pushing the boundaries of myocardial perfusion SPECT. *J. Nucl. Cardiol. 18*, 830−832.
(239) DePuey, E. G. (2012) Advances in SPECT camera software and hardware: Currently available and new on the horizon. *J. Nucl. Cardiol. 19*, 551−581.
(240) Bailey, D. L., and Willowson, K. P. (2013) An evidence-based review of quantitative SPECT imaging and potential clinical applications. *J. Nucl. Med. 54*, 83−89.

DOI: 10.1021/acs.bioconjchem.5b00327
Bioconjugate Chem. 2015, 26, 1413−1438